Synthesis, Characterization and Anticancer Activity of New Gold (III) Complexes with Diamine and Thione Ligands

BY

Muhammad Monim-ul-Mehboob

A Dissertation Presented to the

DEANSHIP OF GRADUATE STUDIES

KING FAHD UNIVERSITY OF PETROLEUM & MINERALS

DHAHRAN, SAUDI ARABIA

In Partial Fulfillment of the

Requirements for the Degree of

DOCTOR OF PHILOSOPHY

In

CHEMISTRY

OCTOBER 2013

KING FAHD UNIVERSITY OF PETROLEUM & MINERALS

DHAHRAN- 31261, SAUDI ARABIA

DEANSHIP OF GRADUATE STUDIES

This thesis, written by **MUHAMMAD MONIM-UL-MEHBOOB** under the direction his thesis advisor and approved by his thesis committee, has been presented and accepted by the Dean of Graduate Studies, in partial fulfillment of the requirements for the degree of **DOCTOR OF PHILOSOPHY IN CHEMISTRY.**

Dr. Anvarhusein A. Isab
(Advisor)

Dr. Abdullah Jafar Al-Hamdan
Department Chairman

Dr. Mohammed I. M. Wazeer
(Co-Advisor)

Dr. Salam A. Zummo
Dean of Graduate Studies

Dr. Mohammed B. Fettouhi
(Member)

6/2/14
Date

Dr. Khaled M. Mazen
(Member)

Dr. Akhtar. A. Naqvi
(Member)

This work is dedicated to my research advisors, honorable teachers,

sincere friends and souls of my beloved parents (late)

who encouraged me for better pursuits in life.

ACKNOWLEDGMENTS

All praises are for Allah Subhanahu Wataala (SBW), Who bestowed me with all His blessings to accomplish this work. All compliments and the blessings of Allah are upon Prophet Muhammad Sallalahu Alaihi Wasallam (SAW), His Progeny and His Great Companions Radiallahu Anhu (RA) who exemplified themselves for us to pursue Sirat-e-Mustaqeem.

I would like to thank KFUPM for financial support as well as providing a conducive academic and research environment. I am thankful to the Chairman, Dr. Abdullah Jafar Al-Hamdan for providing access to all possible research facilities in the Chemistry Department.

With deep sense of gratitude and appreciation, I would like to thank my dissertation advisor Professor Dr. Anvarhusein A. Isab, for his versatile and learned guidance during the research work. His generous cooperation, erudite suggestions, invigorating encouragement and patience, have persisted a source of inspiration for me.

I am very grateful to Professor Dr. M. I. Wazeer as co-advisor for helping me in interpretation of NMR data, writing manuscripts for publications and practical learning on NMR instruments.

I am highly obliged by Associate Professor Dr. M. B. Fettouhi for X-ray single crystal determination of metal complexes, conceptual understanding of Advanced Inorganic Chemistry and scientific writing of PhD dissertation.

My sincere gratitude goes to the other members of my dissertation committee, Dr. Khaled M. Mazen and Dr. Akhtar. A. Naqvi for their cooperation and encouragement.

I am greatly beholden to Professor Dr. Saeed Ahmad, Chemistry Department, UET, Lahore-Pakistan for his encouragement and great support in my scientific triumphs.

I am thankful to M. Arab for guiding me through his NMR expertise, Baha-ud-din for providing synthesis facilities, Ayman al-Majid for elemental analysis and Mansour Zaki for IR and UV-Vis analysis during this research work.

I am also grateful to all faculty and staff members for their kind and cheerful cooperation. My sincere acknowledgment goes to my colleagues Dr. M. Altaf, Dr. B. Al-Maythalony, Dr. Naseer-uz-Zaman, Dr.Tuafik, Dr. Abdulaziz and Dr. Othman. I extend my cordial appreciation to my friends; especially Hanif, Izzat, Atif, Khizar, Zain, Shamsuddin, Zaheer,Umair, Farhan, Zeeshan, Asad, Wajahat, Farrukh, Mobeen, Sajid, Mansha, Daud, Naeem, Waqar and Adeem for their support and cooperation.

I would like to express my greatest gratitude to my parents (late) for their continuous du'aa and support. I must not forget here my family members, my sisters and my brothers, last but not least my nephews and nieces for their cooperation and prayers for my studies.

(Muhammad Monim-ul-Mehboob)

TABLE OF CONTENTS

LIST OF TABLES

LIST OF FIGURES

LIST OF ABBREVIATIONS

ATCC	American Type Culture Collection
AuSTg	Gold thioglucose
AuSTm	Gold sodium thiomalate
Autm	Aurothiomalate
B3LYP	Becke, 3-parameter, Lee-Yang-Parr
bn	Butylenediamine
CCL	Chronic lymphocytic leukemia
CPMAS	Cross Polarization Magic Angle Spinning
Cyclam	1,4,8,11-Tetraazacyclotetradecane
D.P.	Decomposition Point
Dach	1,2-Diaminocyclohexane
Damp	Dichloro[2-(dimethylaminomethyl)phenyl]
DFT	Density Functional Theory
Diap	Diazipane-2-thione
Diaz	Diazinane-2-thione
Dien	Diethylenetriamine
Diphos	Diphenylphosphinoethane
DMEM	Dulbecco's Modified Eagle Medium
DMSO	Dimethylsulfoxide
DNA	Deoxyribonucleic acid
Dppe	1,2-bis(diphenylphosphino)ethane
DSS	2,2-Dimethylsilapentane-5-sulphonate
E. coli	*Escherichia Coli*
EA	Elemental Analysis

ECACC	European Collection of Cell Cultures
ELISA	Enzyme-linked immune-sorbent assay
en	Ethylenediamine
$Et_3PAuSATg$	*Auranofin*
FDA	Food and Drug Administration (USA)
F.Streptococcus	*Fetal Streptococcus*
Far-IR	Far-Infrared
FBS	Fetal Bovine Serum
FID	Free Induction Decay
Gly	Glycine
HBA	Host Bus Adapter
His	L-Histidine
HPC	Heterotrotrpic Plate Counts
IC_{50}	Half maximul inhibitory concentration
Im	Imidazole
Imt	Imidazolidine-2-thione
K. pneumonice	*Klesbiella pneumonia*
LANL2DZ	Los Alamos National Laboratory 2 double ζ
LMCT	Ligand-to-Metal Charge Transfer
LUMO	Lowest Unoccupied Molecular Orbitals
M.P.	Melting Point
MAS	Magic Spinning Angle
Met	L-Methionine
MIR	Mid-Infrared
MTCC	Microbial Type Culture Collection (India)
MTT	Methylthiazol tetrazolium (assay)
N,N'-Et_2-*en*	N,N´-di-ethyl-ethylenediamine

N,N'-*i*Pr_2-*en*	N,N´-di-iso-propyl-ethylenediamine
N,N'-Me_2-*en*	N,N´-di-methyl-ethylenediamine
N-Et-*en*	N-ethyl-ethylenediamine
N-*i*Pr-*en*	N-iso-propyl-ethylenediamine
N-Me-*en*	N-methyl-ethylenediamine
NMR	Nuclear Magnetic Resonance
ORTEP	Oak Ridge Thermal Ellipsoid Plot Program
P. aeruginosa	*Pseudomonas aeruginosa*
PC3	Prostate Cancer 3(human cell line)
Phen	Phenanthroline
pn	Propylenediamine
PPh_3	Triphenylphosphine
RPMI	Roswell Park Memorial Institute (medium)
S. aureus	*Staphylococcus aureus*
S. typhi	*Salmonella typhi*
SD	Standard Deviation
SGC7901	Gastric Cancer 7901 (human cell line)
Terpy	Terpyridine
TMS	Tetramethylsilane
Tu	Thiourea
UV	Ultra violet
Vis	Visible

ABSTRACT

Full Name : Muhammad Monim-ul-Mehboob

Thesis Title : Synthesis, characterization and anticancer activity of new gold (III) complexes with diamine and thione ligands

Major Field : Chemistry

Date of Degree : October 2013

Since the hallmark discovery of anticancer properties of cisplatin, a large number of coordination compounds of platinum and other metals have been investigated for their anticancer potency. In recent years, gold complexes have demonstrated a great potential for the design and development of new anticancer agents. In view of this potential, we prepared several gold(III) complexes and evaluated their antitumor properties.

In this dissertation, two novel series of gold(III) complexes are reported: the first consists of bis-diamines complexes while the second is mixed ligand series containing diamines and thiones. The first series of general formula, $[Au(L)_2]Cl_3$ [where L = 1,2-diaminoethane (en), 1,3-diaminopropane (pn), N-alkyl substituted ethylenediamine (N-R-en) and N,N´-diakyl substituted diamine] was synthesized by reacting auric acid trihydrate ($HAuCl_4 \cdot 3H_2O$) with diamine ligands in 1:2 molar ratio. The second series of general formula, $[(L´)_2Au(L)]Cl_3$, where L = 1,2-diaminoethane (en), 1,3-diaminopropane (pn), 1,4-diaminobutane (bn) and L´ = 1,3-imidazolidine-2-thione (Imt), 1,3-Diazinane-2-thione(Diaz) and 1,3-Diazipine-2-thione (Diap)] was synthesized by reacting $HAuCl_4 \cdot 3H_2O$ with diamine and thione ligands in 1:1:2 molar ratio.

These complexes of both series were subsequently characterized by elemental analysis, far-IR spectroscopy and solution as well as Solid state NMR measurements. The mid-IR and NMR data show the coordination of diamine ligands to Au(III) *via N* donor atoms. The crystal structure of one of the complexes was determined. The complex is dinuclear with two discrete $[Au(pn)(Cl)]^+$ units bridged by two deprotonated pn ligands in a pseudo square planar coordination geometry at the Au(III) ion. The solid state IR as well as ^{13}C

and ^{15}N NMR data for $[(L')_2Au(L)]Cl_3$ complexes indicate that Au(III) centre is bonded *via* sulfur of thiocarbonyl S=C< site of the thiones and also chelated by the diamines.

Spectroscopic data was essentially evaluated by comparing with calculated data from the built and optimized structure by GAUSSIAN 09 at the RB3LYP level with LanL2DZ bases set. The computational study of $[Au(en)_2]Cl_3$ shows that the gold(III) adopts distorted square planar geometry. The structural features of $[(L')_2Au(L)]Cl_3$ complexes based on thione and diamine mixed ligands are almost similar to $[Au(en)_2]Cl_3$ complex.

The potential anticancer properties of gold(III) complexes were evaluated *in vitro* against prostate PC3, gastric SGC7901 and ovarian A2780/A2780 *cis* cancer cell lines. The third series, previously synthesized, with general formula, $[Au(L)Cl_2]Cl$ [where L 1,2-diaminoethane (en), 1,3-diaminopropane (pn), 1,4-diaminobutane (bn)] was also used for comparison with $[Au(L)_2]Cl_3$. Generally, $[Au(diamine)_2]^{3+}$ complexes demonstrate better anticancer properties in PC3 cells, whereas $[Au(diamine)Cl_2]^{1+}$ type displays better anticancer properties in SGC7901 and A2780/A2780 cis cells. The complex $[Au(en)_2]Cl_3$ was recognized as most cytotoxic agent with activity as good as of clinically used drug cisplatin on prostate PC3 cancer cells. In this study, cytotoxicity data for second series of gold(III) complexes against C6 glioma cell lines are also reported, and the results indicate some complexes have cytotoxicity comparable to cisplatin. The *in vitro* cytotoxic study of Au(III)-thione complexes against C6 glioma cell line also leads to conclusion that the structural features e.g. ring size of thione ligand (Imt and Diaz) as well as Au(III) chelate ring size with diamine (en, pn and bn) may affect in vitro cytotoxicity of complex. The Imt containing Au(III) complexes are relatively better cytotoxic agents than those containing Diaz. Some of our complexes show *in vitro* cytotoxicity comparable to cisplatin.

In order to investigate the mode of action of these compounds, experiments were performed on reactivity towards amino acids as potential binding partner in human body. The chemical and biological data presented in this dissertation provide the basis for not only understanding the existing status of gold-based anticancer drugs, but also a rationale for future drug design strategies.

ملخص الرسالة

الاسم الكامل: محمد منعم المحبوب

عنوان الرسالة: تصنييع و توصيف سلسلة جديدة من معقدات الذهب (III) و تقييم سميتها ضد مجموعة من الخلايا السرطانية

التخصص: الكيمياء

تاريخ الدرجة العلمية: 26 \11\ 1434 الموافق ل 2\10\2013

منذ إكتشاف السمة المميزة لخصائص (cisplatin) المضادة للسرطان , فإنه قد تم البحث في عدد كبير من مركبات البلاتين التساهمية وغيره من المعادن لدراسة إمكانية إستخدامها كمضاد للسرطان. خلال السنوات الحالية أظهرت معقدات الذهب إمكانات كبيرة في تصميم وتطوير عوامل مضادة للسرطان. إدراكا لهذه الامكانات قمنا بتحضير عدد من معقدات الذهب (III) وتقييم خصائصها المضادة للأورام.

في هذه الاطروحة تم توثيق سلسلة جديدة من معقدات الذهب (III) : ثنائي امينات و كذلك مختلط المتصلات من نوع ثنائي امينات والثيونات. السلسلة الاولى للصيغة العامة $[Au(L)_2]Cl_3$, حيث L = 1,2 ثنائي أمينو إيثان (en), 1,3 ثنائي أمينوبروبان (pn) , إيثيلين ثنائي امين N- مرتبط بالألكيل (N-R-en) و ثنائي أمين -N,N´ مرتبط بثنائي ألكيل تم تحضيره بتفاعل حمض الاوريك ثلاثي التميه ($HAuCl_4 \cdot 3H_2O$) مع كلاب ثنائي أمين بنسبة مولارية 1:2 . السلسلة الثانية للصيغة العامة $[(L´)_2Au(L)]Cl_3$ حيث L = ثنائي أمينو إيثان (en), 1,3 ثنائي أمينوبروبان (pn) , 1,4 ثنائي أمينو بيوتان (bn) و L´ = 1.2 ايميدازوليداين- 2- ثيون (Imt) ، 1,3 ثنائي أثينان -2- ثيون (Diaz) و 1,3- ثنائي أثيباين -2- ثيون (Diap) تم تحضيره بتفاعل $HAuCl_4 \cdot 3H_2O$ مع كلابات ثنائي أمين وثيون بنسبة مولارية 2:1:1.

لقد تم توصيف معقدات كلا السلسلتين بعد ذلك باستخدام جهاز تحليل العناصر وجهاز مطيافية الاشعة تحت الحمراء وجهاز الرنين النووي المغناطيسي الخاص بالسوائل والحالة الصلبة. نتائج جهازي الرنين النووي المغناطيسي ومطيافية الاشعة تحت الحمراء تظهر رابطة تناسقية لكلابات ثنائي أمين مع Au(III) عبر ذرات N المانحة. و قد تم تحديد التركيب البلوري لأحد هذه المعقدات. المعقد ثنائي النواة بوحدتين $[Au(pn)(Cl)]^+$ مرتبطتين بجسر من كلابتين من pn منزوع البروتونات بشكل هندسي تناسقي مستوي مربع مشوه عند ايون Au(III). مطيافية الاشعة تحت الحمراء للحالة الصلبة بالاضافة إلى نتائج الرنين النووي المغناطيسي ^{13}C و ^{15}N لمعقدات $[(L´)_2Au(L)]Cl_3$ تؤشر أنّ ذرة Au(III) المركزية مرتبطة عبر موقع ذرة الكبريت للثيو كاربونيل S=C< للثيون و بكلاب مع ثنائي الامين.

لقد تم تقييم النتائج المطيافية بمقارنتها مع النتائج المحسوبة من الاشكال المبنية المحسنة باستخدام GAUSSIAN 09 على مستوى RB3LYP مع مجموعة قواعد LanL2DZ. الدراسة الحسابية للمعقد $[(L´)_2Au(L)]Cl_3$ تظهر أن

Au (III) يعتمد شكل هندسي مربع مستوي مشوّه. المميزات في التركيب لمعقدات $[(L´)_2Au(L)]Cl_3$ المتكونة من خليط متصلات الثيون و كلابات ثنائي الامين تشبه إلى حد بعيد معقد $[Au(en)_2]Cl_3$.

لقد تم تقييم قدرة خصائص معقدات عنصر الذهب (III) المضادة للسرطان في المختبر على خطوط خلايا سرطان البروستات PC3 والمعدة SGC7901 والمبيض A2780/A2780cis. السلسلة الثالثة للصيغة العامة والمحضرة مسبقا من $[Au(L)Cl_2]Cl$ حيث L= 1,2 ثنائي أمينو إيثان (en) 1,3 ثنائي أمينوبروبان (pn) , 1,4 ثنائي أمينو بيوتان (bn). تم إستخدامها ايضا للمقارنة مع $[Au(L)_2]Cl_3$. بشكل عام معقدات $[Au(diamine)_2]^{3+}$ تظهر خصائص أفضل ضد خلايا سرطان البروستات PC3, بينما النوع $[Au(diamine)Cl_2]^+$ يظهر خصائص أفضل لمقاومة خلايا سرطان A2780/A2780cis, SGC7901. لقد وجد أن معقد $[Au(en)_2]Cl_3$ العامل الاكثر سمية للخلايا السرطانية وبفاعلية تضاهي العقار المستخدم طبيا لخلايا سرطان البنكرياس PC3 ، cisplatin. نتائج سمية الخلايا للسلسلة الثانية لمعقدات عنصر الذهب (III) على الخلايا السرطانية الدبقية C6 قد تم توثيقها في هذه الدراسة. وقد أظهرت النتائج تقارب في سمية الخلايا مع cisplatin. الدراسة المخبرية لسمية الخلايا لمعقدات Au(III)–ثيون على الخلايا الدبقية C6, أدت أيضا إلى استنتاج تأثير الخصائص الشكلية كحجم الحلقة ونوع الكلاب (Diaz ,Imt) بالإضافة إلى حجم حلقة كلاب ثنائي أمين (en, pn and bn) على السمية الخلوية للمعقد. معقدات Au(III) التي تحتوي متصل Imt لديها عوامل سمية خلوية أفضل من التي تحوي متصل Diaz. بعض من معقداتنا أظهر سمية خلوية مخبريا مقاربة لعقار cisplatin.

للتعرف على طريقة عمل هذه المعقدات , تم القيام بمجموعة من التجارب على فعاليتها على الاحماض الامينية باعتبارها الطرف المرتبط في جسم الانسان. النتائج الكيميائية والحيوية الموجودة في هذه الاطروحة لا تزودنا بمبادئ العقاقير المضادة للسرطان التي تحوي عنصر الذهب فقط, بل تعطي الاساس المنطقي لإستراتيجيات تصميم أدوية مستقبلية.

CHAPTER 1

INTRODUCTION

Platinum-based drugs such as cisplatin, carboplatin and oxaliplatin are among the most active anticancer agents and have been widely used in the treatment of a variety of cancers [1–15]. The structures of some platinum complexes effective as anticancer agents are shown in Figure 1.1. Cisplatin and carboplatin are known to be particularly effective against solid tumor types such as testicular, ovarian, head and neck cancers and, small-cell lung cancer. Carboplatin has approximately the same spectrum of activity as cisplatin but reduced toxicity [12–14]. Oxaliplatin is particularly effective in the treatment of primary advanced colorectal cancer and cisplatin-resistant ovarian cancers [16–18].

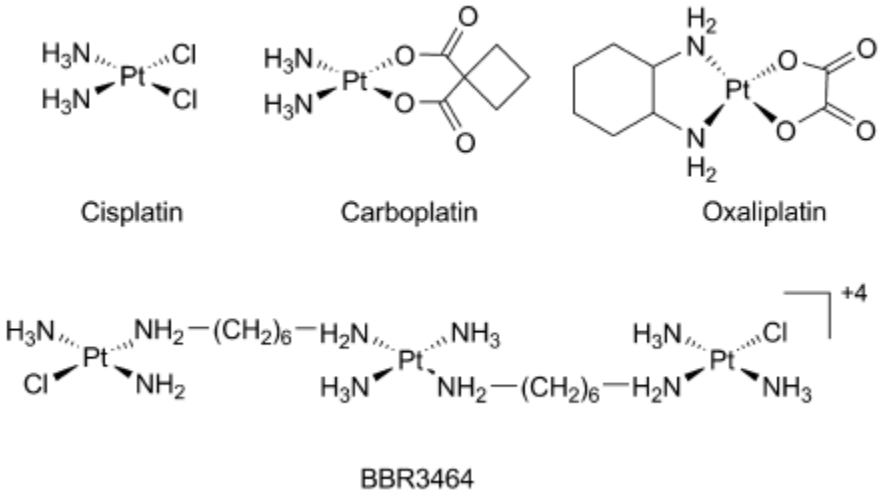

Figure 1.1 Structures of some some anticancer platinum compounds

Although platinum-based drugs are widely used for the treatment of a variety of cancers [1–12] yet they are associated with severe side effects as well as acquired or intrinsic resistance [1]. These limitations encouraged scientists to investigate the complexes of other transition metals for example, palladium, ruthenium and gold. Among the non-platinum transition metal complexes tested so far, gold complexes have demonstrated a great promise for the design and development of anticancer agents.

Gold-based drugs, such as gold(I) thiomalate [*myocrisin* $(Autm)_n$], gold(I) thioglucose [*solganol* $(Autg)_n$] and *auranofin* [2,3,4,6-tetra-*o*-acetyl-1-thio-β-D-glucopyranosato-S) triethylphosphine gold(I)] have been successfully used over many years for the treatment of rheumatoid arthritis [19–22]. Besides curing arthritis, a large number of phosphine-gold(I) complexes, especially, *auranofin* and $[Au(dppe)_2]Cl$ (dppe = 1,2-bis(diphenylphosphino) ethane), are known to exhibit promising antitumor properties [23–27]. $K[Au(CN)_2]$ and gold(I) thiocyanate complexes have also been investigated as chemotherapeutic agents, including mainly the studies of antitumor and anti-HIV activity [28,29]. The structures of some important gold drugs with their trade names are shown in Figure 1.2.

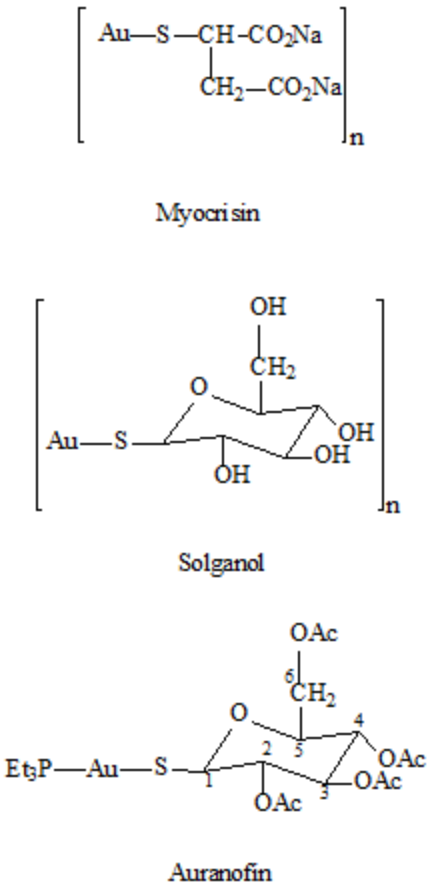

Figure 1.2 Structures of some gold-based drugs

In recent years, gold(III) complexes have become the focus of interest due to the reason that they are isoelectronic and generally isostructural to platinum(II) complexes such as cisplatin, the most widely used anticancer drug. It is, therefore, anticipated that they will have activity similar to that of platinum(II) antitumor drugs [30-34]. Cytotoxic activities of a number of gold(III) compounds have been evaluated. However, compared to gold(I) and platinum(II)-complexes, the gold(III) complexes have not been well explored chemically or electrochemically because they are highly reactive. Since gold(III) complexes have high redox potential and relatively poor stability, their use as anticancer drugs was questioned under physiological conditions [35].

Given that the mammalian environment is generally reducing, compounds of gold(III) were expected to be reduced *in-vivo* to gold(I) and metallic gold, which make them less effective as drugs. Recently, new gold(III) compounds with much higher stability have been synthesized using better ligands that usually have nitrogen atoms in the donor groups [36].

Messori *et al.* described the *in vitro* activity of a series of gold(III) complexes, $[Au(en)_2]Cl_3$ (**I**), $[Au(dien)Cl]Cl_2$ (**II**), $[Au(cyclam)](ClO_4)Cl_2$ (**III**), $[Au(terpy)Cl]Cl_2$ (**IV**), and $[Au(phen)Cl_2]Cl$ (**V)** as shown in Figure 1.3 against the A2780 ovarian cancer cell line and a cisplatin-resistant variant [33,37] The relative order of cytoxicity was Au(terpy) >> Au(phen) > Au(en), Au(dien) >> Au(cyclam). Interestingly the three most active compounds retained activity against the cisplatin-resistant cell line. All of these complexes showed significant cytotoxic effects against the A2780 human ovarian cancer cell line, comparable to or even greater than cisplatin, and they were able to overcome resistance to cisplatin to a large extent.

A number of gold compounds have exhibited potent anticancer activity in *in vitro* assays against a number of human cancer cell lines [38–40]. Gold(III) complexes have been proved to be potent inhibitors of enzymes or proteins that are directly or indirectly involved in cancer growth and progression [41–43].

In the light of the above mentioned medicinal role of gold compounds, it is important to study the coordination chemistry of gold(III) from the point of view of designing new drugs as well as to understand the biochemical mechanism of action of the known anticancer complexes.

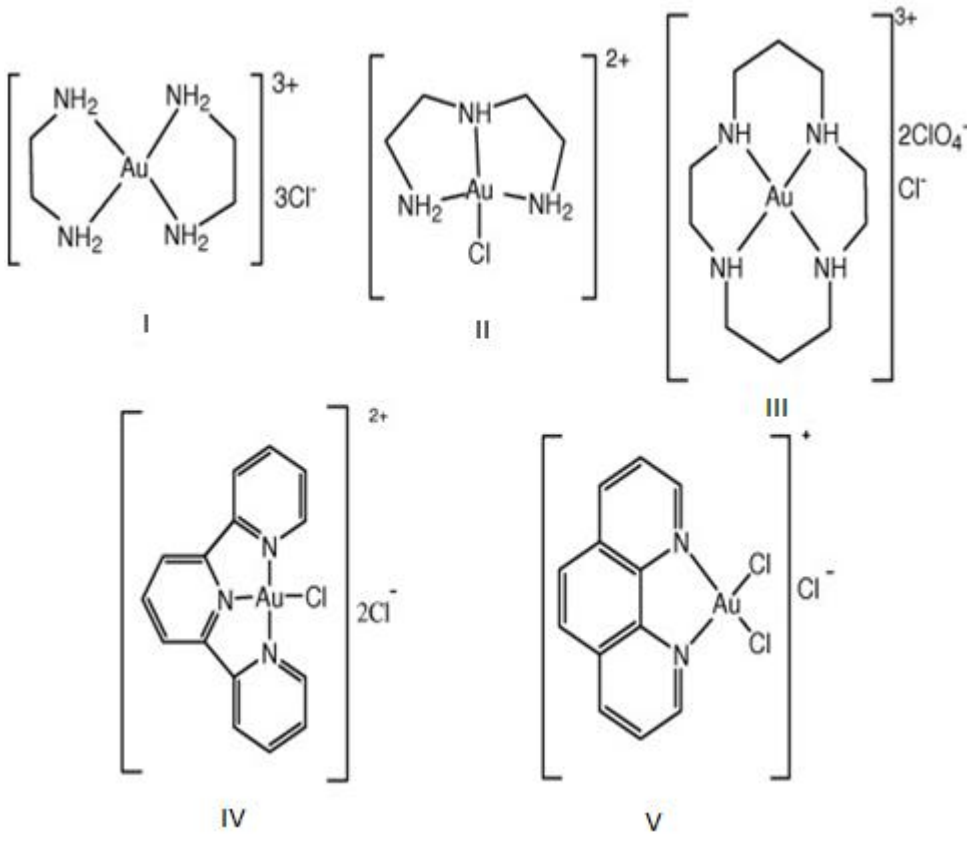

Figure 1.3 Structures of potential anticancer gold (III) poly-amine/imine complexes

1.1 Current Status of the Problem

1) Cisplatin has been used as an anticancer agent for the last few decades but found to be highly toxic.
2) Carboplatin is a second-generation platinum drug against a limited number of cancers with relatively lower toxicity.
3) Oxaliplatin was accepted for clinical use as recently as 2003 and used in combination with 5-fluorouracil against advanced metastatic colorectal cancers.
4) Scientists are striving to develop new types of non-platinum drugs. The main aim is to design anticancer drugs with enhanced efficacy but low toxicity.

5) Metal complexes offer an opportunity for the discovery of new antitumor drugs with truly new mechanisms of action by varying structural features in order to improve the physico-chemical and biological properties.

6) Recent advances in this area demonstrated a great promise for the utilization of non-platinum complexes in cancer chemotherapy.

7) Our interest in using gold for the development of anticancer agent arises from the fact that this metal has extensively been employed in medicinal inorganic chemistry during the last decades.

8) Some gold(III) complexes, isoelectronic with antitumor platinum(II) complexes, have recently been evaluated in *in vitro* tests, showing significant cytotoxic effects.

1.2 Aim of the Present Research

1) The focus of the present study is to synthesize and characterize several new gold(III) complexes with a number of diamine ligands with the general formula, [Au*(diamine)*$_2$]Cl_3 as well as -mixed-ligands gold(III) complexes of diamines and thiones with the general formula, [*(thione)*$_2$Au*(diamine)*]Cl_3.

2) The current work includes gold(III) complexes bidentate chelating ligands that is of ethylenediamine *(en)* and propylenediamine *(pn)* type. These *en* and *pn* are different sized ligands which will form chelate rings around Au(III) center. The thione ligands of different ring size i.e. Imidazolidine-2-thione (Imt),1,3-Diazinane-2-thione (Diaz) and 1,3-Diazipane-2-thione (Diap) will also affect coordinating ability towards Au(III) center. These different chelate size of

coordinated diamines and ring sizes of thiones are expected to demonstrate different reactivities and establish structure-activity relationships (SARs).

3) Furthermore, we will also evaluate the newly synthesized complexes for their potential anticancer activity.

The study is helped to lead us the discovery of new type of anticancer drugs. If we are successful it will not only benefit the people who suffer from cancer in Kingdom of Saudi Arabia but also the cancer victims of the entire world.

CHAPTER 2

LITERATURE REVIEW

For half a century, the field of metal-based anticancer drugs has been dominated by the precious metal, platinum. The discovery of platinum's anticancer properties was made unintentionally during an experiment in 1965 [44], conducted at Michigan State University by Barnett Rosenberg. He used a platinum electrode to apply an electric field to a colony of *E. coli,* which was observed to inhibit their growth [45]. A meticulous investigation into the cause of this effect concluded that the platinum electrode was breaking down to generate platinum-(II) species *in situ,* which was stopping the cells from multiplying. This observation led to the development of *cis*-diamminedichloridoplatinum(II), commonly known as cisplatin, being approved by the American Food and Drugs Administration (FDA) for cancer therapy in December, 1978 [46]. Since that it has become the most widely used anticancer drug, with an estimated 70 % of patients receiving the compound as part of their treatment [47,48].

Cisplatin was heralded as a completely novel type of anticancer agent, and its discovery encouraged inorganic chemists to devise and test other precious metal-based therapies [49]. Metal compounds offer a huge unexplored chemical gap concerning modern drug design and development based on their different kinetics, geometries and reactivities compared to classical non-metal organic drugs.

The fortuitous discovery of the anticancer properties of cisplatin, its platinum-(II) analogues and their wide clinical application in current cancer treatments promoted a

great deal of interest in the area of metal-based anticancer agents [50]. Cisplatin exhibits clinical activity against a wide range of different kinds of cancers. It remains one of the most significant anticancer agents in the clinical armamentarium [51]. However, it experiences both intrinsic and acquired resistance in cancer cell lines [52–55]. Cisplatin resistance is thought to occur primarily by cells resisting DNA platination leading to the exit at G2/M phase of cell cycle and inhibiting apoptosis. In addition, drug-efflux in resistant cell lines has been shown to be greater than the influx due to the up-regulation of multi drug resistance (MDR) genes and the production of antiporters such as glycoprotein [52].

Whilst the chemotherapeutic success of platinum is undeniable, it is by no means the perfect drug. It is not effective against many common types of cancer, drug resistance is common and it has a deplorable range of side effects, which can include nerve damage, hair loss and nausea. Disappointingly however, the countless clinical candidates in fifty years later, there have only been two more worldwide drug approvals for precious metal-containing anticancer drugs: carboplatin and oxaliplatin, both of which are direct analogues of cisplatin, approved in 1993 and 2002 respectively. The mode of action of these platinum complexes is known: the chloride or dicarboxylate ligands are hydrolysed within the cell to generate a bis-aqua species, which binds irreversibly to DNA – usually to two adjacent guanine bases [56] and the cell, unable to replicate, defaults to apoptosis (controlled cell death) [49,57].

Platinum-containing compounds such as cisplatin, carboplatin and oxaliplatin are widely used in the treatment of a variety of cancers. Newer, second generation platinum compounds like carboplatin and oxaliplatin were designed to improve efficacy

particularly against cell lines that demonstrate second pass cisplatin resistance [58]. Tolerance to cisplatin-induced DNA damage has been suggested as a fundamental mechanism of drug resistance [59].

In the early 1980s, the rapidly emergent interest as well as demand has enthused for the design of alternative platinum and non-platinum-based anticancer agents in cancer chemotherapy in order to overcome both intrinsic and acquired resistance in cancer cell lines. Consequently, in recent years the interest in non-platinum metal complexes for cancer chemotherapy has been rapidly growing. Such consideration has further been stimulated by the possibility of developing new agents with a different mode of action and clinical profile from the well-established platinum based metallodrugs [60].

To circumvent the problem of drug-resistance in cisplatin-resistant cells, gold(III)-based complexes have been designed as a potential alternative to cisplatin [61,62]. Gold(III) complexes exhibit iso-electronic and iso-structural features with platinum-(II) and have similar uptake and DNA interference activity [62]. In addition, the higher charge of gold(III) compared to platinum(II) is an added advantage for binding with DNA [63]. Among the several classes of metal complexes that have been taken into consideration as potential anticancer agents starting from the 1980's, only a few investigations have focused on d^8 square planar gold(III) complexes in spite of their stringent similarity to platinum (II) complexes [64–68]

In this context, a number of research reports are available in the literature on gold (I) drugs, but only a few reports appeared about the biological actions of gold(III) complexes [69,70]. However, owing to their relatively less solubility profile and being kinetically

more labile than the corresponding Pt(II) complexes, the gold(III) complexes were found to deviate from the platinum(II) compounds.

During the 1990s, the gold(III) compounds emerged as potential anticancer agents showing improved stability both in solid and solution phases, lower toxicity and favorable *in-vitro* pharmacological profiles. For example in 1996, Parish, Buckley, Elsome and co-workers reported a series of cytotoxic gold(III) compounds with tridentate damp ligands [damp = (dimethylamino)methyl]phenyl)] with encouraging results towards the anticancer activity (see Figure 2.1) [71–75]. Parish *et al.* also described [76] the chemical and biological studies of dichloroido-2-{(dimethylamino)methyl)phenyl}gold (III) complex. Abbate *et al.* [72] explained crystal structure and solution chemistry of the cytotoxic complex 1,2-dichloroido(o-phenanthroline)gold(III) chloride.

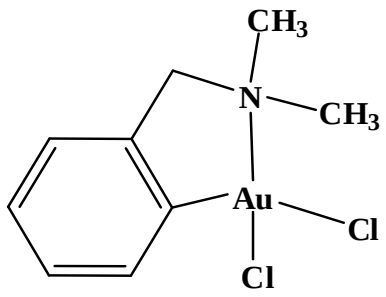

Figure 2.1 Structure of [(Damp)$AuCl_2$]

We refer, in particular, to gold(III) porphyrinates (see Figure 2.2) [77], and to a variety of organogold(III) compounds [78]. Potent cytotoxic actions were investigated *in vitro* for most of the compounds. Some compounds are evidently shown the ability to overcome cisplatin resistance.

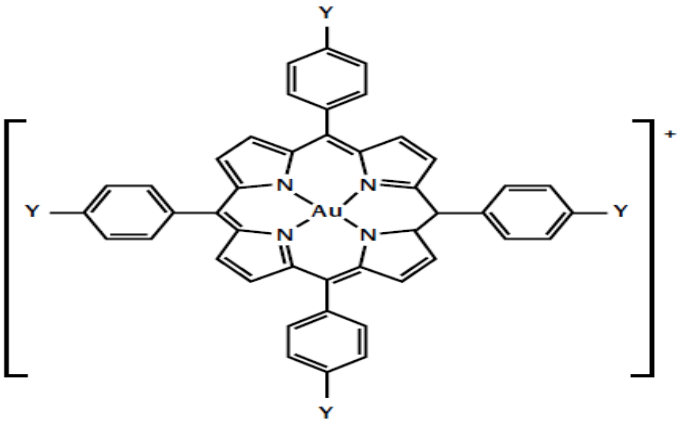

Figure 2.2 Representing structure of gold(III) porphyrin complexes

Abbate *et al.* reported the crystal structure and solution chemistry of the cytotoxic complex 1,2-dichloro(*o*-phenanthroline)gold(III) chloride (see Figure 2.3) [72].

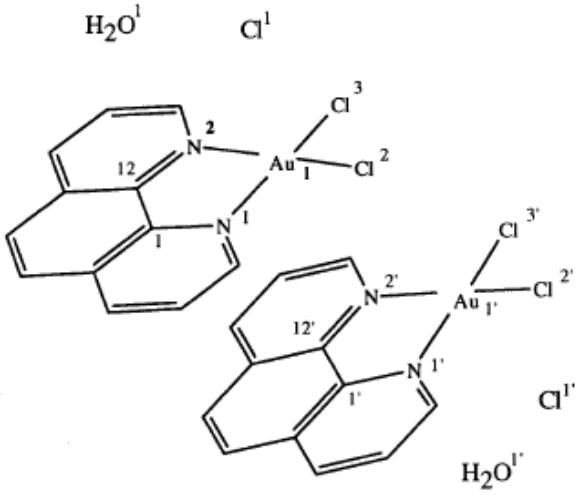

Figure 2.3 Structure of [{(Phen)$AuCl_2$}Cl·H_2O]$_2$

In 2002, Marcon, Minghetti and Cinellu realized that some novel gold(III) complexes, bearing the *bipyridyl* ligand (see Figure 2.4), might be favorably employed for anti-proliferative effects on various human cancer cell lines [35].

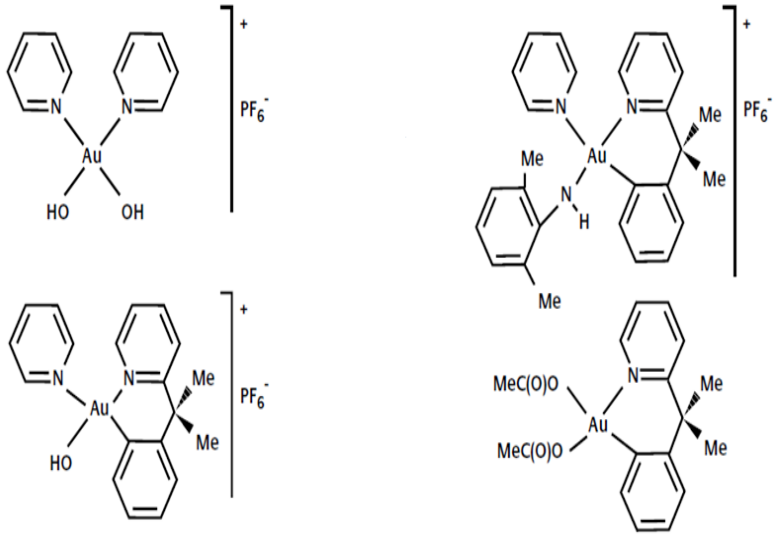

Figure 2.4 Schematic drawing of Au(III) bipyridine complexes

S. Zhu *et al.* described the synthesis, structures, and electrochemistry of gold(III) ethylenediamine complexes and interactions with Guanosine 5'-Monophosphate [71]. Further, a number of other gold(III) complexes have been developed with anticancer activity. Gabbiani *et al.* elaborated a review on gold(III) compounds as anticancer drugs [31]. We refer, in particular, to gold(III) dithiocarbamates (see Figure 2.5) [79].

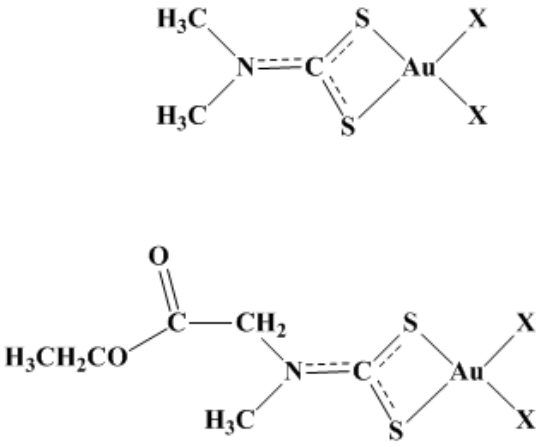

Figure 2.5 Structures of gold(III) dithiocarbamate complexes [X=Cl or Br]

In 2006**,** Casini *et al.* described a series of dinuclear gold(III) complexes with a "Au_2O_2" diamond core and with *bypiridyl* ligands exhibiting interesting *in vitro* biological properties [80].

Several lines of evidence suggest that gold(III) compounds produce their antiproliferative effects through innovative and nonconventional modes of action. For instance, the hypothesis that their biological effects are mediated by an anti-mitochondrial mechanism rather than by direct DNA damage, as it is the case for cisplatin and its analogs, has gained much credit during the last few years. A. Bindoli *et al.* proposed thioredoxin reductase as a target for gold compounds acting as potential anticancer drugs [81]. Other targets were proposed in recent times such as the proteasome [82,83], histone deacetylases [84,85], a few kinases [86,87], transcription factors containing zinc finger motifs, etc.

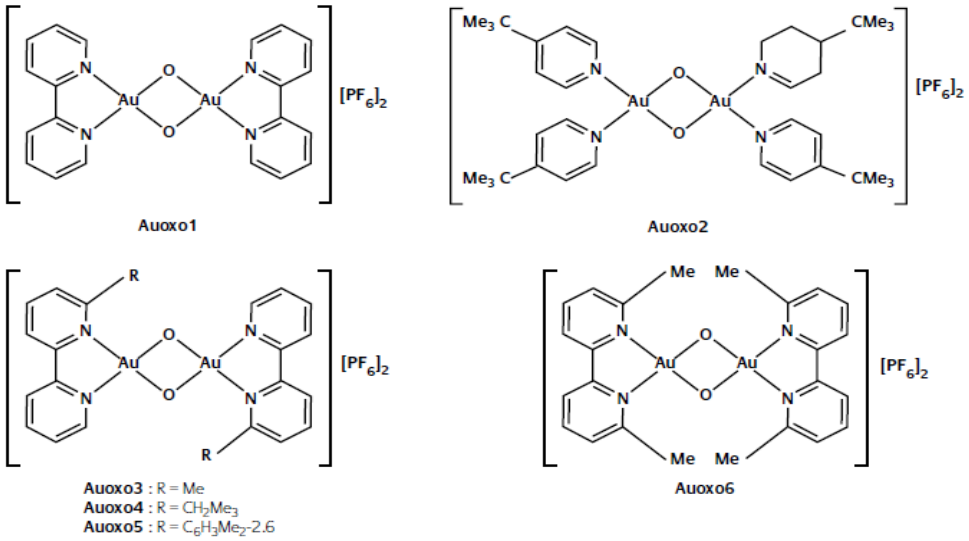

Figure 2.6 Schematic drawings of dinuclear gold(III) oxo complexes.

Figure 2.6 illustrates Auoxo type gold(III) complexes in which Auoxo3 is a ca. 1:1 mixture of the *cis* and *trans* isomer while Auoxo4 and Auoxo5 are, as depicted, only *trans* isomers.

It is now a quite accepted opinion that the remarkable cytotoxic effects documented for several gold compounds are mainly the consequence of metalation and inactivation of selected crucial proteins [88]. In contrast to the availability of such diverse anticancer agents as mentioned above, gastric and prostate cancer inhibiting gold(III) agents have rarely been explored.

Maiore *et al.* recently evaluated gold(III) derivatives of 2-substituted pyridines for their biological and pharmacological behavior [88]. Palanichamy *et al.* identified four gold(III) compounds, $[Au(Phen)Cl_2]PF_6$, and its derivatives, exhibiting anticancer activity in both cisplatin sensitive and cisplatin resistant ovarian cancer cells [89]. Gabbiani *et al.* described remarkable anticancer properties *in vitro* for Au(III)bipy, Auoxo6 and Au_2phen compounds [90]. Kouodom *et al.* suggested rational design of gold(III)-dithiocarbamato

peptidomimetics for the targeted anticancer chemotherapy [91]. Lessa *et al.* reported gold(I) and gold(III) complexes with glyoxaldehyde *bis*(thiosemicarbazones) as cytotoxic agents against human tumor cell lines and inhibition of thioredoxin reductase activity [92]. In this connection, an attractive strategy has astutely been designed to regulate the chemical and physical behavior of biologically pertinent tetra-coordinate gold(III) complexes. Such concept is executed by inclusion of appropriate bidentate ligands in the well-known gold(III) complexes having anticancer properties.

Intrigued by these observations and motivated by our continued search to better understand the chemical and physical behavior of biologically relevant tetracoordinate gold(III) complexes, the compounds, $[Au(en)_2]Cl_3$ and $[Au(N\text{-}pr\text{-}en)_2]Cl_3$ have been prepared, and subsequently characterized. Finally, their cytotoxicity has been tested *in vitro* in human gastric carcinoma SGC7901 cell line and prostate PC3 cancer cell lines. Other physicochemical studies like solution ^{13}C as well as solid ^{13}C, ^{15}N NMR and DFT calculation studies were also performed.

In this study, we tried to analyze the potential of $[Au(en)_2]Cl_3$ over its N-alkyl substituted analogue and to evaluate if it inhibits cancer cell proliferation or induction of slow growth of cancer cells. To the best of our knowledge, gold(III) diamine complexes and their derivatives have rarely been explored as anticancer agents against gastric, prostate and ovarian cancer cell lines.

With such frame of mind, we have recently reported $[Au(\textit{en})_2]Cl_3$ (**1**) and $[Au(N\text{-}pr\text{-}\textit{en})_2]Cl_3$ (**4**) complexes, demonstrating effective cytotoxicity against human gastric and prostate cancer cell lines [93–95]. $[Au(Dach)_2]Cl_3$ complexes have also been presented as

anticancer agents [96]. Such persuasive results triggered us to continue further studies on gold(III) complexes with various alkyldiamines ligands in order to investigate the effects of chelate ring size and basicity of amine-N of alkyldiamines ligands.

Hence, new gold(III) diamine complexes have been prepared and characterized by various analytical and spectroscopic techniques. Anticancer properties of a new series of Au(III) alkanediamine complexes, with general formulae of $[LAuCl_2]Cl$ and $[Au(L)_2]Cl_3$ [where L = ethylenediamine (*en),* propylenediamine (*pn),* butylenediamine (*bn)* and *N-alkyl* substituted ethylenediamine (*N-R-en*)], against a panel of cancer cell lines are reported here. The cytotoxic properties have been evaluated *in vitro* against human prostate PC3, gastric SGC7901 and ovarian A2780 / A2780 cis cancer cell lines. The effectiveness of these complexes (**1**-**10**) has been assessed in terms of IC_{50} on the SGC7901 and PC3 cancer lines, and compared to the commercially available cisplatin. The representative complexes (**1**) and (**8**) have also been studied as potential cytotoxic agents based on their IC_{50} data in the cisplatin-sensitive A2780 and cisplatin resistant A2780 cis ovarian cell lines.

Metal complexes of heterocyclic thiones have found great interest in recent research due to their potential medicinal applications [97–102]. Considerable work has been carried out on thione complexes with gold(I) [103]. On the other hand, very little is known about gold(III) complexes with thiones.

Heterocyclic thiones as ligands in metal complexes have attracted considerable attention because of their relevance to biological systems and the versatility in their coordination modes. These thiones are potentially ambidentate or multi-functional donors with either

the exocyclic S or heterocyclic N atoms available for coordination, thus yielding a variety of interesting complexes with geometries of variable nuclearity and great structural diversity [104].

Milavanovic *et al.* have evaluated *in vitro* the cytotoxic properties of $[Au(en)Cl_2]^+$ against chronic lymphocytic leukemia (CCL) cells and have shown comparable cytotoxicity profiles to cisplatin [105]. A. Casini *et al.* (2008) have studied the anti cancer activities in a series of $[Au(en)_2]Cl_3$ type complexes. They reported that $[Au(en)_2]Cl_3$ showed similar activities compared to cisplatin [106].

Our research group has recently reported that the $[Au(en)Cl_2]Cl$ complex causes minimal histological changes in kidney and liver of rats, reflecting its relative safety as compared to other clinically established anti-neoplastic drugs [95]. Likewise, we have reported $[Au(en)_2]Cl_3$ as a promising candidate as an anticancer agent [93]. For that reason, $[Au(en)_2]Cl_3$ might be a promising chemo-preventative and chemo-therapeutic agent against human gastric carcinogenesis.

Such optimistic literature reports on Au(III) complexes prompted us to carry out the synthesis of a number of mixed-ligand complexes $[Au(\textit{diamine})Cl_2]^+$ with thiones such as Imt, Diaz and Diap. Accordingly, we have synthesized mixed ligand gold(III) complexes by using different diamines and thiones. These complexes have been characterized by CHNS analysis, Solid state IR and solid as well as solution NMR spectroscopic methods. Finally, the prepared Au(III)-thione complexes have also been evaluated *in vitro* as cytotoxic agents against C6 glioma cancer cell line.

CHAPTER 3

OBJECTIVES

The aim of this research is to synthesize new gold(III) complexes as potential anticancer agents. The main goals of the research work are as follows:

3.1 Synthesis of Gold(III) Complexes

3.1.1 Synthesis of Gold(III) Complexes of Diamines

The un-substituted and mono/dialkylsubstituted diamines as chelating bidentate ligands as shown in Figure 3.1 were used to synthesize the following gold(III) four coordinated complexes:

i. $[Au(\textit{diamine})_2]Cl_3$

where diamine = 1,2-Diaminoethane(en) or 1,3-Diaminopropane(pn)

ii. $[Au(\textit{N-alkyl-1,2-diaminoethane})_2]Cl_3$

where alkyl =Me, Et, *n*-Pr, *iso*-Pr

iii. $[Au(\textit{N,N´-dialkyl-1,2-diaminoethane})_2]Cl_3$

where alkyl =Me, Et, *n*-Pr, *iso*-Pr

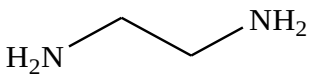

1,2-Diaminoethane(en)

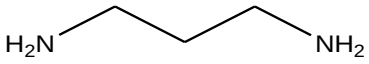

1,3-Diaminopropane(pn)

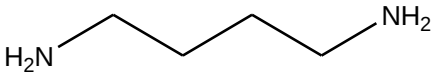

1,4-Diaminobutane(bn)

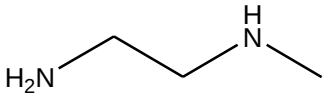

N-Methyl-1,2-diaminoethane (N-Me-en)

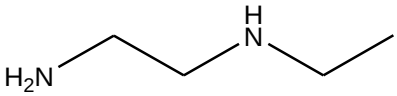

N-Ethyl-1,2-diaminoethane (N-Et-en)

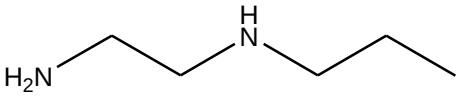

N-*n*-Propyl-1,2-diaminoethane (N-*n*-Pr-en)

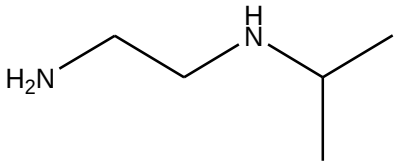

N-*iso*-Propyl-1,2-diaminoethane (N-*iso*-Pr-en)

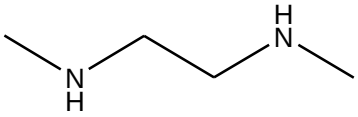

N,N´-di-Methyl-1,2-diaminoethane (N,N´-di-Me-en)

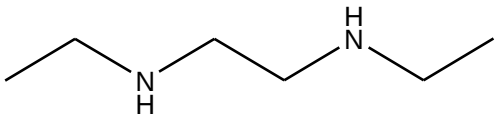

N,N´-di-Ethyl-1,2-diaminoethane (N,N´-di-Et-en)

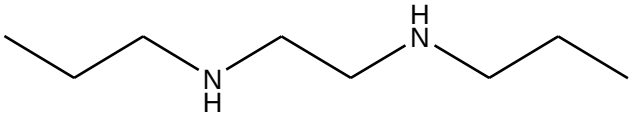

N,N´-di-*n*-Propyl-1,2-diaminoethane (N,N´-di-*n*-Pr-en)

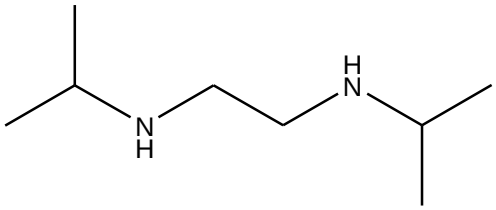

N,N´-di-*iso*-Propyl-1,2-diaminoethane (N,N´-di-*iso*-Pr-en)

Figure 3.1 Structures of diamine ligands used in this study

3.1.2 Synthesis of Gold(III) Complexes of Thione and Diamine Ligands

The un-substitued diamine and thione ligands were used to synthesize the following gold(III) complexes:

i. [*(thione)*$_2$Au*(en)*]Cl_3

ii. [*(thione)*$_2$Au*(pn)*]Cl_3

iii. [*(thione)*$_2$Au*(bn)*]Cl_3

where *en* =1,2-diaminoethane (ethylenediamine), *pn* =1,3-diaminopropane (propylenediamine), *bn*= 1,4-diaminobutane (butylenediamine) and thione= 1,2-imidazolidine-2-thione (Imt) or 1,3-Diazinane-2-thione (Diaz) or 1,4-Diazipane-2-thione (Diap) as shown in Figure 3.2

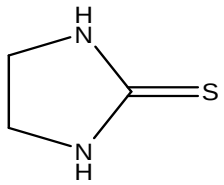

Imidazolidine-2-thione

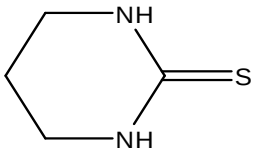

1,3-Diazinane-2-thione

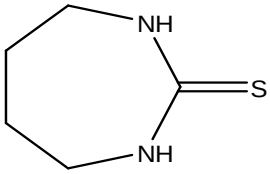

1,3-Diazepane-2-thione

Figure 3.2 Structures of thione ligands used in this study

3.2 Characterization of Gold(III) Complexes

The complexes 3.1.1 (i, ii and iii) and 3.1.2 (i, ii and iii) were characterized by melting point (MP) and elemental analysis (EA) techniques.

3.3 Structural Analysis of Gold(III) Complexes

The complexes were then structurally analyzed by Mid Infrared (MIR), Far Infrared (FIR) and Ultra-Violet (UV)/Visible (Vis) spectroscopic methods; ^{1}H, ^{13}C, ^{15}N solution and ^{13}C, ^{15}N solid state Nuclear Magnetic Resonance (NMR) measurements. X-ray crystallography was employed for structure determination of crystalline complexes.

3.4 Study of Anticancer Properties of Gold(III) Complexes

The anticancer properties of gold complexes werer studied *in-vitro* against a panel of human cancer cell lines in order to evaluate their potential as possible anticancer agents.

CHAPTER 4

EXPERIMENTAL

4.1 Chemicals

$HAuCl_4 \cdot 3H_2O$ was obtained from Strem Chemicals Co., while acetone, absolute ethanol, acetonitrile, D_2O and CD_3OD were obtained from Fluka Chemicals Co. 1,2-Diaminoethane, 1,3-Diaminopropane, 1,4-Diaminobutane, N-ethyl-1,2-diaminoethane, N-propyl-1,2-diaminoethane and N-isopropyl-1,2-diaminoethane were purchased from Sigma Aldrich. N, N′-dimethyl-1,2-diaminoethane, N, N′-diethyl-1,2-diaminoethane, N, N′-dipropyl-1,2-diaminoethane and N, N′-diisopropyl-1,2-diaminoethane were obtained from Alfa Aesar.

Imidazole, L-histidine and L-glycine were obtained from Sigma-Aldrich, L-^{13}C3-cysteine, L- methionine were obtained from Isotech, USA. Sodium tetrachloroaurate (III) dihydrate, Imidazolidine-2-thione (Imt), 1,3-Diazinane-2-thione (Diaz), 1,3-Diazipane-2-thione (Diap), Imidazole, were purchased from Sigma-Aldrich.

Potassium cyanide was purchased from Fisher Scientific Co. Potassium thiocynate was obtained from J. T. Baker Chemicals Co. The ^{15}N label diamines ligands and ^{15}N and ^{13}C label potassium cyanide were obtained from Cambridge Isotope Labs, USA. All other reagents as well as solvents were obtained from Aldrich Chemical Co., and used as received.

4.2 Cell lines

Human gastric SGC7901 and prostate PC3 cancer cell lines were provided by American Type Culture Collection (ATCC). Cells were cultured in Dulbecco's Modified Eagle Medium (DMEM) supplemented with 10 % Fetal Calf Serum (FCS), penicillin (100 kU L^{-1}) and streptomycin (0.1 g L^{-1}) at 37 ºC in a 5 % CO_2 -95 % air atmosphere. MTT (3-(4,5-Dimethylthiazol-2-yl)-2,5-diphenyltetrazolium bromide, a yellow tetrazole) was purchased from Sigma Chemical Co, St.Louis, MO, USA.

Human cisplatin sensitive A2780 and cisplatin resistant A2780 cis ovarian carcinoma cell lines were provided by the European Centre of Cell Culture (ECACC) Salisbury, UK. Cell culture reagents were purchased from Gibco-BRL, Basel, Switzerland. Glioma C6 cancer cell line was obtained from ATCC, Georgetown University, Washington DC, USA.

4.3 Synthesis of Gold(III) Complexes

All reactions were generally carried out under an atmosphere of nitrogen using research grade chemicals and solvents. All complexes were subsequently characterized by melting point (MP) and elemental analysis (EA) techniques. Elemental analyses were performed on Perkin Elmer Series 11 (CHNS/O), Analyzer 2400. Melting points for complexes were carried out on BÜCHI 510 melting point apparatus.

4.3.1 Synthesis of Gold(III) Diamine Complexes

Gold complexes of ethylenediamine $[Au(en)_2]Cl_3$ and N-substituted ethylenediamine $[Au(N\text{-}Pr\text{-}en)]Cl_3$ were prepared according to the reported procedures [71] and the purity

of these compounds was checked by elemental analysis. The procedure of synthesis is described here for $[Au(pn)_2]Cl_3$ complex. $HAuCl_4 \cdot 3H_2O$ (0.20 g, 0.50 mmol) was dissolved in 5 mL of deionized H_2O. 1.0 mL of ca. 1.0 mmol aqueous solution of 1,3-diaminopropane was added to this solution. An orange precipitate was formed after stirring for 3 hr. The precipitate was removed by filtration. The filtrate was kept in hood for crystallization after addition of 20 mL of ethanol. The very pale yellow precipitate, which formed immediately, was filtered off and air-dried [93–95]. Similar procedures were followed for the reported complexes **(1-7)** shown in Figure 4.1 as explained in Schemes I, II and III. Products were characterized by melting point (M.P.) and elemental analysis (EA) as given in Table 4.1.

Using un-substituted diamines

$$HAuCl_4 \cdot 3H_2O + 2\ en \rightarrow [Au(en)_2]Cl_3 + HCl$$

$$HAuCl_4 \cdot 3H_2O + 2\ pn \rightarrow [Au(pn)_2]Cl_3 + HCl$$

Scheme I

Using substituted monoalkyl diamines

$$HAuCl_4 \cdot 3H_2O + 2\ N\text{-}R\text{-}en \rightarrow [Au(N\text{-}R\text{-}en)_2]Cl_3 + HCl$$

where R= Me, Et, *n*Pr and *i*Pr

Scheme II

Using substituted dialkyl diamines

$$HAuCl_4 \cdot 3H_2O + 2\ N,N'\text{-}R_2\text{-}en \rightarrow [Au(N,N'\text{-}R_2\text{-}en)_2]Cl_3 + HCl$$

where R= Me, Et, *n*Pr and *i*Pr

Scheme III

4.3.1.1 Preparation of $[Au(pn)_2]Cl_3$ complex

$HAuCl_4 \cdot 3H_2O$ (0.20 g, 0.50 mmol) was dissolved in 5 mL of deionized H_2O. 1.0 mL of a 1.0 M aqueous solution of 1,3-diaminopropane (*pn*) was added to it. An orange precipitate formed, which was collected by filtration. 30 mL of ethanol was added to the filtrate. The very pale yellow precipitate was immediately formed. The precipitate was filtered off and air-dried [93–95].

4.3.1.2 Synthesis of Crystalline Gold(III) Diamine Complex

The suitable quality crystals for X-ray analysis were obtained by dissolving both $HAuCl_4 \cdot 3H_2O$ (0.21 g, 0.53 mmol) and *pn* (0.08 g, 1.08 mmol) in minimum volume of methanol. Both solutions were mixed and stirred for 2 hr. The yellow precipitate formed was separated by filtration. The filtrate was kept in the hood under the dark for the crystallization. After one week, light yellow crystals of $[Au_2(pn)_2Cl_2]Cl_2 \cdot H_2O$ complex were obtained. The crystalline product was characterized by melting point and elemental analysis (Table 4.1).

Table 4.1 Elemental analysis of Au(III) diamine complexes

Complex	M. P. (ºC)	Found (Calculated) %		
		%C	%H	%N
$[Au(en)_2]Cl_3$ (**1**)	296	11.95(11.34)	4.14(3.81)	13.56(13.28)
$[Au(pn)_2]Cl_3$ (**2**)	227-228	16.26(15.35)	4.94(4.72)	12.28(11.93)
$[Au_2(pn)_2Cl_2]Cl_2 \bullet H_2O$ (**2a**)	235-237	10.37(10.29)	2.95(2.88)	7.89(8.00)
$[Au(N\text{-}Pr\text{-}en)_2]Cl_3$ (**4**)	139-141	23.41(23.68)	6.20(5.48)	11.30(11.04)
$[Au(N\text{-}i\text{Pr}\text{-}en)_2]Cl_3$ (**5**)	107-109	24.54(23.66)	6.05(5.56)	11.38(11.04)
$[Au(N,N'\text{-}Et_2\text{-}en)_2]\,Cl_3$ (**6**)	210	28.68(26.90)	7.70(6.02)	11.43(10.46)
$[Au(N,N'\text{-}i\text{Pr}_2\text{-}en\,)_2]Cl_3$ (**7**)	239	32.37(32.47)	7.66(6.81)	9.55(9.47)

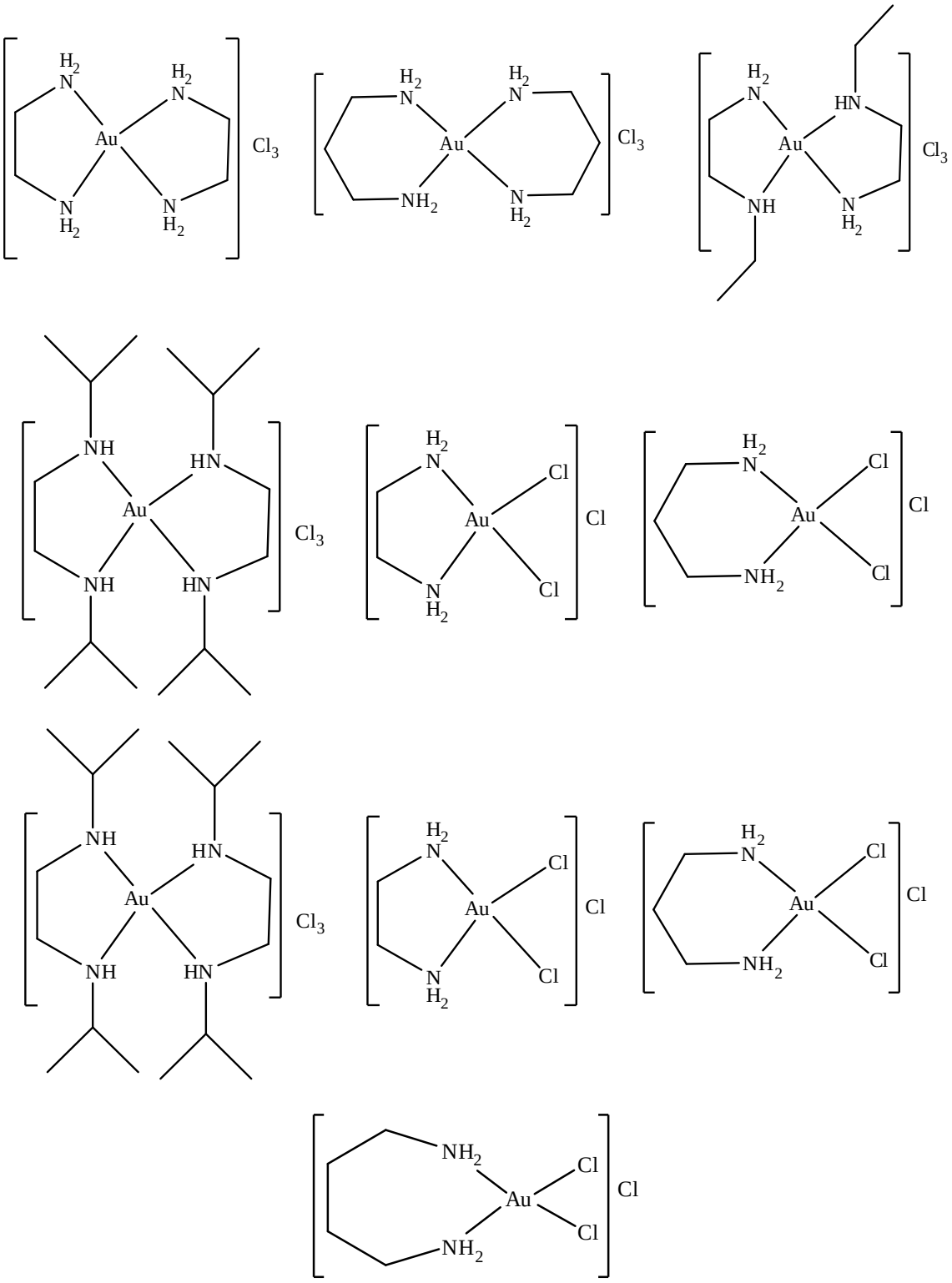

Figure 4.1 Possible structures of gold(III) diamine complexes

4.3.2 Synthesis of Gold(III) Diamine and Thione Complexes

Imidazolidine-2-thione (Imt), 1,3-Diazinane-2-thione (Diaz), 1,3-Diazipane-2-thione (Diap) were prepared according to the published procedure [98]. Firstly, [(diamine)$AuCl_2$]Cl complexes were prepared according to the literature [94]. Later, [(diamine)Au(thione)$_2$]Cl were synthesized as follows: 0.6 mmol of [(diamine)$AuCl_2$]Cl was dissolved in 20 mL distilled H_2O (solution 1). 1.2 mmol of thione was dissolved in 40 mL methanol (solution 2). Both solutions were mixed in a round bottom flask and refluxed at 60 ^oC for 2 hr. The resulting solution was filtered, concentrated and allowed to precipitate. The resulted precipitate was dried and the filtrate is kept in the refrigerator for crystallization. Products were characterized by melting point and elemental analysis (Table 4.2). Possible structures of gold(III) thione complexes are shown in Figure 4.2.

Using Diamine and Imidazolidine-2-thione (Imt)

$HAuCl_4 \cdot 3H_2O$ + diamine + 2 Imt → [(*diamine*)Au(Imt)$_2$]Cl_3 + HCl

where diamine= *en*, *pn* and *bn*

Scheme 1V

Using Diamine and 1,3-Diazinane-2-thione (Diaz)

$HAuCl_4 \cdot 3H_2O$ + diamine + 2 Diaz → [(*diamine*)Au(Diaz)$_2$]Cl_3 + HCl

where diamine= *en*, *pn* and *bn*

Scheme V

Using Diamine and 1,4-Diazipine-2-thione (Diap)

$HAuCl_4 \cdot 3H_2O$ + diamine + 2 Diap → [(*diamine*)Au(Diap)$_2$]Cl_3 + HCl

where diamine= *en*, *pn* and *bn*

Scheme VI

Table 4.2 Elemental analysis of Au(III) thione complexes

Complex	M.P. (^oC)	Found (Calculated)			
		%C	%H	%N	%S
$[(Imt)_2Au(en)]Cl_3$ (**11**)	201	17.19(16.92)	3.73(3.55)	14.77(14.80)	11.19(11.30)
$[(Imt)_2Au(pn)]Cl_3$ (**12**)	218	18.88(18.58)	4.05(3.81)	15.00(14.45)	11.04(11.02)
$[(Imt)_2Au(bn)]Cl_3$(**13**)	172	20.30(20.16)	4.20(4.06)	14.19(14.11)	9.99(10.76)
$[(Diaz)_2Au(en)]Cl_3$(**14**)	240	21.04(20.16)	4.28(4.06)	14.30(14.11)	9.91(10.76)
$[(Diaz)_2Au(pn)]Cl_3$(**15**)	212	24.43(24.59)	5.06(5.31)	15.59(15.55)	10.00(9.38)
$[(Diaz)_2Au(bn)]Cl_3$ (**16**)	269	23.18(23.31)	4.72(4.52)	13.50(13.47)	9.95(10.28)
$[(Diap)_2Au(en)]Cl_3$(**17**)	203	24.49(24.59)	5.13(5.31)	15.41(15.55)	9.74(9.38)
$[(Diap)_2Au(pn)]Cl_3$(**18**)	237	23.37(23.31)	4.67(4.52)	13.54(13.47)	10.01(10.28)

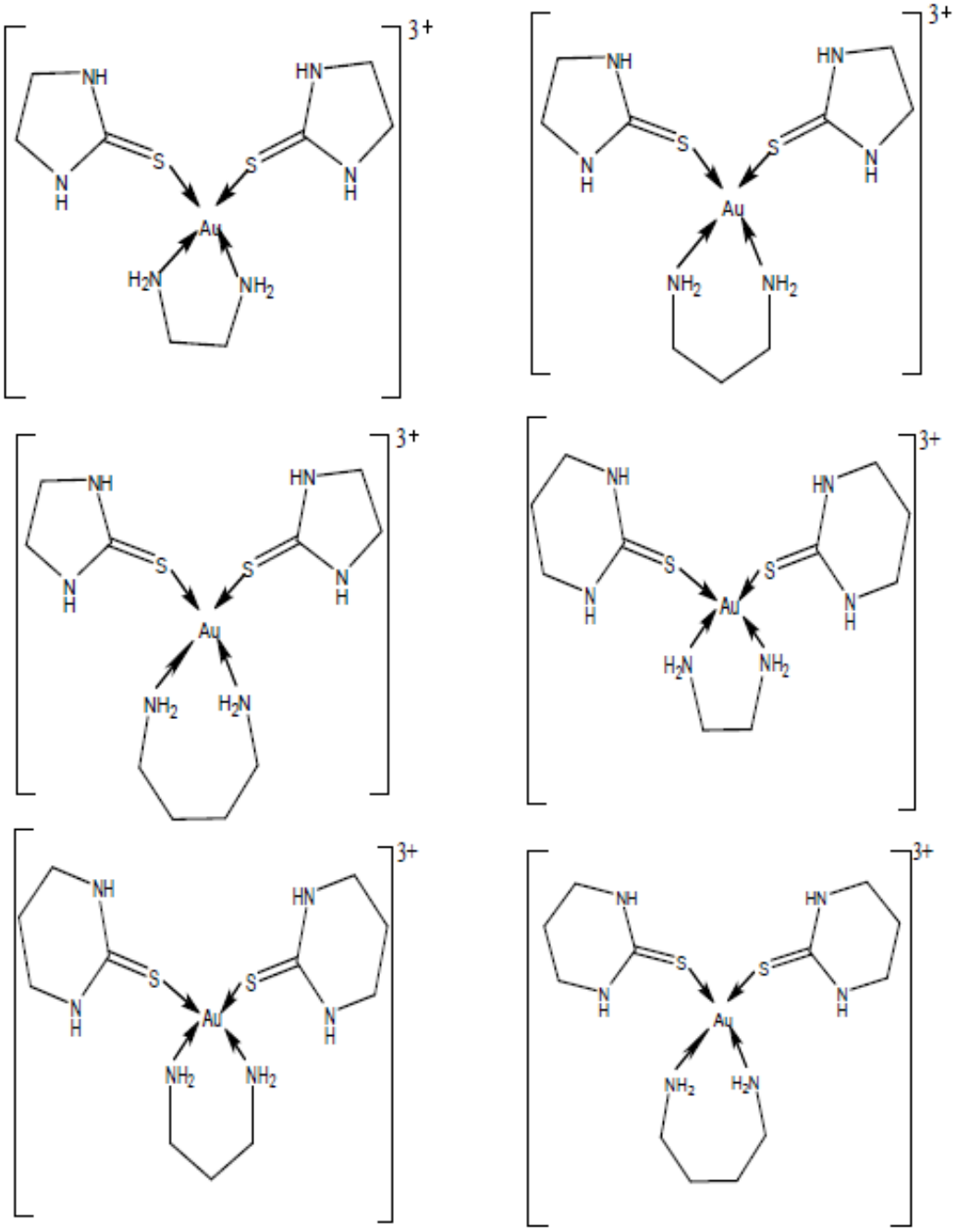

Figure 4.2 Possible structures of gold(III) thione complexes

4.3.3 Synthesis of Cyanido(diamine)Hg(II) complexes

The mercury (II) complexes of diamines were prepared by mixing the solutions of selected diamine (3.5 mmol) and $Hg(CN)_2$ (3.0 mmol) in methanol and refluxing for about 4 hr as given in Schemes VII, VIII and IX. The res ulting colorless solution was filtered and kept in the refrigerator for crystallization. The products were obtained in good yields. They were characterized by melting point and elemental analysis (Table 4.3). Possible structures of cyanido(diamine)Hg(II) complexes are shown in Figure 4.3.

Using un-substituted diamines

$Hg(CN)_2$+ en → [(*en)* $Hg(CN)_2$]

$Hg(CN)_2$+ pn → [(*pn)* $Hg(CN)_2$]

Scheme VII

Using monoalkylsubstituted diamines

$Hg(CN)_2$+ N-Me-en → [(N-R-*en)* $Hg(CN)_2$]

Scheme VIII

Using dialkylsubstituted diamines

$Hg(CN)_2$+ N-N′-diR-en → [(N-N′-diR-*en)* $Hg(CN)_2$]

where R=Me, Et, *i*Pr

Scheme IX

Table 4.3 Elemental analysis of Hg(II)$(CN)_2$-diamine complexes

Complex	M.P. (°C)	Found (Calculated)		
		%C	%H	%N
[(*en*)Hg$(CN)_2$] (**19**)	105	15.54(15.36)	2.78(2.58)	17.79(17.92)
[(*pn*)Hg$(CN)_2$] (**20**)	130	18.93(18.38)	3.23(3.08)	17.27(17.15)
[(N-Me-*en*)Hg$(CN)_2$] (**21**)	75-76	17.97(18.38)	3.38(3.08)	17.13(17.15)
[(N, N′-Me-*en*)Hg$(CN)_2$] (**22**)	60-61	20.84(21.15)	3.33(3.55)	16.62(16.44)
[(N, N′-Et-*en*)Hg$(CN)_2$] (**23**)	95-96	26.34(26.19)	3.44(3.85)	14.98(15.27)
[(N, N′-*i*Pr-*en*)Hg$(CN)_2$] (**24**)	50-52	29.99(30.42)	4.39(4.59)	14.29(14.19)

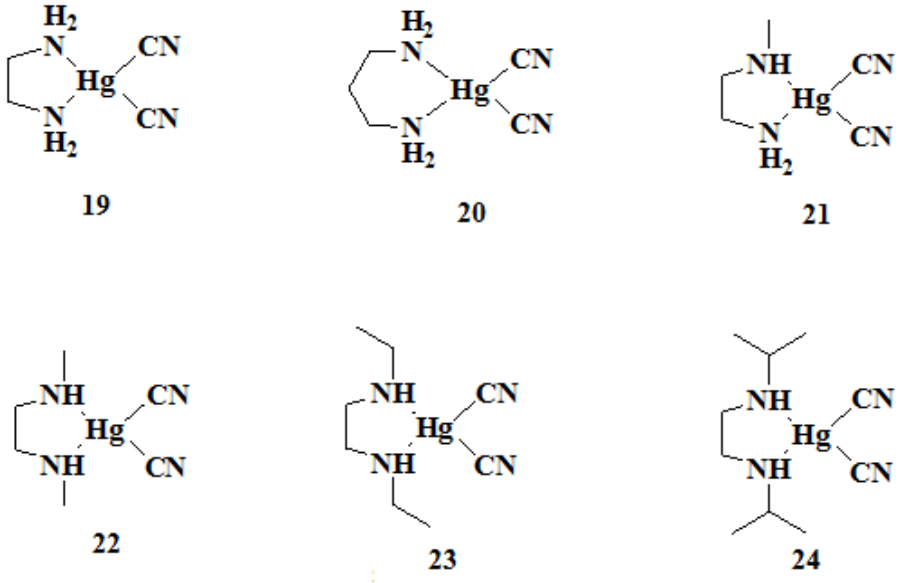

Figure 4.3 Possible structures of Cyanido(diamine)Hg(II) complexes

4.3.4 Synthesis of Cadmium(II) and Mercury(II) Selenocyanate Complexes

A solution of $CdCl_2$ in 10.0 mL distilled water was mixed with equivalent stoichiometric amount of ligand (Histidine or Glycine) in 10.0 mL methanol-water mixture in 1:1 volume ratio. The resulting solution stirred for 30 min, then two equivalents of KSeCN in water was added. The resulting mixture was refluxed with stirring under nitrogen gas for 15 min then heated for ~ 1.5 hr at 70 ^{o}C. The product was filtered, washed and dried. A similar procedure was applied for mercury complexes using $HgCl_2$ instead of $CdCl_2$ as shown in Schemes X and XI. The products were characterized by melting point and elemental analysis (Table 4.4). Possible structures of Cadmium(II) and Mercury(II) selenocyanate complexes are shown in Figure 4.4.

Using Glycine (Gly) and KSeCN as ligands

$$MCl_2 + Gly + 2\ KSeCN \rightarrow [(Gly)M(SeCN)_2]$$

where M(II)=Cd(II) or Hg(II)

Scheme X

Using Histidine (His) and KSeCN as ligands

$$MCl_2 + His + 2\ KSeCN \rightarrow [(His)M(SeCN)_2]$$

where M(II)=Cd(II) or Hg(II)

Scheme XI

Table 4.4 Elemental analysis of Cd(II) and Hg(II) selenocyanate complexes

Complex	M. P. (℃)	Found (Calculated)		
		%C	%H	%N
[(Gly)Cd(SeCN)$_2$] (**25**)	D.P. at 184	1.32 (1.27)	12.15 (12.09)	10.78 (10.57)
[(His)Cd(SeCN)$_2$] (**26**)	D.P. > 205	2.00 (1.90)	20.44 (20.12)	14.88 (14.67)
[(Gly)Hg(SeCN)$_2$] (**27**)	>300	1.10 (1.04)	10.04 (9.89)	9.00 (8.65)
[(His)Hg(SeCN)$_2$] (**28**)	D.P. >140	1.70 (1.60)	17.11 (16.99)	12.64 (12.38)

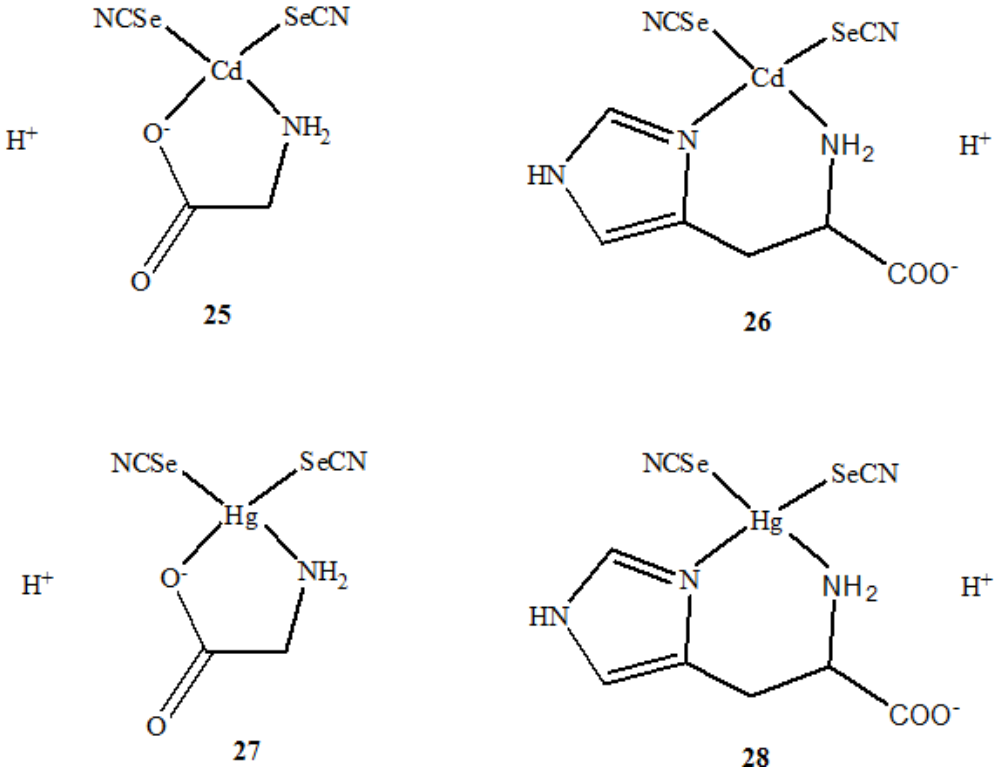

Figure 4.4 Possible structures for M(II)) selencyante of Gly and His complexes

4.4 Spectroscopic Characterization

4.4.1 Elemental Analysis

Elemental analysis (EA) and melting points (M.P.) of gold(III) complexes were performed on Perkin Elmer Series 11 (CHNS/O), Analyzer 2400 and BŪCHI 510 melting point apparatus respectively. The melting points and CHN/CHNS results of metal complexes are given in Tables 4.1, 4.2, 4.3 and 4.4**.**

4.4.2 Mid-IR and Far-IR studies

The solid state Mid-IR spectra of the ligands and their gold(III) complexes were performed on a Perkin–Elmer FTIR 180 spectrophotometer or NICOLET 6700 FTIR using KBr pellets over the range 4000–400 cm^{-1} and solid state Far-IR spectra were recorded for complexes at 4 cm^{-1} resolution at room temperature using CsCl disks on a Nicolet 6700 FT-IR with Far-IR beam splitter.

4.4.3 UV-Vis Studies

Lambda 200, Perkin-Elmer UV-Vis spectrometer was employed for recording and monitoring the electronic spectra. All electronic spectral data obtained for the gold (III) complexes were given in tabulated form.

4.4.4 Solution state NMR measurements

The solution ^{1}H and ^{13}C NMR experiments were performed on Jeol 500 MHz NMR Spectrometer at 297 K using ca. 0.10 M solution of the complexes in the deuterated

solvents (D_2O, DMSO, $CDCl_3$ and CD_3OD. etc.). The ^1H NMR spectra were obtained on a Jeol 500 MHz NMR spectrometer operating at a frequency of 500 MHz. ^{13}C NMR spectra were obtained at 125.65 MHz with ^1H broadband decoupling at 297K. The spectral conditions were: 32k data points, 0.967s acquisition time, 1.00 s pulse delay and 45^o pulse angle. ^1H and ^{13}C NMR Chemical shifts (δ) values were referenced to tetramethylsilane (TMS).

^{15}N NMR spectra were obtained on Jeol 500 MHz Spectrometer operating at frequency 50.55 MHz with ^1H broadband decoupling at 297K. The spectral conditions were: 32k data points, 0.128 s acquisition time, 2.00 s pulse delay and 45^o pulse angle. ^{15}N NMR chemical shifts (δ) values were referenced to -342.68 ppm of enriched $^{15}NH_4NO_3$ in D_2O solvent.

4.4.5 Solid state NMR measurements

Solid state NMR showed more sensitivity to coordination geometry rather than solution NMR, which is expected from the removal of the solvent effects, fluxional processes and other averaging processes that may be present in the solution state. It has the added advantage that it provides the three principal components of the shielding tensor, rather than just the average value observed in solution spectra. These components can be calculated from the intensities of the spinning side bands in the Solid state spectra. Under the conditions of magic-angle spinning (MAS), the isotropic chemical shift δ_I, given by Equation 1, is equivalent to the chemical shift observed in solution

$$\delta \mathbf{I} = \mathbf{1/3}\,(\delta\,\mathbf{11} + \delta\mathbf{22} + \delta\mathbf{33}) \quad \textbf{(Equation 1)}$$

For a nonsymmetrical environment, with $\delta_{11} < \delta_{22} < \delta_{33}$, the chemical shift anisotropy ($\Delta\delta$) is defined as

$$\Delta\delta = \delta 33 - \tfrac{1}{2}(\delta 11 + \delta 22) \quad \textbf{(Equation 2)}$$

For a symmetric tensor, where $\delta_{11} = \delta_{22} = \delta\perp$, then $\delta_{33} = \delta_{//}$; for $\delta_{33} = \delta_{22} = \delta\perp$, then $\delta_{11} = \delta_{//}$. For these cases the shift anisotropy is defined as

$$\Delta\delta = \delta// - \delta\perp \quad \textbf{(Equation 3)}$$

Unlike solution chemical shifts, solid state NMR results can be correlated directly with crystallographic structure determinations when available, and structural predictions can be made in the absence of crystallographic data.

Solid state ^{13}C NMR measurement

The $^{13}C\{^{1}H\}$ solid state NMR spectra were obtained on a JEOL LAMBDA 500 spectrometer operating at 125.65 MHz, corresponding to magnetic strength of 11.74 T. Samples were packed into 6 mm zirconium oxide rotors at ambient temperature of 278 K. Cross-polarization and high power decoupling were employed. Pulse delay of 7.0 s and a contact time of 5.0 ms were used in the CPMAS experiments. The magic angle spinning rates were from 2 kHz to 4 kHz. Carbon chemical shifts were referenced to TMS by setting the high frequency isotropic peak of solid adamantane to 38.56 ppm [107].

Solid state ^{15}N NMR measurement

Natural abundance ^{15}N spectra were also recorded on a JEOL LAMBDA 500 spectrometer, using a contact time of 5 ms and a pulse delay of 10 s. Samples were packed into 6 mm zirconium oxide rotors at ambient temperature of 278 K. Cross-polarization and high power decoupling were employed. The magic angle spinning rates were between 2 kHz to 4 kHz. All ^{15}N spectra were referenced to $^{15}NH_4NO_3$ peak (δ_{iso}) =

-358.63 ppm relative to CH_3NO_2, (δ_{iso}) = 0 ppm [108]. The ^{15}N chemical shifts were referenced to an external enriched solid $^{15}NH_4Cl$ sample to 40.73 ppm [108] and converted to the standard CH_3NO_2 by a chemical shift of -380.0 ppm for NH_3 [107]. The center peaks were differentiated from the spinning side-bands by recording the spectra at two different spinning speeds.

Both the ^{15}N spectra and ^{13}C spectra, containing spinning side-band manifolds, were analyzed using a program HBA[109] based on Maricq and Waugh [110] which were developed at Dalhousie University, Canada, and University of Tübingen, Germany.

Solid state ^{199}Hg NMR measurement

Solid state cross-polarization magic-angle spinning (CPMAS) $^{199}Hg\{^1H\}$ NMR spectra were obtained at ambient temperature of 298 K on the same spectrometer operating at a frequency of 89.30 MHz. Contact times of 20 ms were used with a proton pulse width of 6 μs, with a recycle delay of 10 s. Approximately 5000 FID (free induction decays) were collected and transformed with a line broadening of 100 Hz. Chemical shifts were referenced using an external sample of solid $[Hg(DMSO)_6](O_3SCF_3)_2$ with chemical shift δ_{Hg} = -2313 ppm from $Hg(CH_3)_2$ [111].

4.5 X-ray structure determination

The crystal structure determination was carried out on Bruker Single Crystal X-ray Diffractometer. For crystalline gold(III) complexes, X-ray quality single crystals were mounted in a thin-walled glass capillary on a Bruker-Axs Smart Apex diffractometer equipped with graphite monochromatized Mo Kα radiation (λ = 0.71073 Å). The data were collected using SMART software [112]. The data integration was performed using SAINT [113]. An empirical absorption correction was carried out using SADABS [114]. The structure was solved with direct methods and refined by full matrix least square methods based on $\mathbf{F}^2$, using the structure determination package SHELXTL [115] based on SHELX 97 [116]. Graphics were generated using ORTEP-3 [117] and MERCURY [118]. For complex $[Au_2(pn)_2Cl_2]Cl_2.H_2O$ **]**, both of the hydrogen atoms of the disordered water molecule could not be placed reliably. All other H atoms were placed a calculated positions using a riding model. Crystallographic data, experimental and structure refinement details of complex **(2a)** are presented in Table 4.5.

Table 4.5 Crystallographic data and experimental details of crystal structure of (2a)

Parameters	Values
Molecular formula	$C_6H_{18}Au_2Cl_2N_4 \cdot 2(Cl) \cdot H_2O$
Formula weight	699.99
Crystal size/mm	0.40 × 0.33 × 0.27
Wavelength/Å	0.71073
Temperature/K	295 (2)
Crystal symmetry	Monoclinic
Space group	*C*2/*c*
a/Å	28.864 (3)
b/Å	8.4074 (7)
c/Å	13.0740 (12)
α/°	90
β/°	91.377 (3)
γ/°	90
V/ $Å^3$	3171.8 (5)
Z	8
D_c/Mg m^{-3}	2.932
μ(Mo-Kα)/mm^{-1}	19.15
F(000)	2544
θ Limits/°	2.5–28.3
Collected reflections	9266
Unique reflections(R_{int})	2266
Observed reflections[$F_o > 2\sigma(F_o)$]	2774
Goodness of fit on F^2	1.06
R_1(F), [I> 2σ (I)]	0.054
wR_2 (F^2), [I> 2σ(I)]	0.129
Largest diff.peak, hole/e $Å^{-3}$	2.86

4.6 Computational study

The structures of some complexes were built and optimized using GAUSSIAN 09 Revision A.1 program package [119] and GAUSSIAN 03, Revision B.04 program package [120] at DFT/B3LYP level with LANL2DZ (Los Alamos ECP plus double-zeta) basis set [121,122]. Geometry optimization for the built structures was also carried out using the same software program.

4.7 Anticancer properties

Human gastric cancer SGC7901 cells and prostate cancer cells PC3 were incubated. Trypan blue dye exclusion analysis and MTT assay were used to detect cell proliferation and assess the inhibitory effect of gold (III) complexes on the proliferation of SGC7901 and PC3 cells. In one culture plate, human gastric cancer SGC7901 and PC3 cells were treated with the gold(III) complex and the control (water) and in the second plate, only the $[Au(en)_2]Cl_3$ and SGC7901 cells were kept in these two sets for an entire day (24 h) and for 3 days (72 h). In other sets, compounds **1** and **4** with fixed concentration were employed to determine the growth inhibitory effect for both PC3 and SGC7901 cells. After being treated with compounds **1** and **4**, cell viability was examined by MTT assay.

4.7.1 Assessment of cell proliferation

MTT assay was used to obtain the number of living cells in the sample. SGC7901 and PC3 cells were seeded on 96-well plates at a predetermined optimal cell density to ensure exponential growth in the duration of the assay. After 24 h pre-incubation, growth medium was replaced with experimental medium containing the appropriate drug or

control. Six duplicate wells were set up for each sample, and cells untreated with drug served as control. Treatment was conducted at 24 h and 72 h sequentially. After incubation, 10 μL MTT (6 g/L, Sigma) was added to each well and the incubation was continued for 4 h at 37 °C. After removal of the medium, MTT stabilization solution (dimethylsulfoxide: ethanol = 1:1) was added to each well, and shaken for 10 min until all crystals were dissolved. Then, optical density was detected in a micro plate reader at 550 nm wavelength using an ELISA reader. Each assay was performed in triplicate. Cell number and viability were determined by trypan blue dye exclusion analysis.

4.7.2 *in vitro* Cytotoxic assay for cisplatin sensitive prostate (PC3) and cisplatin resistance gastric (SGC7901) cells

MTT assay was used to obtain the number of living cells in the sample. SGC7901 and PC3 cells were seeded on 96-well plates at a predetermined optimal cell density to ensure exponential growth in the duration of the assay. After 24 h pre incubation, growth medium was replaced with experimental medium containing the appropriate drug or control. Six duplicate wells were set up for each sample, and cells untreated with drug served as control. Treatment was conducted at 24, and 72 h respectively. After incubation, 10 μL MTT (6 g/L, Sigma) was added to each well and the incubation was continued for 4 h at 37 °C. After removal of the medium, MTT stabilization solution (dimethylsulfoxide: ethanol = 1:1) was added to each well, and shaken for 10 min until all crystals were dissolved. Then, optical density was detected in a micro plate reader at 550 nm wavelength using an ELISA reader. Each assay was performed in triplicate. Cell number and viability were determined by trypan blue dye exclusion analysis.

Prostate PC3 and Human gastric SGC7901 cells were used in this study. Cells were cultured in Dulbecco's Modified Eagle Medium (DMEM) supplemented with 10 % fetal calf serum (FCS), penicillin (100 kU L^{-1}) and streptomycin (0.1 g L^{-1}) at 37 ºC in a 5 % CO_2 -95 % air atmosphere. Human gastric SGC7901 cells, prostate PC3 were incubated with these compounds at fixed concentrations or with water as control to assess the inhibitory effect on cell proliferation. The standard MTT assay has been used to assess inhibitory effect on cells growth. The cell survival versus drug concentration is plotted. Cytotoxicity was evaluated with reference to the IC_{50} value. The half maximal inhibitory concentration (IC_{50}) is a measure of the effectiveness of a compound in inhibiting biological or biochemical function. According to the FDA, IC_{50} represents the concentration of a drug or compound or complex that is required for 50 % inhibition *in vitro*. It is evaluated from the survival curves as the concentration needed for a 50 % reduction of survival. IC_{50} values are expressed in μM [123]. IC_{50} values were calculated from dose-response curves obtained in replicate experiments.

4.7.3 *in vitro* Cytotoxic assay for cisplatin sensitive (A2780) and cisplatin resistance (A2780 cis) ovarian cancer cell line

Adrent human ovarian adenocarcinoma (A2780) cells and cisplatin-resistant ovarian (A2780 cis) cells were cultured in complete RPMI 1640 medium containing 100 units/mL penicillin, 100 μg/mL streptomycin and 10 % fetal bovine serum (FBS). The cisplatin-resistant cell line A2780 cis is developed by chronic exposure of the parent cisplatin-sensitive A2780 cell line. In order to retain resistance, 1 μM cisplatin needed to add to the media for A2780 cis every 2-3 passages. The two cell lines were grown at 37

^{o}C in a humidified atmosphere of 95 % air and 5 % CO_2. Experiments were performed on cells within 10 passages. Viable cells were counted using the trypan blue exclusion method.

Drug effects on exponentially growing cancer cells were determined using MTT assay. A2780 and A2780 cis cells were seeded at a density of 6,000 cells/100 µL per well in 96-well plates and allowed to attach for 24 hr at 37 °C under 5 % CO_2. After the attachment period, cancer cells were exposed to drugs at different concentrations in RPMI 1640 medium without FBS and antibiotics. Sample solutions were prepared by dissolving in water and diluted with water to a series of different concentrations. The final concentration of water in medium was 1 % v/v. After 6 hr drug exposure, the medium with sample solutions at different concentrations was removed by aspiration and fresh drug-free complete medium with FBS and antibiotics were added and the cells were incubated for additional 66 h. At 72 h after drug addition, 100 µL MTT reagents (0.5 mg/mL in PBS) were added to each well after removal of medium, and cells were incubated for a further 4 h at 37 °C. Later, the MTT reagent was discarded, and the purple precipitate was dissolved in 100 µL DMSO. The absorbance of formazan, a metabolite of MTT, in the resulting solution was photometrically measured at a wavelength of 595 nm using a microplate reader (Tecan Instruments Inc., Research Triangle Park, NC, USA). Experiments were performed in three replicate wells for each drug concentration and carried out independently at least three times.

4.7.4 Assay for inhibitory effect of $[(diamine)AuCl_2]^{1+}$ complexes (8-10) on prostate (PC3) and gastric (SCG7901) cancer cells

MTT assay was used to obtain the number of living cells in the sample. Human gastric cancer SGC7901 and prostate cancer PC3 cells were seeded on 96-well plates at a predetermined optimal cell density i.e.ca 6,000 cells/100 µL per well in 96-well plates to ensure exponential growth in the duration of the assay. After 24 h pre incubation, growth medium was replaced with experimental medium containing the appropriate drug using Au (III) diamine complex or control using water. Six duplicate wells were set up for each sample, and cells untreated with drug served as control. In one sets of culture plate, human gastric cancer SGC7901 and human prostate PC3 cells were treated with the complexes **(1), (4)** and **(8-10)** as drug and the control (water) for 24, 48 and 72 h. In other sets, complexes **(1), (4),** and **(8-10)** with fixed concentration i.e. 10 µM were employed to determine the growth inhibitory effect for both PC3 and SGC7901 cells separately. After incubation, 10 µL MTT (6 g/L, Sigma) was added to each well and the incubation was continued for 4 h at 37 °C. After removal of the medium, MTT stabilization solution [Dimethylsulfoxide (DMSO): Ethanol = 1:1] was added to each well, and shaken for 10 min until all crystals were dissolved. Then, optical density was detected in a micro plate reader at 550 nm wavelength using an Enzyme-Linked Immuno-Sorbent Assay (ELISA) reader. After being treated with Au(III) diamine complexes, cell viability was examined by MTT assay. Each assay was performed in triplicate. MTT assay for inhibitory effect has been used for complexes **(8-10)** against PC3 and SGC7901 cells. These cells were treated with various concentrations of complexes **(8-10)** for 24-72 h. The results are shown in Figures 2-7.

4.7.5 *in vitro* Cytotoxicity of Au(III)thione complexes on C6 glioma cells

C6 glioma cells were seeded at 2 x 10^4 cells/well in 100μL DMEM, containing 10 % FBS in 96-well tissue culture plate, and incubated for 72 h at 37 ^oC, 5 % CO_2 in air and 90 % relative humidity in CO_2 incubator in order to evaluate the *in vitro* cytotoxicity of $[(thione)_2Au(diamine)]Cl_3$ complexes (**11-16**).

160, 80, 40, 20, 10 and 5 μg/mL sample solutions were prepared in DMEM. 100 μL of each sample solution were added to the incubated C6 glioma cells and further incubated for 20 hours. The medium was discarded and 100 μL DMEM containing MTT (5 mg/mL) was added to the same cells and again incubated in CO_2 incubator at 37 ^oC in dark for 4 h. The dark purple crystals of formazan were produced in the cells at the bottom of the wells.

The medium of culture from each well was aspirated cautiously to prevent disruption of the cell monolayer. 100 μL of DMSO was added in each well and mixed thoroughly to dissolve the formazan crystals, producing a purple solution. The absorbance of the 96 well plates was taken at 570 nm with Labsystems Multiskan EX-ELISA (Enzyme-linked immune-sorbent assay) reader against a reagent blank.

4.8 Biological activity

The biological activity of cyanido(diamine)Hg(II) and M(II)selenocyanate complexes [M(II)=Cd(II) or Hg(II)] are evaluated by antimicrobial assay and test for bacterial strain (antibacterial assay) respectively.

4.8.1 Antimicrobial assay

Antimicrobial activity was measured as described in the literature [124,125]. It was evaluated by the minimum inhibitory concentration (MIC) on four microorganisms, namely *Escherichia coli (E.Coli), Heterotrotropic Plate Counts (HPC), Pseudomonas aeruginosa (P. aeruginosa) and Fecal Streptococcus (FS).* Each analysis was carried out in duplicate to maintain the maximum accuracy. Dosage of each chemical started from 10 μg/ml and continued until MIC was reached. A maximum dose of 1000 μg/ml was used as a stopping criterion. The complex (**19**) and its derivatives (**21-24**) are relatively insoluble in water however; the bioactivities are carried out in water. As tested complexes are more soluble in DMSO, analysis is repeated for all the compounds in duplicate. Complexes were dissolved in water and in DMSO separately to note any effect of solubility. Some of the results show slight improvement in DMSO as compared to water. However, it should be noted that solutions prepared in water was kept in shaker prior to analysis at least for 24 hr and a homogenous sample was used for analysis.

4.8.2 Antibacterial assay

Standard type culture of *Escherichia coli* (MTCC 443), *Klebsiella pneumoniae* (MTCC 109), *Pseudomonas aeruginosa* (MTCC 1688), *Salmonella typhi* (MTCC 733) and *Staphylococcus aureus* (MTCC 737) were obtained from Microbial Type Culture Collection (MTCC) Chandigrah India. The agar well diffusion technique [126] was used to screen the antibacterial activity. Antibacterial activities were screened *in vitro* by using nutrient agar plates obtained from Himedia (Mumbai). The plates were prepared by pouring 20 ml of molten media into a sterile Petri dish and allowed to solidify for 5 minutes. A sterile cork borer of diameter 6.0 mm was used to make wells in the agar plates. Inoculums were swabbed uniformly on the surface of agar plates. 0.1 mg/well were loaded on 6.00 mm diameter well. The plates were allowed to stand for 1 h for diffusion then incubated at 37 ° C for 24 h. At the end of incubation, inhibition zones were measured.

4.9 Interaction studies of Gold(III) complexes using NMR spectroscopy

Interaction of the gold(III) complexes with some biologically important ligands has been studied using ^{1}H and ^{13}C NMR measurements.

4.9.1 NMR measurements

All NMR measurement were carried out on a JEOL LAMBDA 500 MHz NMR spectrophotometer at 298 K using 0.05 M solution of $[Au(pn)_2]Cl_3$ complex (Figure 4.5) in D_2O. ^{13}C NMR spectra were obtained at 125.65 MHz with ^{1}H broadband decoupling. The spectral conditions were: 32 k data points, 0.967 s acquisition time, 1.00 s pulse delay and 45˚ pulse angle.

NMR samples were prepared by mixing $[Au(pn)_2]Cl_3$ complex in D_2O with Imidazolidine-2-thione, Thiourea, Glycine, Methionine, Histidine and Imidazole ligands abbreviated as Imt, Tu, Gly, Met, His and Im as shown in Figure 4.6 respectively in 1:1 molar ratio in order to study the interaction between them.

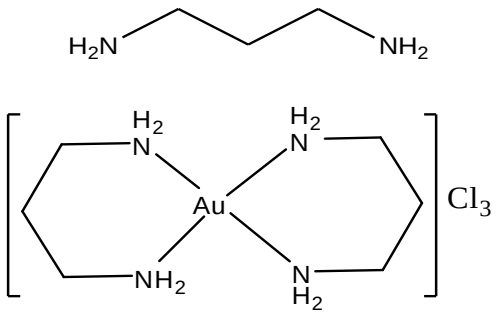

Figure 4.5 Structures of pn and $[Au(pn)_2]Cl_3$ complex

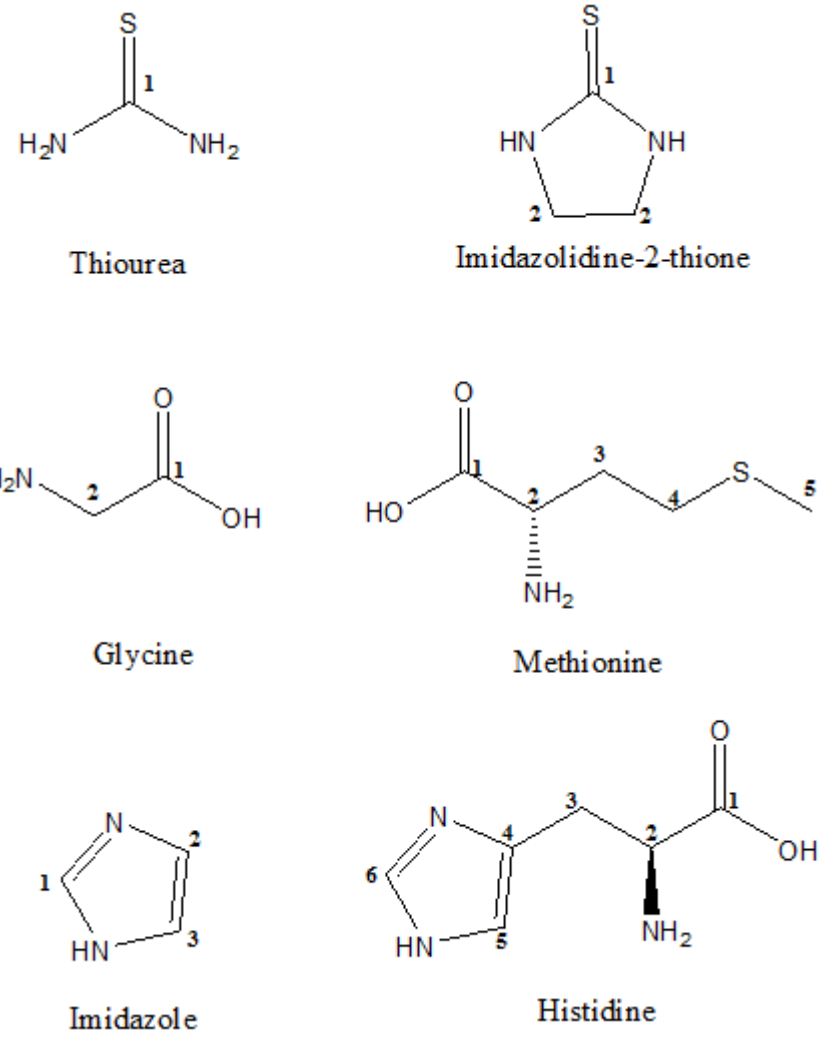

Figure 4.6 Structures of ligands used in the NMR studies of interactions

CHAPTER 5

RESULTS AND CONCLUSION

5.1 Gold(III) Diamine Complexes

This work reports the synthesis of some $[Au(diamine)_2]Cl_3$ complexes where diamine = 1,2-diaminoethane (*en*), 1,3-diaminopropane (*pn*), alkyl-substituted 1,2-diaminoethane (N-R-*en*) and diakyl-substituted 1,2-diaminoethane (N,N´-R_2-*en*).

5.1.1 Mid-IR Studies

The characteristic mid-IR vibration bands for the free ligands and their corresponding gold(III) complexes are shown in Table 5.1. Solid state IR spectrum of complex (**1)** shows clear signals for the presence of N-H frequency at 3396 cm^{-1}, while in case of complex (**4)**, the N-H frequency appears at 3538 cm^{-1} indicating the strong coordination of ligand with the metal center. The C–N stretching bands showed a slight shift to higher frequency in the complex. It indicates a shorter C–N bond in the complex as compared to the free ligand.

Solid state IR spectra of complexes (**2)** and **(2a)** showed signals for the presence of N-H vibration at 3413 and 3442 cm^{-1} respectively. The C–N stretching bands in the complexes (**2)** and **(2a)** showed a large shift to higher wave numbers 1203 and 1198 cm^{-1} respectively, indicating that the C–N bond in the complex is relatively stronger than that in the free *pn* ligand. The N-H band appears at much higher frequency in N-alkyl-

substituted diamine complexes than that in the unsubstituted diamines complexes [93]. For example, the N-H frequency shift is about 150 and 180 cm^{-1} in complexes (**3)** and **(4)** respectively, while this shift is about 56 cm^{-1} in complex (**2)**. The larger N-H wave number shifts designate the strong coordination of ligands in complexes (**3)** and (**4)** with the gold(III) centre. This may be due to lone pair donation to the gold(III) center, which is facilitated by the alkyl group bound directly to the nitrogen donor atom as substituent.

Table 5.1 Mid-IR frequencies, ν(cm^{-1}) for Au(III) diamine complexes

Compound	ν(N-H)	ν(C-N)
en[b]	3393	1093
(**1**)	3396	1043
pn	3357 m, 3282 m	1093 w
(**2**)	3413	1203
(**2a**)	3442	1198
N-Et-*en*	3276 br	1130 m
(**3**)	3426	1042
N-pr-*en*[a]	3358 m	1127
(**4**)	3538	1163
N-ipr-*en*	3300 m, 3289 m	1174 m
(**5**)	3476	1124

[a] Published work [93] and [b] Published work [94]

5.1.2 Far-IR studies

The characteristic Far-IR vibration bands for the free ligands and their corresponding gold(III) complexes are shown in Table 5.2. There is a characteristic stretching frequency at 367 cm^{-1} for Au-Cl bond in trihydrate auric acid ($HAuCl_4 \cdot 3H_2O$). The absence of such stretching band in bis(diamine) gold(III) indicating the replacement of two monodentate chloride by bidentate diamine ligands. That is also confirmed by the presence of stretching frequencies of Au-N bond indicating coordination of diamine *via* N-donor atoms to gold(III) center. Far-IR data showed signals at 378 and 476 cm^{-1} & 375 and 415 cm^{-1} that could be assigned for the stretching frequencies of the Au–N bond of complexes $[Au(en)_2]Cl_3$**(1)** and $[Au(N\text{-}Pr\text{-}en)_2]Cl_3$ (**4**) respectively [94,127].

Table 5.2 Far-IR frequencies, ν(cm^{-1}) for Au(III) diamine complexes

Compound	ν(Au-Cl)	ν(Au-N)
$HAuCl_4 \cdot 3H_2O$	367	--
$[Au(en)_2]Cl_3$ (**1**)	--	378, 476
$[Au(N\text{-}Pr\text{-}en)_2]Cl_3$ (**4**)	--	375, 415

[a] Published work [94]

5.1.3 UV-Vis studies

UV-Vis data showed absorption in the region of 250–350 nm (40000–28570 cm^{-1}) which correspond to LMCT (Ligand to metal charge transfer) transitions. The absorption spectrum of trihydrate auric acid $HAuCl_4 \cdot 3H_2O$ gives a characteristic absorption band at 320 nm [128]. Therefore, a signal at 300 nm with high extinction coefficient (Ɛ) could be assigned to Cl→Au charge transfer. Such a transition of high extinction coefficient cannot be assigned to the symmetry forbidden d–d transition. According to crystal field theory, the LUMO orbital is d_{x2-y2} for d^8 complexes, so LMCT (ligand to metal charge transfer) could be due to $p_\sigma \rightarrow d_{x2-y2}$ transition. It is also evident that the electronic spectra of these compounds are stable and consistent which means that the gold center remains in +3 oxidation state.

5.1.4 Solution state NMR studies

Table 5.3 shows the ^{13}C NMR chemical shifts of diamine ligands and their corresponding gold(III) complexes in solution. Downfield shifts were observed for ^{13}C resonances in the gold(III) complexes relative to the free diamine ligands. There is third non-equivalent carbon directly bonded to NH due to deprotonation of NH_2 in coordinated *pn:* $NHCH_2CH_2CH_2NH_2$ of complex (**2a**). These downfield shifts may be due to the σ-donation of nitrogen lone pair to the metal center that causes the deshielding of the carbons adjacent to the coordinating-NH groups. The downfield shift is greater for the substituted diamine ligand than that for the unsubstituted diamine ligand. For example, in case of complex (**2**), the change in chemical shift of C1 signal is observed as 3.37 ppm, while in case of complexes (**3**) and (**4**), the change in chemical shift of C-1 signal

observed is 13.64 and 7.78 ppm respectively. Similar trend of change in chemical shift has been observed in complex (**5**).

A significant downfield shift was observed at 50.69 ppm for complex (**1**) with respect to the free ethylenediamine (*en*) ligand at 37.32 ppm (Table 5.3). This can be attributed to the donation of nitrogen lone pair to the gold that causes deshielding of the carbon(s) next to the bonding nitrogen. But the upfield shift of compound $[Au(en)_2]Cl_3$ (**1**) as compared to $[(en)AuCl_2]Cl$ (**8**) may be due to the lone pair donation of nitrogen is slightly less effective as compared to that of the compound (**8**) which is having two Cl^- atom directly bonded to gold. It is also worth-mentioning that the only one signal at 50.69 ppm for $[Au(en)_2]Cl_3$ (**1**) indicates that the tetra-coordinate gold(III) complex is adopting the regular square planar geometry thereby causing two carbons in similar environment. But the shifts vary significantly from one ligand to the other, suggesting different degrees of σ-donation from the ligand to the metal (Table 5.3). For instance, complexes $[Au(en)_2]Cl_3$ (**1**) and $[Au(N\text{-}Pr\text{-}en)_2]Cl_3$ (**4**) even though they have the same basic skeleton of ethylenediamine (*en*), the chemical shifts of the C-1 and C-2 carbons of $[Au(N\text{-}Pr\text{-}en)_2]Cl_3$ (**4**) appear at 48.61 and 57.52 ppm respectively. The chemical shifts of C-2 and C-3 of the ligand in complexes (**1, 4** and **6**) demonstrate that they are in similar environment even after complexation with the metal center. It is may be due to cyclic bond strain for the *endo*-cyclic carbon atom of metal chelate. Such a higher shift is may be as a result of inductively withdrawing effect of the nitrogen atom which is coordinated to the gold(III).

Table 5.3 Solution state ^{13}C NMR chemical shifts of Au(III) diamine complexes

Compound	^{13}C (δ in ppm)			
	C-1	C-2	C-3	C-4
en[a]	37.32			
(**1**)	50.69			
pn	37.61	25.79		
(**2**)	40.98	27.94		
(**2a**)	40.66	26.31	38.06*	
N-Et-*en*	36.41	44.4	44.37	11.42
(**3**)	50.05	57.38	49.1	10.59
N-pr-*en*[a]	40.83	51.41	51.63	22.8
(**4**)	48.61	57.52	58.03	36.39
N-ipr-*en*	36.58	42.27	52.58	19.07
(**5**)	37.95	52.29	57.52	21.26

[a]Published work [93]

* Third non-equivalent carbon directly bonded to NH due to deprotonation in coordinated *pn* $NHCH_2CH_2CH_2NH_2$ ligand of complex (2a)

5.1.5 Solid state NMR

The ^{13}C and ^{15}N CPMAS NMR spectral data for complexes (**1)** and (**2)** are shown in Table 5.4. It is observed that ^{13}C isotropic chemical shift of diamines moves towards downfield region upon coordination as compared with the free ligands. A similar trend has been observed in ^{13}C solution state NMR.

In the case of solid state NMR spectroscopy, we observe only the isotropic signals due to the carbon and nitrogen indicating small anisotropies due to the sp^3 hybridizations of these atoms. The chemical shift of 51.82 ppm in Solid state ^{13}C NMR, for complex **(1)** is slightly higher than that of the solution NMR chemical shift 50.69 ppm (Table 5.4) which is a clear indication of the stability of the prepared complex as well as the conservation of the bond topology in solution as in the solid form. The ^{15}N NMR chemical shift for $[Au(en)_2]Cl_3$ is -317.36 while for 1,2-ethylenediamine dihydrochloride (*en*·2HCl), it appeared at -342.68 ppm. This deshielding can be attributed to the lone pair electron donation of the nitrogen atom of ethylenediamine (*en*) ligand to gold(III).

Recently, Mironov and Afanas'eva published data on complex (**2)** [129]. These authors reported that a ring-open form of complex (**2**) is possible. However, our solution and solid ^{13}C NMR data indicate only two resonances as given in Table 5.3 and Table 5.4 respectively. This clearly shows that complex (**2**) is a bis-chelated of gold(III). The open chain complex should give more than two resonances in ^{13}C NMR. This is also corroborated by solid state ^{15}N NMR data in which only one ^{15}N signal is observed.

Table 5.4 Solid state ^{13}C and ^{15}N NMR data of Au(III) diamine complexes

Compound	^{15}N	^{13}C	
	$^{15}NH_2$	C-1	C-2
en•HCl[a]	-342.68	37.79	
$[Au(en)Cl_2]Cl$[a] (**6**)	-342.09	53.76	
$[Au(en)_2]Cl_3$[b] (**1**)	-317.36	51.82	
pn•HCl	-343.12	37.81	26.17
$[Au(pn)_2]Cl_3$ (**2**)	-365.28	41.34	30.95

[a]Published work [94] and [b]Published work [93]

5.1.6 Crystal structure of complex (2a)

The crystal structure of complex **(2a)** is shown in Figure 5.1. Selected bond lengths and bond angles are given in Table 5.5 and Table 5.6. It is a dinuclear ionic complex with two $[Au(pn)(Cl)]^+$ units bridged by two deprotonated molecules of 1,3-propylenediamine ligand. There are two chloride ions and one water molecule in the outer sphere of the complex. The coordination geometry around the Au(III) ions is pseudo-square planar and each metal atom is coordinated by two NH and one NH_2 donor groups of the two deprotonated 1,3-propylenediamine bridging ligand molecules, and one chloride anion. The dinuclear cations contain two six-member chelate cycles AuN_2C_3 and the four-member cycle Au_2N_2.

In the central Au_2N_2 four-member ring of the dimer complex Au2–N1 & Au2–N3 bond distances 2.039 (1) & 2.019 (1) Å are shorter than Au1–N1 & Au1–N3 bond distances 2.048 (1) & 2.052 (1) Å. The Au-N bond distances vary from 2.019 (1)–2.052 (1) Å and correspond to those found in the amine Au (III) complex [130] Au1–Cl1 and Au2–Cl2

bond lengths are 2.298 (4) and 2.288 (4) Å respectively as given in Table 5.12. The N–Au1–N and N–Au2–N bond angles vary in the ranges 79.0 (4)–174.9 (4) ° and 80.0 (4)–173.6 (5) ° respectively. The bond angles around both gold(III) ions in binuclear complex are different from each other. These observations provide an additional evidence for the presence of slightly different geometry around both gold(III) ions in this binuclear complex.

In this binuclear complex the Au···Au distance [3.0549 (8) Å] is longer than the one reported [3.004 (2) Å] for Au(III) complexes with primary amine ligands [130–132]. This metal···metal distance is also longer than the one in metallic gold [2.884 Å]. However, it is short enough to illustrate aurophilic (Au···Au) interaction in complex **(2a)**. The presence of Cl^- counter ions, lattice water molecule and –NH, $–NH_2$ groups of the 1,3-propylenediamine ligand result in hydrogen bond formation in the solid state structure of compound **(2a)**, which leads to the formation of a three-dimensional hydrogen bonded network as shown in Figure 5.2 and Figure 5.3.

Table 5.5 Selected bond lengths (Å) for the crystal structure of complex (2a)

Bond	Length (Å)
Au1—Cl1	2.298 (4)
Au2—Cl2	2.288 (4)
Au1—N2	2.041 (12)
Au1—N3	2.039 (12)
Au1—N1	2.019 (11)
Au1—Au2	3.0549 (8)
Au2—N4	2.042 (12)
Au2—N3	2.048 (11)
Au2—N1	2.052 (11)

Table 5.6 Selected bond angles (º) for the crystal structure of complex (2a)

Bonds	Angle (°)
N1—Au1—N2	94.5 (5)
N1—Au1—N3	80 (4)
N2—Au1—N3	173.6 (5)
N1—Au1—Cl1	176.3 (3)
N2—Au1—Cl1	89.1 (4)
N3—Au1—Cl1	96.4 (3)
N1—Au1—Au2	41.8 (3)
N2—Au1—Au2	133.9 (3)
N3—Au1—Au2	41.7 (3)
Cl1—Au1—Au2	134.99 (11)
N4—Au2—N3	95.9 (5)
N4—Au2—N1	174.9 (4)
N3—Au2—N1	79 (4)
N4—Au2—Cl2	89.2 (3)
N3—Au2—Cl2	174.4 (3)

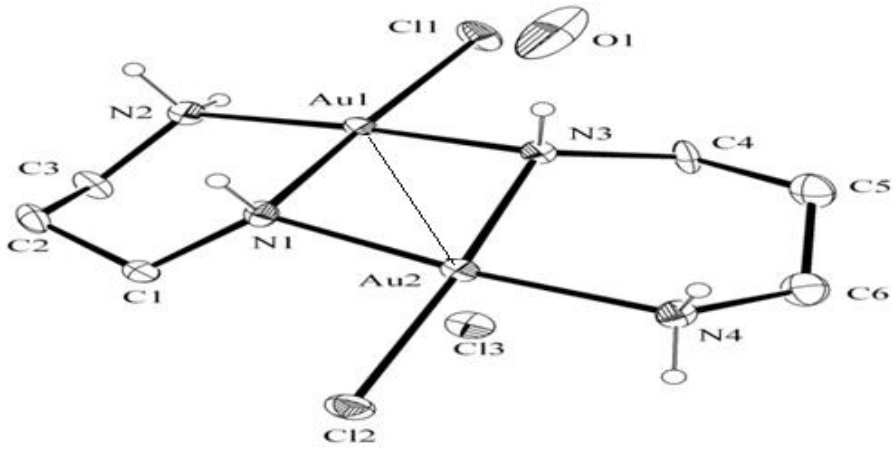

Figure 5.1 A view of the molecular structure of the dimeric complex (2a)

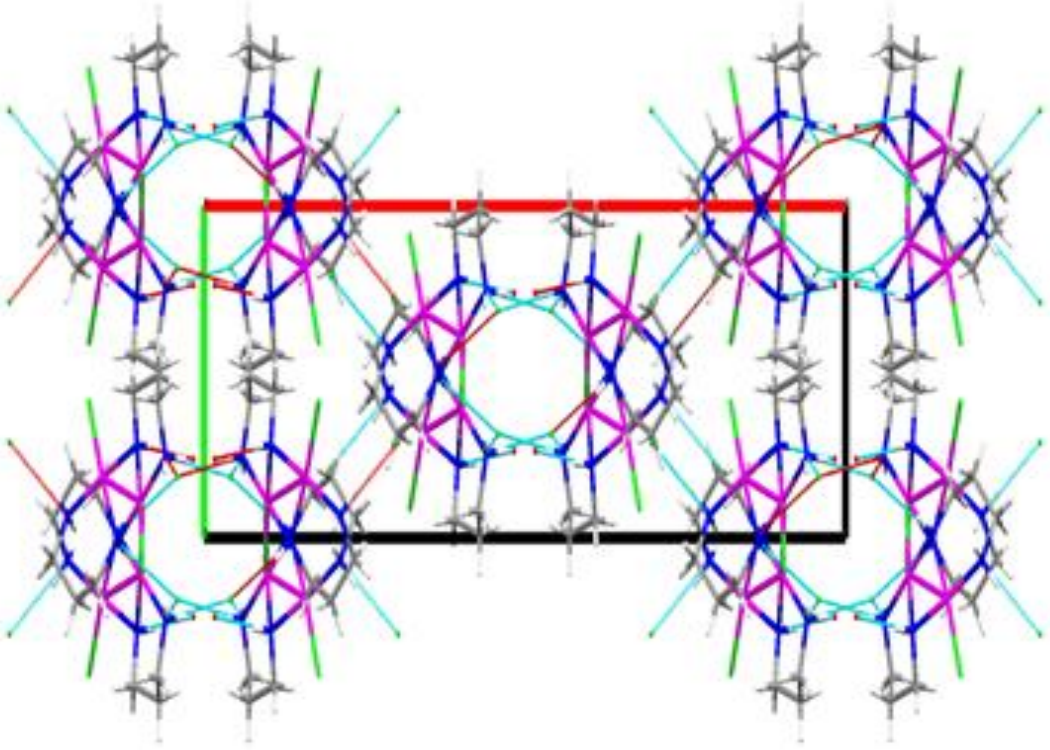

Figure 5.2 View of the hydrogen bonded network of complex (2a) in the unit cell.

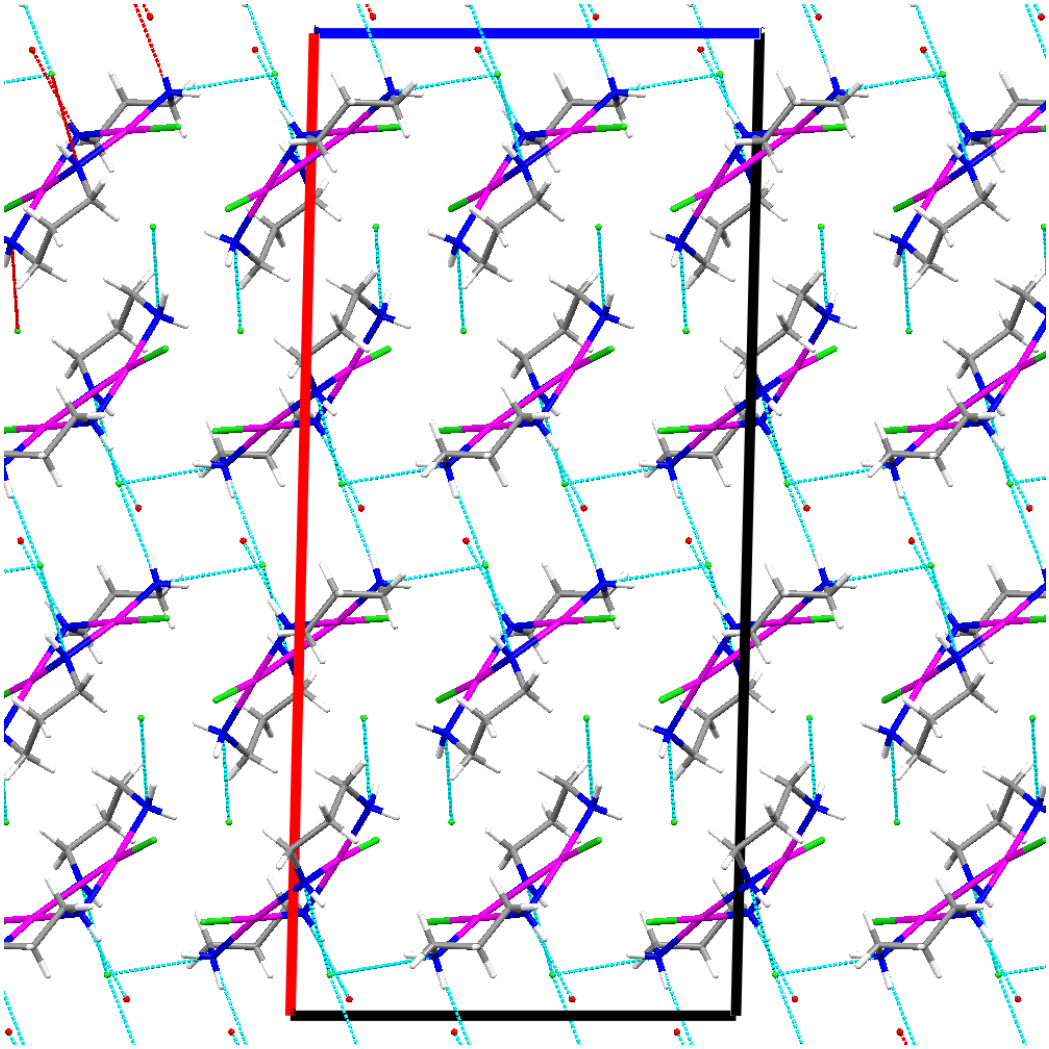

Figure 5.3 View of the hydrogen bonded network of complex (2a) in the unit cell

5.1.7 Computational analysis

B3LYP optimized structure was analyzed computationally for complex $[Au(en)_2]^{3+}$ **(1)** using B3LYP/LanL2DZ level of theory which shows acceptable for the experimental values from the crystal structure of the gold(III) complex with ethylenediamine (*en*) [71]. Selected bond lengths and torsion angles of the computationally optimized structure are presented in Table 5.7 and Table 5.8 respectively. The computational results show that complex $[Au(en)_2]^{3+}$ **(1)**, has a slightly distorted square planar geometry as shown in Figure 5.4.

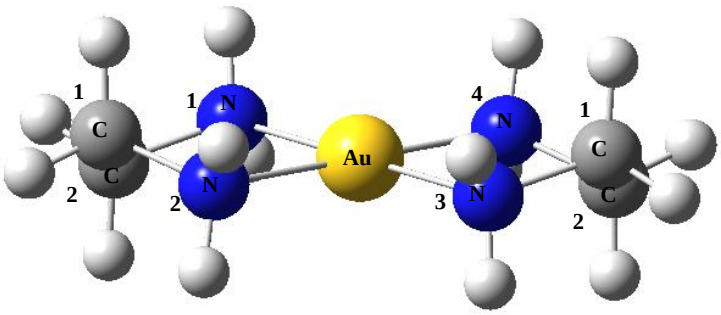

Figure 5.4 Computationally optimized structure of $[Au(en)_2]^{3+}$ complex

Table 5.7 Selected bond lengths (Å) drived computationally for $[Au(en)_2]^{3+}$ structure

Bond	Length (Å)
Au-N (1)	2.1207
Au-N (2)	2.1218
Au-N (3)	2.1196
Au-N (4)	2.1226

Table 5.8 Selected torsion angles (º) drived computationally for $[Au(en)_2]^{3+}$ structure

Bonds	Torsion angle (º)
N(1)–Au–N(2)	82.287
N(1)–Au–N(4)	97.714
N(2)–Au–N(3)	97.7
N(3)–Au–N(4)	82.299
N(2)–Au–N(1)–C(2)	-14.755
N(4)–Au–N(1)–C(2)	165.246
N(3)–Au–N(1)–C(2)	62.855
Au–N(1)–C(2)–C(1)	41.005
Au–N(2)–C(1)–C(2)	40.153

5.1.8 Effect of $[Au(diamine_{)2}]^{3+}$ complexes on cell proliferation

The cytotoxicity assay was performed with complexes (**1)** and (**4)** on PC3 and SGC7901 cells. The experimental PC3 and SGC7901 cells were treated with various concentrations of (**1)** and **(4)** for 24-72 hours and the cell viability was determined as described in the experimental section by MTT assay and the results are shown in Table 5.9 and in Figure 5.5, Figure 5.6 and Figure 5.7.

Figure 5.5 shows that cell proliferation of PC3 and SGC7901 cells was significantly reduced after 24 hrs of treatment with $[Au(en)_2]Cl_3$. From Figure 5.5, it is also quite clear that complex $[Au(en)_2]Cl_3$ (**1),** showed concentration dependent cytotoxic effect on cancerous cells PC3 and SGC7901. This observation is comparable with the report published by Milovanovic *et al.* on gold(III)-monoethylenediamine complexes on chronic lymphocytic leukemia (CLL) cells [105]. The same complex (**1)** was already found to exhibit relevant cytotoxicity properties when tested on human ovarian cancer cell lines i.e., A2780 and A2780 cis [37].

Time dependent activity studies revealed that after 72 hr of the experiment with complex (**1)** on SGC7901 cell, the cell proliferation is bit higher than that of the PC3 cells at fixed 10 μM concentration as shown in Figure 5.6. In Figure 5.7, the cytotoxicity results demonstrate that the complex (**1)** at 10 μM concentrations has higher cytotoxic effect in comparison with the same concentrations of complex (**4)**.

Table 5.9 Effect of $[Au(en)_2]^{3+}$complex on cell proliferation of gastric cancer cell line

Compound	Day 1 (24 hr)	Day 3 (72 hr)
Control	0.56 ± 0.03	1.30 ± 0.14
$[Au(en)_2]Cl_3$ (**1**)	0.28 ± 0.03	0.45 ± 0.08

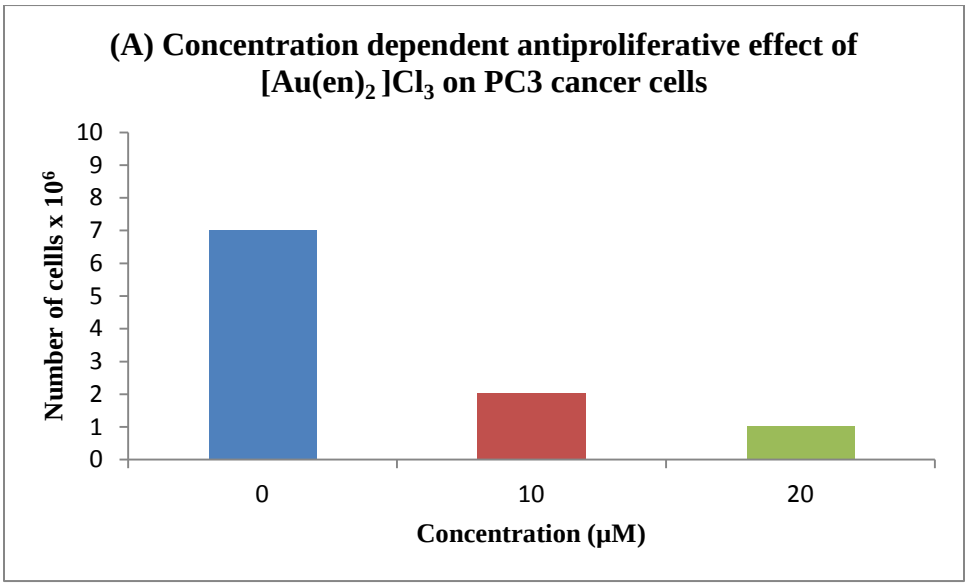

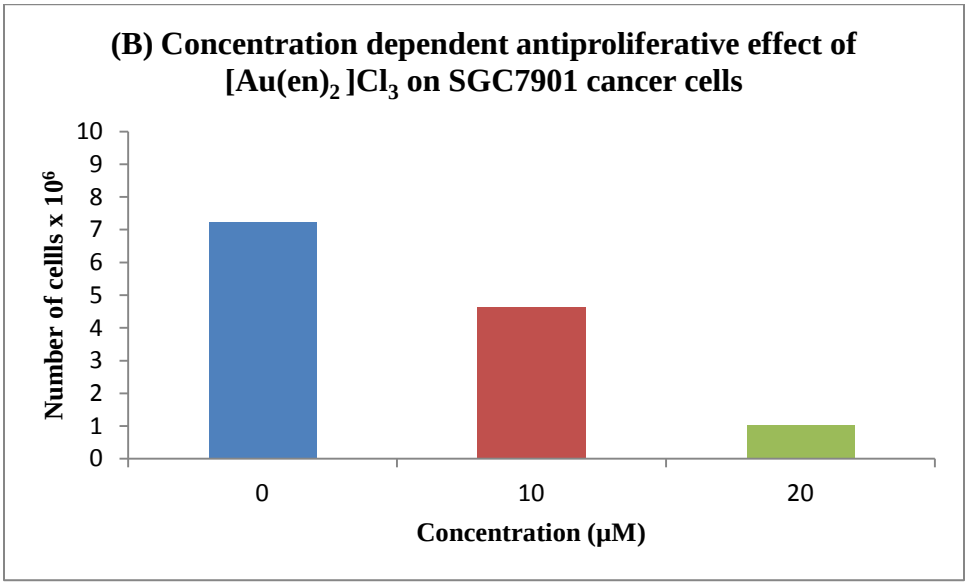

Figure 5.5 Concentration dependent antiprolifrative effect of complex (1) on A) PC3 and B) SGC7901 cells

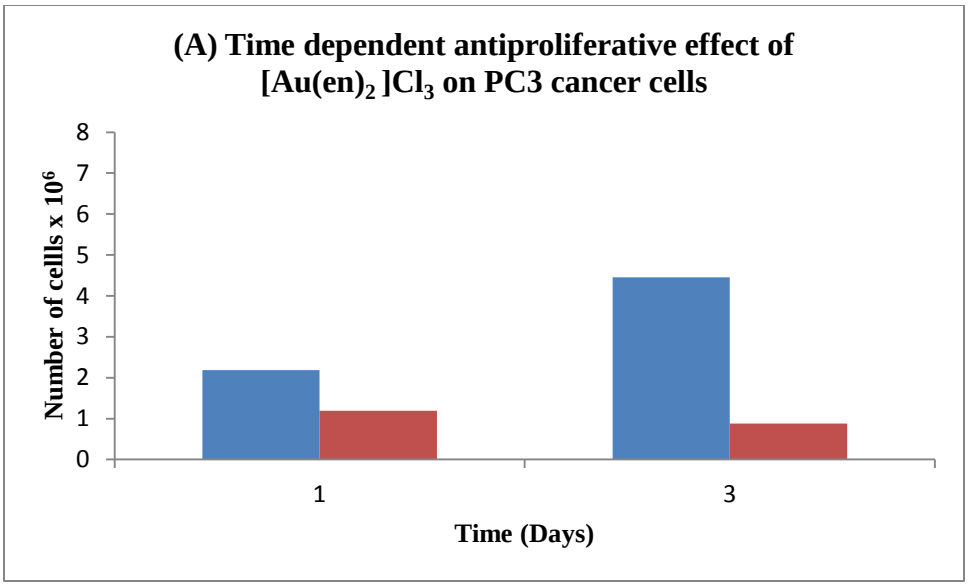

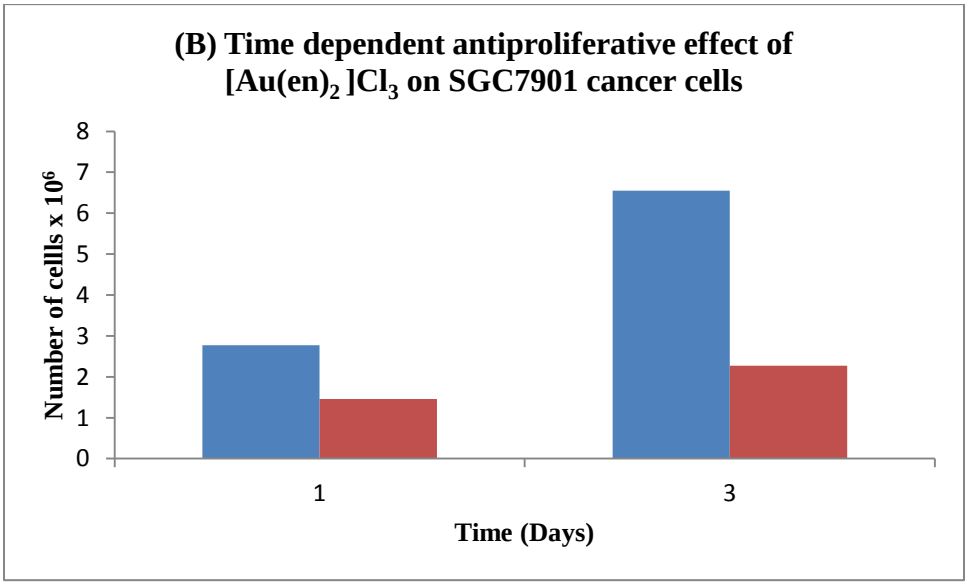

Figure 5.6 Time dependent antiprolifrative effect of complex 1 on (A) PC3 and (B) SGC7901 cells

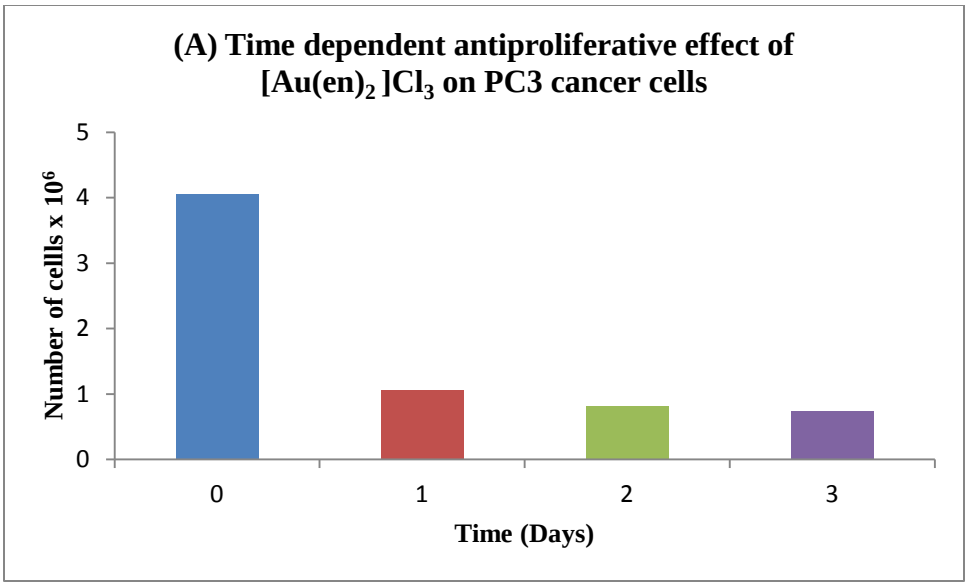

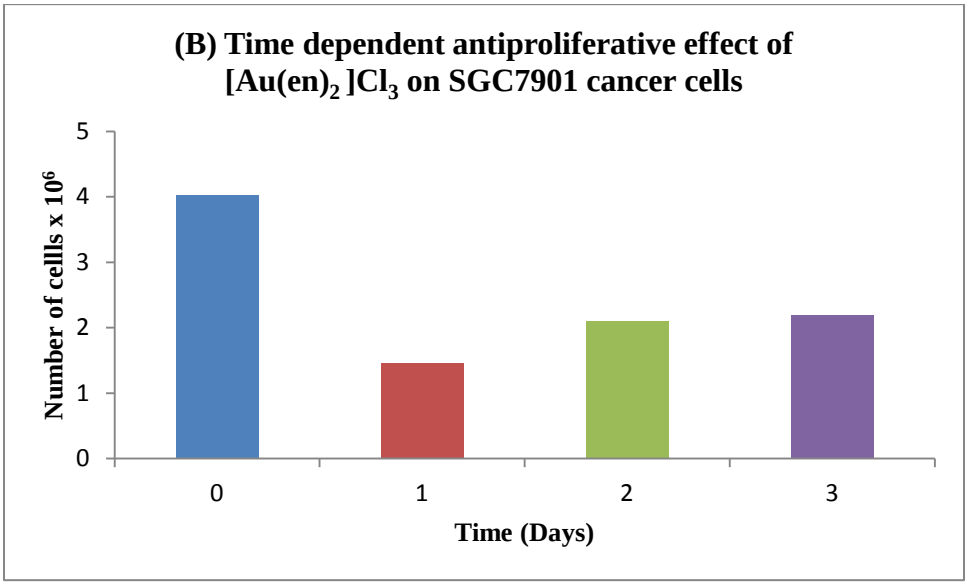

Figure 5.7 Time dependent antiprolifrative effect of complex 1 on (A) PC3 and (B) SGC7901 cells

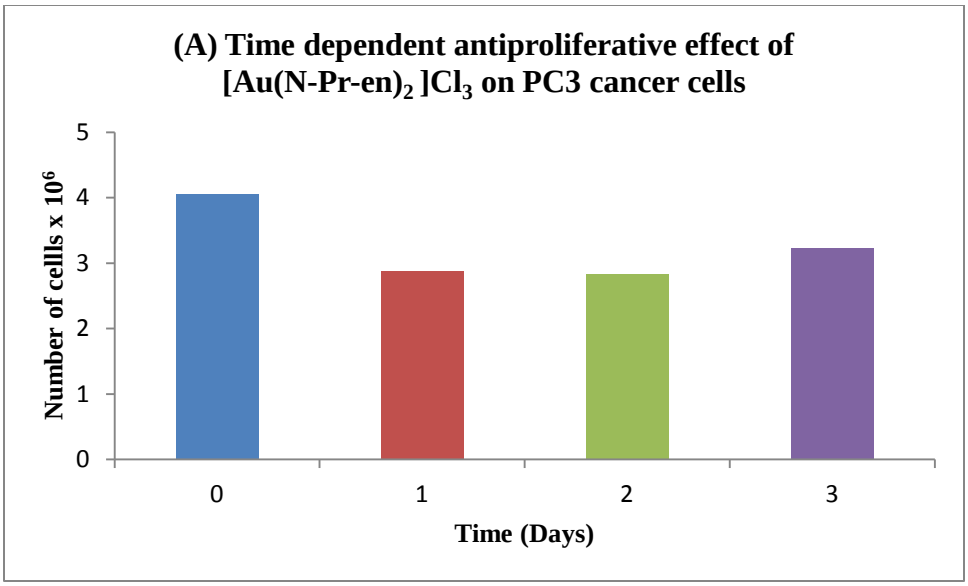

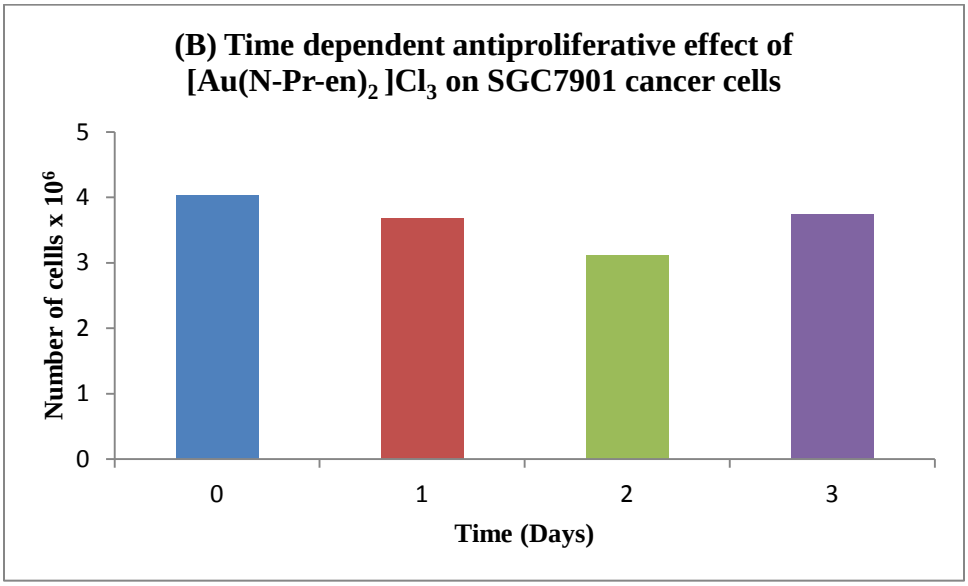

Figure 5.8 Time dependent antiprolifrative effect of complex 4 on (A) PC3 and (B) SGC7901 cells

5.1.9 *in vitro* Cytotoxicity of $[Au(diamine)_2]^{+3}$complexes (1-5) on prostate (PC3) and gastric (SCG7901) cancer cells

The preliminary studies were reported on two gold(III) complexes, formulae $[Au(en)_2]Cl_3$ (**1**) and $[Au(N\text{-}pr\text{-}en)_2]Cl_3$ (**4**) against prostate cancer cell lines (PC3) and gastric carcinoma cell lines (SGC7901). It is clearly observed that $[Au(en)_2]Cl_3$(**1**) has better anticancer activity than $[Au(N\text{-}pr\text{-}en)_2]Cl_3$(**4**) [93]. Casini *et al.* [106,133] have checked several gold(III) complexes for their cytotoxic effects against selected human cancer cell lines. They reported the *in vitro* cytotoxic properties of [Au(6-1,1-dimethylbenzyl)-2,2´-bipyridine)$_2$] complex which indicated two fold higher activity as compared to cisplatin against A2780 ovarian cancer cells.

The cytotoxic study was extended to a new series of gold(III) diamine complexes. A pioneer attempt was also made to evaluate *in vitro* cytotoxic effect of gold(III) diamine complexes against androgen-resistant prostate PC3 and human gastric SGC7901 cancer cells using MTT assay. The representative gold complexes (**1**) and (**4**) demonstrated a comparable cytotoxicity, as shown in Figure 5.7, whether the drug exposure was for 24, 48 or 72 hr [93]. For that reason, we used a 3-day exposure protocol to assess IC_{50} value. Cisplatin was included for comparison.

The IC_{50} data for Au(III) complexes (**1-5**) showed reasonable cytotoxicity in the 1-6 μM range for PC3 cells, as given in Table 5.10. For PC3 cells, complex (**1**) was recognized as effective cytotoxic agent like cisplatin while complexes (**2-5**) demonstrated about 4 to 6 fold lower potency. Complexes (**6-8**) showed almost 7-9 fold lower cytotoxicity as compared to cisplatin. For SCG7901 cells, complexes (**1-5** and **8**) show slightly lower

cytotoxicity with respect to cisplatin whereas complexes **(6-7)** almost two fold more cytotoxic than cisplatin. Complexes (**6-7**) may be potential anticancer agents for cisplatin resistant SCG7910 cells.

An independent assessment of complexes (**1-5**) reveals an interesting feature that SGC7901 gastric cancer cells exhibit 7 to 8 fold intrinsic resistance relative to the PC3 cancer cells with respect to cisplatin. Nevertheless, only 2-fold or less resistance to complexes (**2-5**) was observed for PC3 as shown in Table 5.10. This suggests that the intrinsic factors regulating cellular sensitivity to cisplatin and complex (**1)** are different for PC3 and SGC7901 cells. The factors affecting sensitivity of PC3 and SGC7901 cells are analogous in complexes (**2-5**). There is no doubt that the present results in the study will be helpful for further exploiting and defining the potential role of gold(III) complexes in combat against prostate and gastric cancers.

The inhibitory effect of complexes (**2)** to (**5**) on the proliferation of rapidly dividing cells may be attributed to the induction of cell cycle blockage, interruption of the cell mitotic cycle, apoptosis or necrosis.

Even though the exact mechanisms on anti-proliferation of [Au(diamine)Cl_2]Cl complexes remains vague, the inhibitory effect of complex (**6-8)** on the proliferation of rapidly dividing cancer cells may be attributed to the induction of cell cycle blockage, interruption of the cell mitotic cycle, apoptosis and necrosis.

Table 5.10 *in-vitro* Cytotoxicity of Au(III) diamine complexes on PC3 and SGC7901 cell lines

Complex	[a]IC_{50} (μM)		Fold Resistance SGC7901/PC3 ratio
	PC3	SGC7901	
Cisplatin	1.1± 0.1	7.3± 0.5	6.6
(**1**)	1.0 ± 0.1	8.5 ± 0.6	8.5
(**2**)	6.2 ± 0.4	8.1 ± 0.5	1.3
(**3**)	4.2 ± 0.3	9.5 ± 0.1	2.3
(**4**)	4.6 ± 0.4	9.7 ± 0.7	2.1
(**5**)	6.8 ± 0.4	9.6 ± 0.1	1.4
(**8**)	7.5 ± 0.08	4.1 ± 0.26	0.55
(**9**)	9.3 ± 0.10	3.3 ± 0.07	0.35
(**10**)	8.0 ± 0.71	7.9 ± 0.01	0.99

[a]IC_{50} data are given with ± SD.

Each experiment was performed independently at least 3 times.

5.1.10 Inhibitory effect of $[(diamine)AuCl_2]^{1+}$ complexes (8-10) on prostate (PC3) and gastric (SGC7901) cancer cells

All gold(III) complexes showed concentration dependent cytotoxic effect in cancer cell lines SGC7901 and PC3 as illustrated in Figure 5.9 to Figure 5.14.

The cell proliferation of PC3 and SGC7901 cells is significantly reduced after 24 hrs of treatment with complex (**8**) as shown in Figure 5.9. This observation is consistent with the report published by Milovanovic *et al.* on gold(III)-monoethylenediamine complexes on chronic lymphocytic leukemia (CLL) cells [105]. The same compound was found to exhibit pertinent cytotoxic properties when tested in different human ovarian cancer cell lines A2780. The time dependent activity revealed that the cell proliferation on SGC7901

cells is slightly higher than that of the PC3 cells at fixed 10 μM concentration after 72 hrs of the experiment with complex (**9**).

The MTT results showed the effect of complexes **(8-10**) on prostate cancer cells growth, where the first two complexes (**8**) and **(9**) demonstrated inhibition in cancer cells growth in PC3, while the last complex (**10**) did not show any significant changes in cancer cells growth in PC3. Thus, complexes (**8**) and (**9**) might prove to be reasonably good candidates as anticancer drugs for prostate cancer.

The MTT results also showed the effect of complexes (**8-10**) on gastric cells growth, where the first complexes (**8**) demonstrated inhibition in cancer cells growth in SGC7901, while the last two complexes **(9)** and (**10)** did not show any major changes in cancer cells growth in SGC7901. Thus, complex (**10**) might prove to be practically good candidate as anticancer drug for gastric cancer.

Even though the exact mechanisms of anti-proliferation of [Au(diamine)Cl_2]Cl complexes remains uncertain, the inhibitory effects of complexes (**8-10**) on the proliferation of rapidly dividing PC3 and SCG7901 cells may be accredited to the induction of cell cycle blockage, interruption of the cell mitotic cycle, apoptosis and necrosis [134–136].

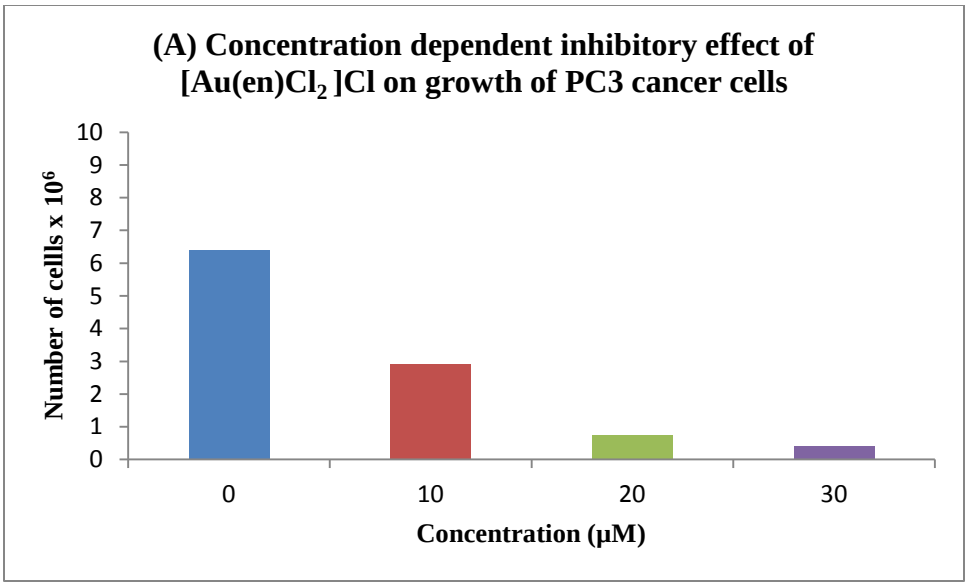

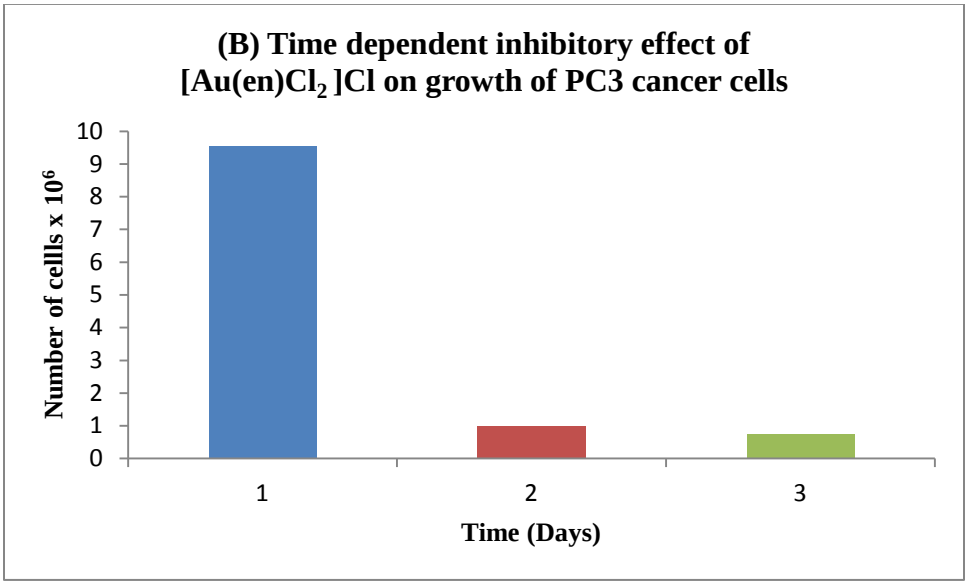

Figure 5.9 (A) Concentration dependent and (B) Time dependent inhibitory effect of complex 8 on PC3 cells growth

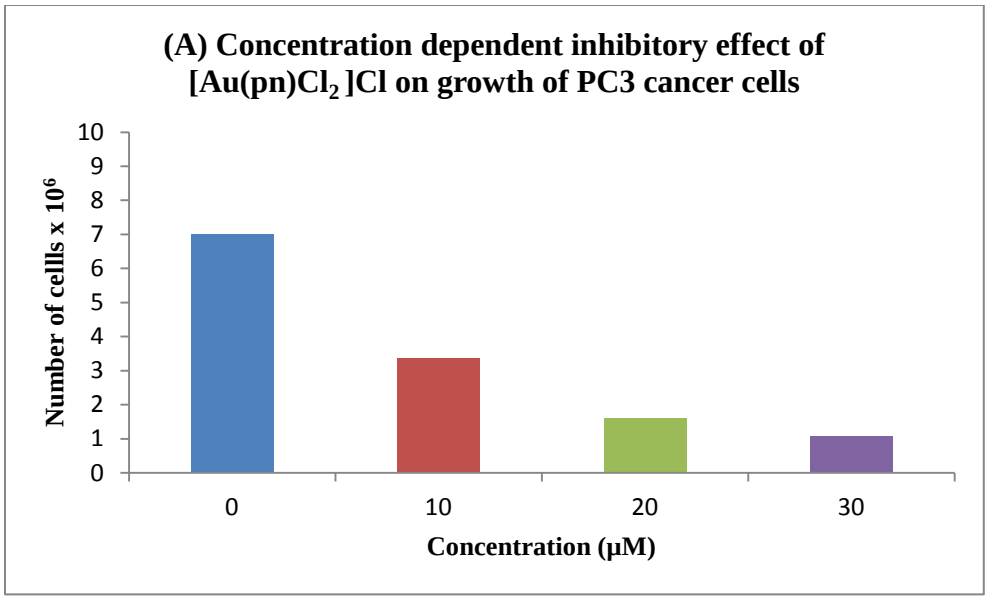

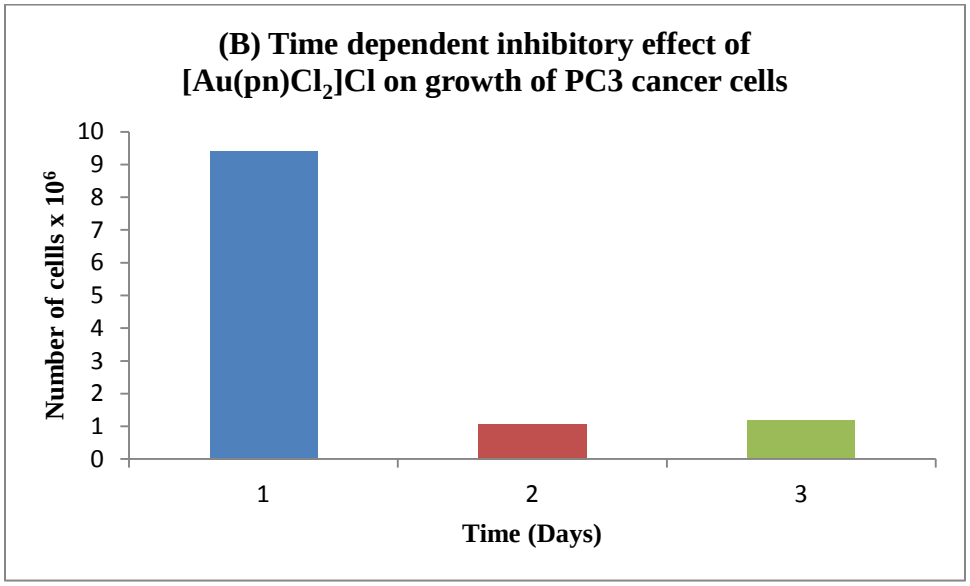

Figure 5.10 (A) Concentration dependent and (B) Time dependent inhibitory effect of complex 9 on PC3 cells growth

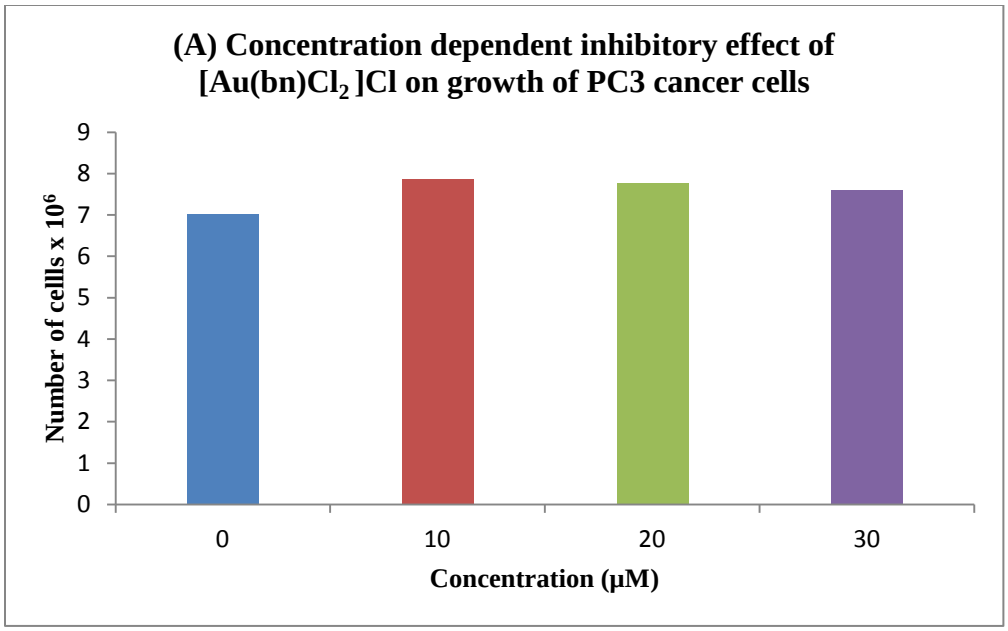

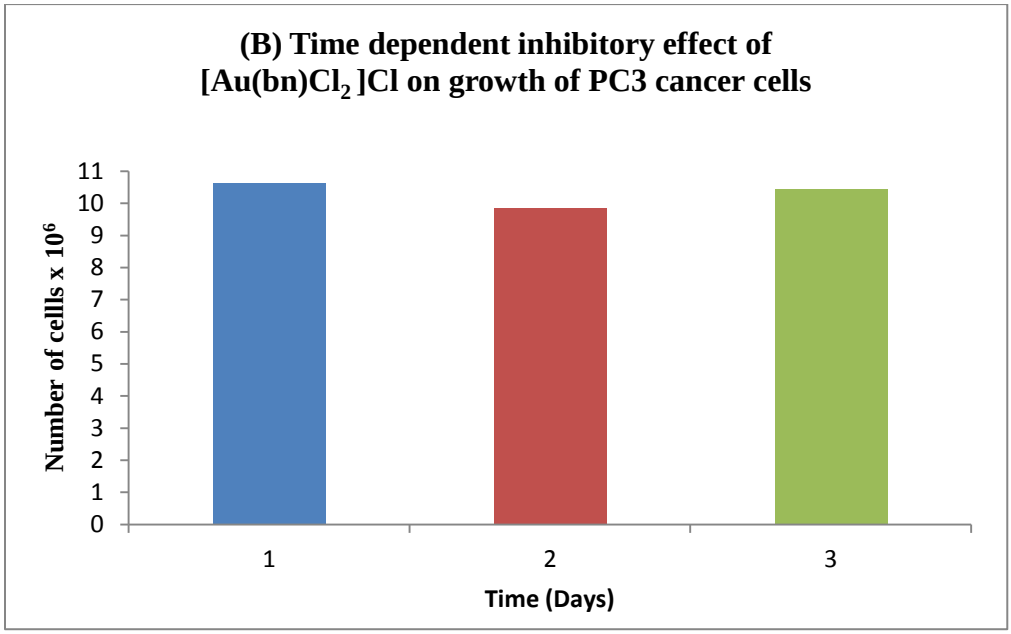

Figure 5.11 (A) Concentration dependent and (B) Time dependent inhibitory effect of complex 10 on PC3 cells growth

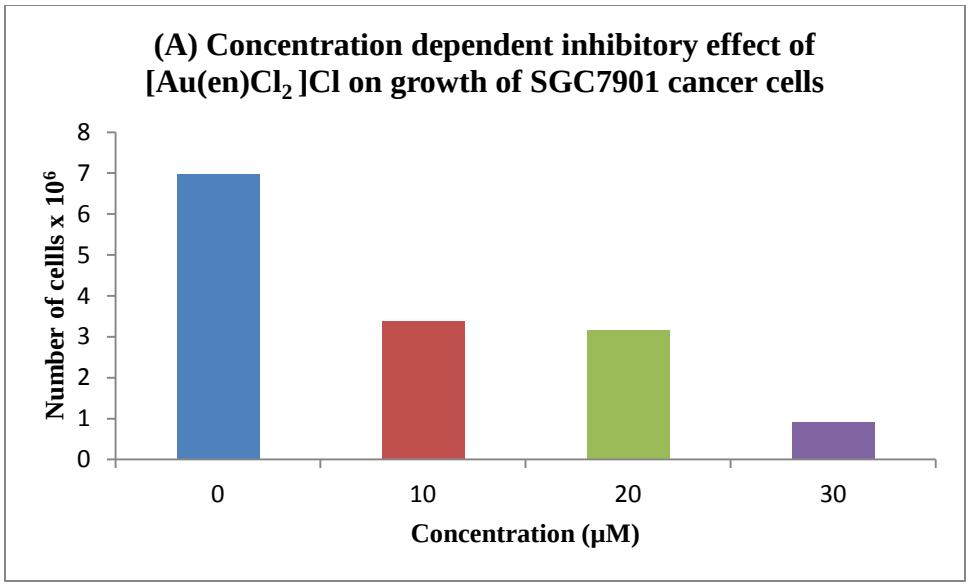

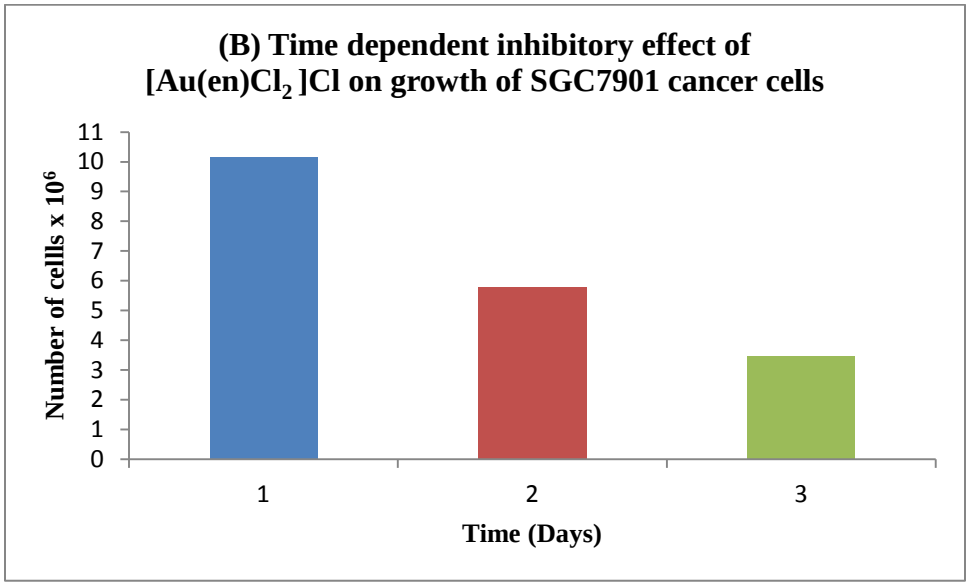

Figure 5.12 (A) Concentration dependent and (B) Time dependent inhibitory effect of complex 8 on SGC7901 cells growth.

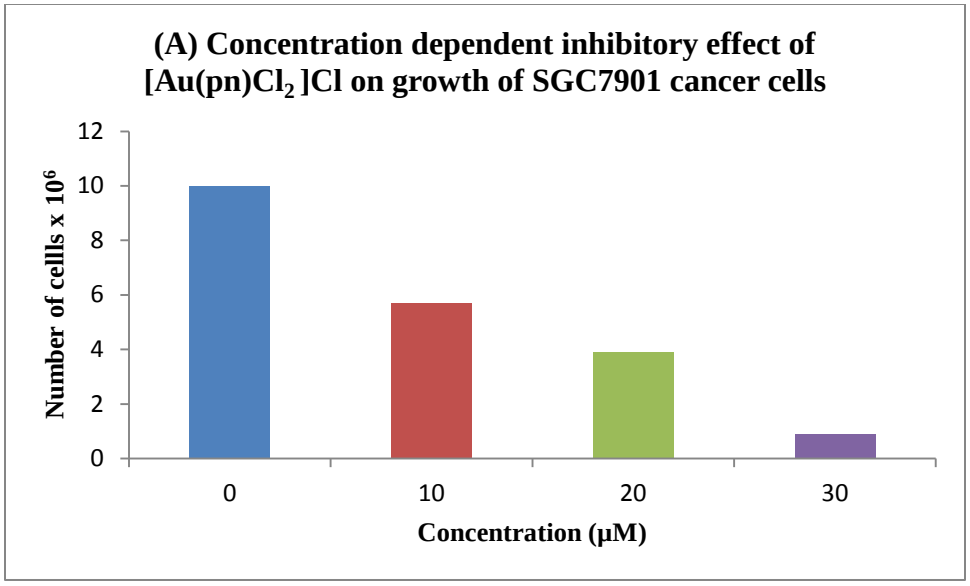

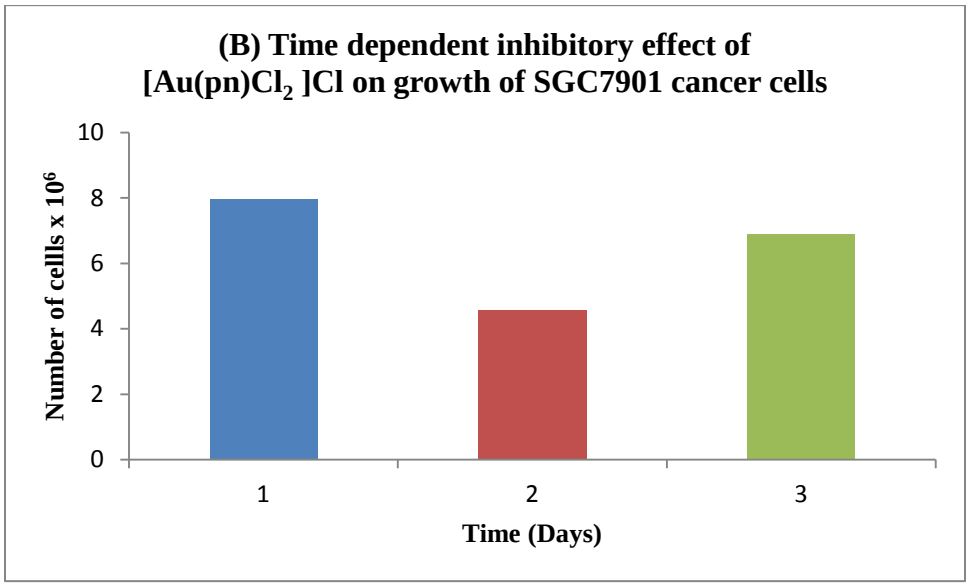

Figure 5.13 (A) Concentration dependent and (B) Time dependent inhibitory effect of complex 9 on SGC7901 cells growth

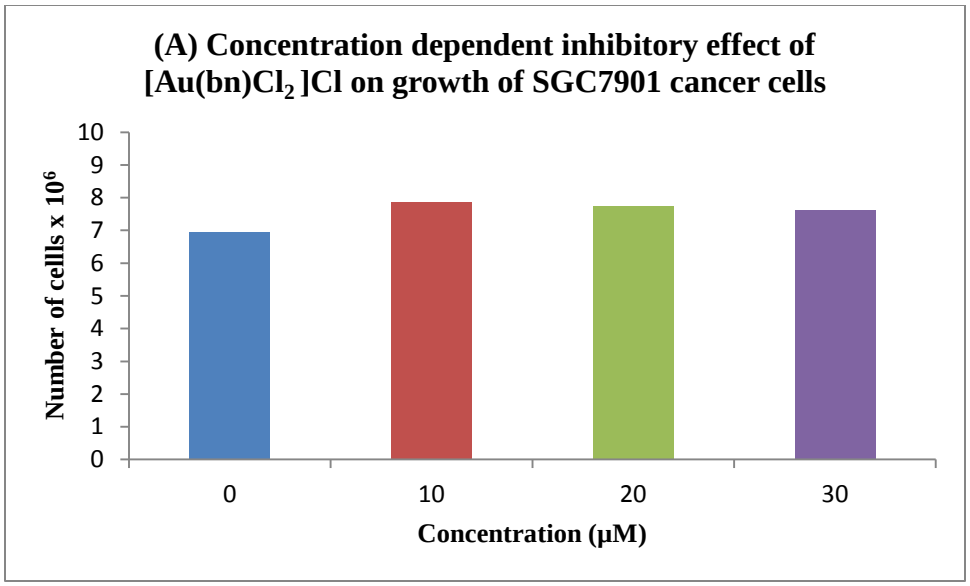

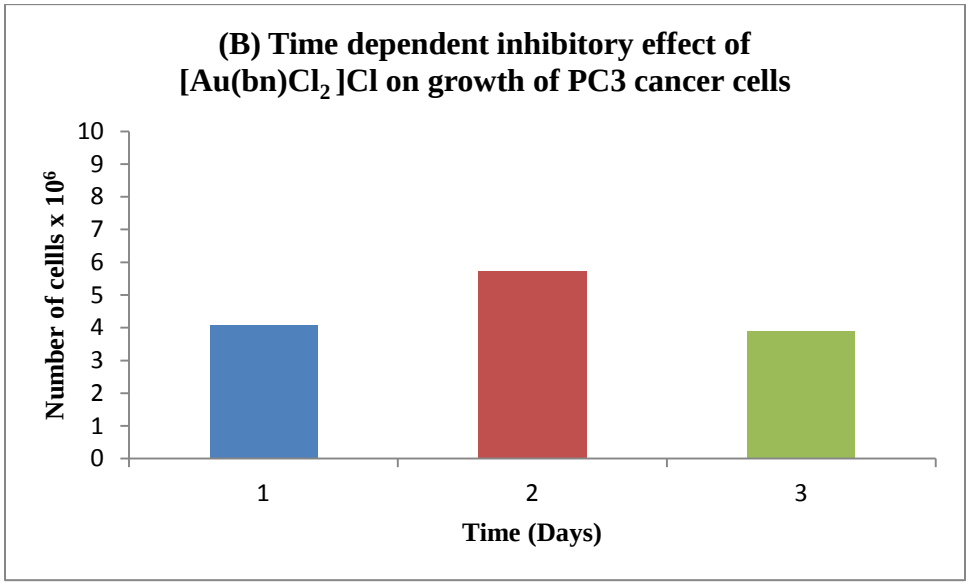

Figure 5.14 (A) Concentration dependent and (B) Time dependent inhibitory effect of complex 10 on SGC79013 cells growth

5.1.11 *in vitro* Cytotoxicity of Au(III) diamine complexes on ovarian cancer cell lines

The *in vitro* cytotoxicity of Au(III) diamine complexes (**1**) and **(8**) was evaluated in terms of IC_{50} on cisplatin sensitive ovarian A2780 cancer cells and cisplatin resistant ovarian A2780 cis cancer cells. The IC_{50} (μM) data are shown in Table 5.11. The cisplatin-resistant cell line A2780 cis is developed by chronic exposure of the parent cisplatin-sensitive A2780 cell line. In order to retain resistance, 1.0 μM cisplatin needs to be added to the media for A2780 cis every 2-3 passages.

IC_{50} data for cisplatin sensitive A2780 shows that [Au(*en*)$_2$]Cl_3 (**1**) and [Au(*en*)Cl_2]Cl (**8**) with IC_{50} values 4.6 and 5.0 are three times less *in vitro* cytotoxic agent than that of cisplatin with IC_{50} value 1.5, whearas IC_{50} data for cisplatin resistant A2780 cis cancer cell line shows that [Au(*en*)$_2$]Cl_3 (**1**) is slightly stronger cytototoxic agent while [Au(*en*)Cl_2]Cl (**8**) is slightly weaker cytotoxic agent than cisplatin with IC_{50} value of 12.8. Cisplatin has been included for comparison. Casini et al [29] also reported A2780 and A2780 cis data for the complex (**1**), and these are in agreement with our study.

Table 5.11 *in vitro* Cytotoxicity of Au(III) diamine complexes on ovarian cell lines

Complex	[a]IC_{50}		Fold Resistance
	A2780	A2780 cis	A2780 cis/A2780
Cisplatin	1.5 ± 0.2	12.8 ± 0.5	8.4
$[Au(en)_2]Cl_3$**(1)**	4.6 ± 0.3	10.6 ± 0.4	2.3
$[Au(en)Cl_2]Cl_3$**(8)**	5.0 ± 0.3	14.3 ± 0.5	2.9

[a]IC_{50} data are given with ± SD.

Each experiment was performed independently at least 3 times.

5.2 Gold(III) Complexes of Diamine and Thione Ligands

This work reports the synthesis of some $[(thione)_2Au(diamine)]Cl_3$ complexes where thione = 1,3-imidazolidine-2-thione (Imt), 1,3-Diazinane-2-thione (Diaz) and diamine = diaminoethane (*en*), 1,3-diaminopropane (*pn*) or 1,4-diaminobutane (*bn*).

5.2.1 Mid-IR characterization

The selected mid-IR frequencies are given in Table 5.12. The vibrational frequency for thione ligands ν(C=S) shows red shift upon complexation as a result of electron donation from sulfur to the metal center that promote Π-back donation to thione Π* orbital, this causes weakening of the C-S bond [66]. On the other hand, the N-H vibrational frequency, ν(N-H), was found to shift to higher wave number (blue shift) indicating the strengthening of N-H bond in complex compared to the free ligand, as a result of electron donation form sulfur.

Table 5.12 Mid-IR frequencies, ν(cm^{-1}) of Au(III) thione complexes

Compound	$\nu_{(N-H)}$, cm^{-1}	$\nu_{(C=S)}$, cm^{-1}
Imt	3200	506
$[(Imt)_2Au(en)]Cl_3$ **(11)**	3426 w	495
$[(Imt)_2Au(pn)]Cl_3$ **(12)**	3426 s	497
$[(Imt)_2Au(bn)]Cl_3$ **(13)**	3400 w	496
Diaz	3166	516
$[(Diaz)_2Au(en)]Cl_3$ **(14)**	3423 w	503
$[(Diaz)_2Au(pn)]Cl_3$ **(15)**	3444 m	505
$[(Diaz)_2Au(bn)]Cl_3$ **(16)**	3413 sh	506
Diap	3143	519
$[(Diap)_2Au(en)]Cl$ **(17)**	3418 m	507
$[(Diap)_2Au(pn)]Cl$ **(18)**	3428 m	509

5.2.2 Solution state NMR characterization

The ^{13}C NMR chemical shifts of thione and their complexes are given in Table 5.13. In ^{13}C resonances at 182.11 and 45.38 ppm correspond to S=C< (free Imt) and C-CH_2-NH (free Imt) respectively. The upfield chemical shift for S=C< carbon of Imt from 182.1 to about 175.8 ppm accounts for coordination of sulphur atom of of S=C< towards Au(III) centre. Chemical shifts at 173.34, 41.20 and 19.07 ppm correspond to S=C<, CH_2-NH and C-CH_2-C carbon atoms of free Diaz respectively. The larger upfield chemical shift for carbon of S=C< (bound Diaz) from 173.34 to about 166.51 ppm is consistent the ligation of sulfur of S=C< towards Au(III) center [137]. The smaller upfield shifts of C-CH_2-NH (bound Diaz) and C-CH_2-C (bound Diaz) also corroborates the binding of carbon of S=C< (bound Diaz) to Au(III). The evident upfield shift of carbon of S=C< bound thione in $[(thione)_2Au(diamine)]Cl_3$ with respect to free thiones indicates coordination of thiones through sulphur of S=C< to Au(III) centre as shown in Table

5.13. The ^{1}H NMR spectra for $[(thione)_2Au(diamine)]Cl_3$ complexes are very complicated because of the strained structures of diamine ligands and non-equivalency of hydrogen environments in the complexes [138]. ^{1}H NMR data were, therefore, found to be non-descriptive for such complexes.

Table 5.13 Solution state ^{13}C chemical shifts (ppm) for Au(III) thione complexes

Compound	S=C<(Imt)	C-CH_2-NH(Imt)		
Free Imt	182.11	45.38		
$[(Imt)_2Au(en)]Cl_3$ **(11)**	175.73	45.1		
$[(Imt)_2Au(pn)]Cl_3$ **(12)**	175.93	45.06		
$[(Imt)_2Au(bn)]Cl_3$ **(13)**	175.94	45.06		
	S=C<(Diaz)	C-CH_2-NH(Diaz)	C-CH_2-C(Diaz)	
Free Diaz	173.34	41.2	19.07	
$[(Diaz)_2Au(en)]Cl_3$ **(14)**	166.56	36.68	18.42	
$[(Diaz)_2Au(pn)]Cl_3$ **(15)**	166.59	36.33	18.42	
$[(Diaz)_2Au(bn)]Cl_3$ **(16)**	166.51	38.38	18.4	
	S=C<(Diap)	C-CH_2-NH(Diap)	C-CH_2-C(Diap)	C-CH_2-C(Diap)
Free Diap	163.34	40.13	18.34	16.07
$[(Diap)_2Au(en)]Cl_3$ **(17)**	159.23	37.13	18.01	15.79
$[(Diap)_2Au(pn)]Cl_3$ **(18)**	159.02	36.43	17.91	15.67

5.2.3 Solid state NMR characterization

The Solid state NMR data for the complexes are given in Table 5.14. The thiocarbonyl resonances in the ligands Imt and Diaz, appear at 180.6 and 175.6 ppm respectively [139]. So it can be seen that thiocarbonyl carbons are de-shielded by about 12 to 17 ppm relative to the free ligand, confirming the coordination through the sulfur atom of the thione group. The high values of ^{15}N chemical shifts are assigned to Imt and Diaz nitrogens, whereas the low value of ^{15}N chemical shift is assigned to the diamine ligands. The ^{15}N shifts of the diamines in the complexes show lower shifts of 5-17 ppm, compared to that in the free ligands. These shifts indicate an increase in electron density at the nitrogen atom, in agreement with literature [138].

Table 5.14 Solid state ^{13}C and ^{15}N NMR chemical shifts of Au(III) thione complexes

Complex	Nucleus	δ_{iso}	σ_{11}	σ_{22}	σ_{33}	Span	Skew	Other
(**11**)	^{13}C	155.41						46.78
	^{15}N	-260.14, -335.83						
(**12**)	^{13}C	177.03	257	183	90	167	0.116	46.58
	^{13}C	154.9	221	163	81	139	0.175	
	^{15}N	-258.2						
(**13**)	^{13}C	176.93	252	193	86	167	0.289	46.29
	^{15}N	-259.6						
(**14**)	^{13}C	166.74	241	186	73	168	0.351	42.70, 19.41
	^{13}C	149.37	223	143	82	141	-0.127	
	^{15}N	-357.6						
(**15**)	^{13}C	167.31						43.48, 19.50
	^{15}N	-337.47						
(**16**)	^{13}C	171.69	244	189	83	161	0.319	44.74, 27.46
	^{15}N	-205.2						

[a]Isotropic shielding, $\sigma_{iso} = (\sigma_{11} + \sigma_{22} + \sigma_{33})/3$

$\Delta\sigma = \sigma_{33} - 0.5(\sigma_{11} + \sigma_{22})$

[b]$\eta = 3(\sigma_{22} - \sigma_{11}) / 2\Delta\sigma$

5.2.4 Computational analysis

Built and optimized structures were analyzed computationally for vibrational frequencies and NMR data using B3LYP/LanL2DZ level of theory, to facilitate the spectroscopic data interpretation. Selected bond length and torsion angles of the computationally optimized structures are presented in Table 5.15 and Table 5.16 respectively. Comparisons of calculated bond lengths show that the C-S bond of thione becomes longer after complexation due to Π-back donation; this agrees with the experimental mid-IR data that shows red shift upon complexation.

Additionally, C-S bonds were longer in Diaz complexes compared to C-S bond length in Imt complexes. It is obviously an indication of larger Π-back donation as well as stronger bond in Diaz complexes. In general, this observation agrees also with the higher up-field shift effect on Diaz C-S carbon as detected by 13C NMR, which clarify the higher back donation in Diaz complexes. After optimization, the built complexes showed square planar structures around the gold(III) center; S-Au-N angles were ranging from 173o to 179o. Optimized geometries of [(thione)2Au(diamine)]Cl3 complexes (11-16) at the B3LYP/LanL2DZ level of theory using Gaussian 09, Revision A. 1 are shown in

Figure 5.15.

Table 5.15 Selected bond lengths (Å) drived computationally for $(thione)_2Au(diamine)]^{3+}$ structures

Bond	$[(Imt)_2Au(en)]^{3+}$	$[(Imt)_2Au(pn)]^{3+}$	$[(Imt)_2Au(bn)]^{3+}$	$[(Diaz)_2Au(en)]^{3+}$	$[(Diaz)_2Au(pn)]^{3+}$	$[(Diaz)_2Au(bn)]^{3+}$
Au-N1	2.163	2.159	2.157	2.167	2.174	2.177
Au-N2	2.173	2.171	2.157	2.167	2.164	2.156
Au-S1	2.473	2.483	2.493	2.474	2.481	2.482
Au-S2	2.471	2.482	2.493	2.474	2.477	2.480
S1-C	1.825	1.824	1.829	1.859	1.851	1.851
S2-C	1.824	1.823	1.829	1.859	1.851	1.852

Table 5.16 Selected torsion angle (°) drived computationally for $[(thione)_2Au(diamine)]^{3+}$ structures

Angle	$[(Imt)_2Au(en)]^{3+}$	$[(Imt)_2Au(pn)]^{3+}$	$[(Imt)_2Au(bn)]^{3+}$	$[(Diaz)_2Au(en)]^{3+}$	$[(Diaz)_2Au(pn)]^{3+}$	$[(Diaz)_2Au(bn)]^{3+}$
S1-Au-N1	93.87	89.37	86.79	93.24	87.37	86.79
S2-Au-N2	91.93	87.43	86.79	93.23	90.20	86.79
N1-Au-N2	81.81	90.71	94.40	81.84	90.73	94.40
S1-Au-S2	92.53	92.66	92.18	91.89	91.76	88.35
S1-Au-N2	174.55	176.96	176.75	173.98	176.16	176.10
S2-Au-N1	173.15	176.16	176.76	173.98	176.96	177.07
Au-S1-C	106.76	107.14	108.57	108.65	110.14	109.41
Au-S2-C	110.77	111.74	108.57	108.66	110.14	109.47

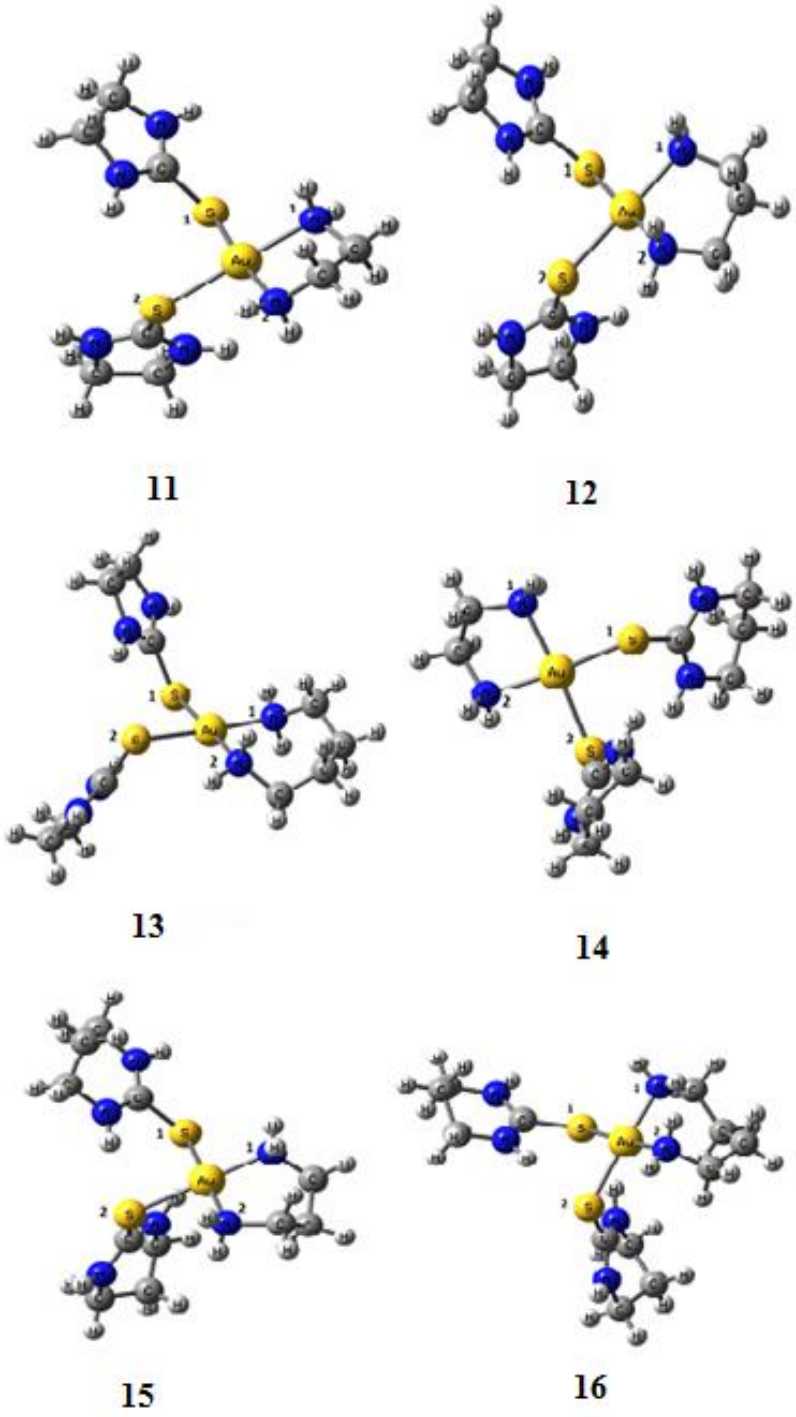

Figure 5.15 Computationally optimized structures of $[(thione)_2Au(diamine)]^{3+}$ complexes

5.2.5 *in vitro* Cytotoxicity of Au(III) thione complexes

The EAE (Experimental Autoimmune Encephalomyelitis) was evaluated for its antiproliferative effect using MTT assay. The $[(thione)_2Au(diamine)]Cl_3$ complexes inhibited the proliferation of C6 glioma cells in a concentration dependent manner. IC_{50} values were calculated from the growth curve using MTT assay (Figure 5.*16*). It showed values of inhibition 42, 36, 73, 152, 62, 61 μg/mL for $[(thione)_2Au(diamine)]Cl_3$ complexes **11, 12, 13, 14, 15 and 16** respectively. Therefore, the $[(thione)_2Au(diamine)]Cl_3$ complexes **11, 12, 15 and 16** were more effective for the C6 glioma cells.

It is evident from IC_{50} values that Imt containing Au(III) complexes (**11-13**) are relatively better cytotoxic agents than Diaz containing Au(III) complexes (**14-16**). As far as cytotoxicity against C6 glioma cells is concerned, the five member thione ring (Imt) is fairly better ligand than the six member thione ring (Diaz). However, the six member Au(III) chelates (**12** and **15**) with 1,3-Diaminopropane (pn) are comparatively better cytotoxic agents than five member chelate (1 and 4) with 1, 2-diaminoethane (en) as well as seven member chelate (**13** and **16**) with 1,4-diaminobutane (bn). It can be concluded that structural features e.g. ring size of thione ligand (Imt and Diaz) as well as Au(III) chelate size with diamine (*en*, *pn* and *bn*) may affect *in vitro* cytotoxicity of complex against C6 glioma cell line.

The MTT results based on phase contrast micrographs showed a decrease in cell density on treatment with different concentrations of extract. Significant numbers of cells were

found to be round, detached and floating at higher concentrations and the samples were photographed after removing dead floating cells to improve the quality of images.

Even though the anticancer efficacy of imidazolidine-2-thione (Imt) and ethylenediamine (*en*) of $[(thione)_2Au(diamine)]Cl_3$ complexes has independently been reported, so far their chemotherapeutic potential as a combined complex has not been analyzed.

The Imidazolidine-2-thione (Imt) containing complexes $[(Imt)_2Au(en)]Cl_3$ (**11**) and $[(Imt)_2Au(pn)]Cl_3$ (**12**) showed toxicity profiles comparable to cisplatin [140] which has been documented to have an overall IC_{50} in the range of 10.9-67.0 µM. Yildrim *et al.* reported the IC_{50} data of some anticancer compounds specifically against glioma C6 cell lines [141]. They tested anti-proliferative activity of novel platinum compounds against C6 glioma cells and demonstrated an IC_{50} range of 16.75-28.75 µg/mL with respect to cisplatin. Comparison with other gold(III) compounds has scarcely been studied.

Pivetta *et al.* analyzed the role of imidazolidine-2-thione as an anticancer agent in combination with other metal ions [142]. They found a high *in vitro* cytotoxicity of imidazolidine-2-thione copper (II) complexes in mouse neuroblastoma N2a cells. Imidazolidine influences apoptosis, a mechanism of programmed cell death functioning to eliminate damaged, mutated or cancerous cells. Chemotherapeutic agents cause simultaneous activation of apoptotic signals and induction of anti-apoptotic factors, such as NF-kappa B and subsequently diminish the overall efficacy of the administered drug. Sharma *et al.* [143,144] described imidazoline to modulate the NF-kappa B pathway by preventing its nuclear translocation and selectively sensitizing the cancer cells toward DNA damaging agent. The pretreatment of cancer cells with the imidazoline causes a

significant increase in apoptosis resulting in augmented efficacy of camptothecin and cisplatin. Comparative studies are required to interpret the functional advantages of alkyl substituted thiones and to establish structure-activity relationship (SAR) using different ring size of thiones (Imt, Diaz and Diap) incorporation in the gold(III) complexes.

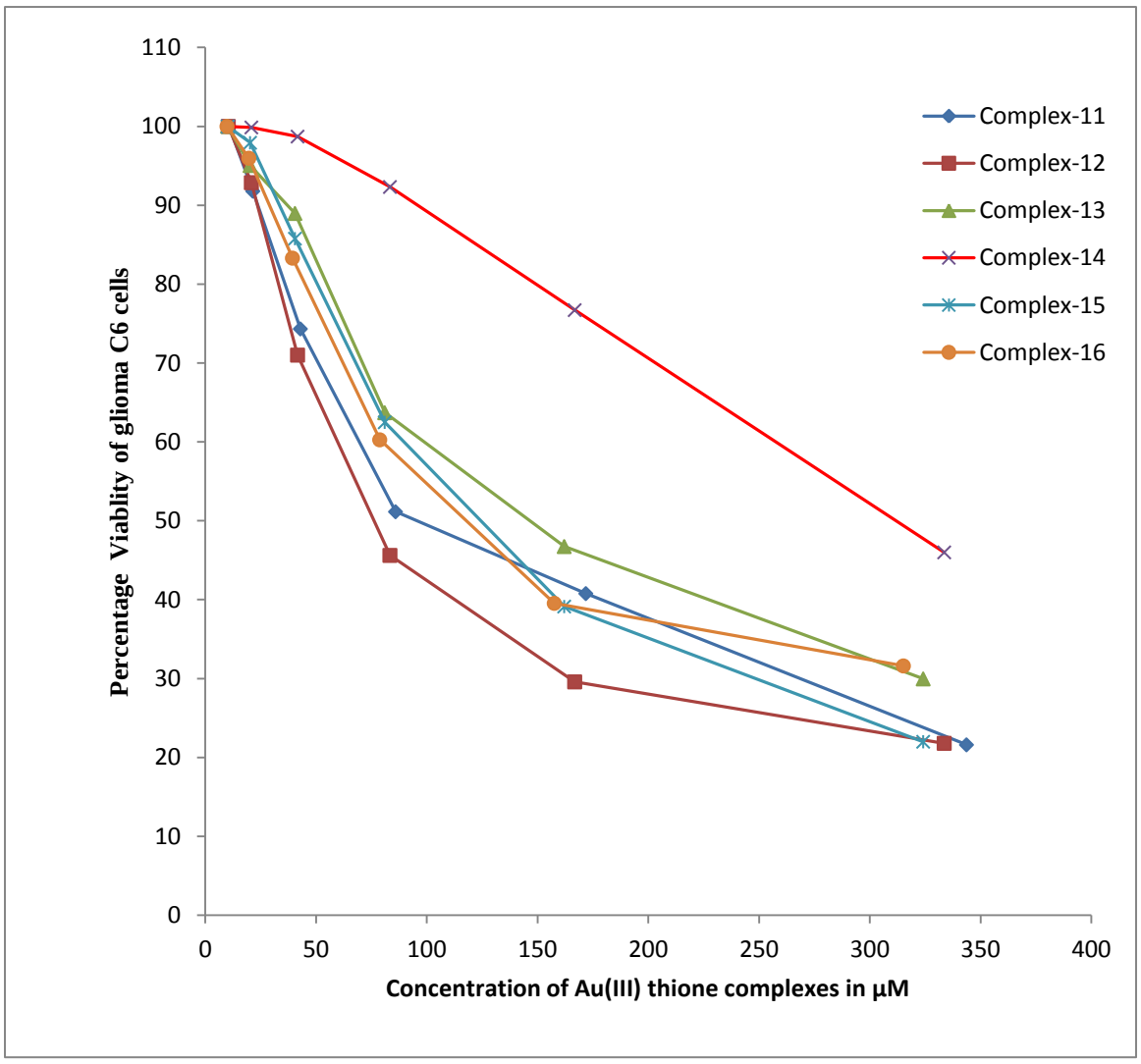

Figure 5.*16 in vitro* Cytotoxicity of Au(III) thione complexes on C6 glioma cell line

5.3 Cyanido(diamine)Mercury(II) complexes

This work reports the synthesis and characterization of some Hg(II) diamine complexes with general formula [(diamine)Hg(II)(cyanido)$_2$] where cyanido = CN^- and diamine = *en*, *pn*, N-Me-*en*, N,N'-Me_2-*en*, N,N'-Et_2-*en* and N,N'-ipr_2-*en*.

5.3.1 Mid-IR Studies

Selected mid-IR bands for the free ligands, Hg(II) precursor and the prepared complexes are given in Table 5.17. A sharp band around 3300 cm^{-1} was observed for all the complexes indicating the presence of diamines. The C≡N stretching frequency of $Hg(CN)_2$ is observed at 2191 cm^{-1}. For all prepared complexes (**19-24**), only one ν(C≡N) mode was observed, at lower frequency compared to the free $Hg(CN)_2$. For example, in case of the complex (**19**), the ν(C≡N) shift appears about 33 cm^{-1} towards lower frequency than that of the cyanide precursor. This is consistent with a significant back donation of electron density from the metal to the empty π* orbitals of cyanide upon coordination to the diamines. The changes in ν(N–H) between ligands and corresponding complexes are small and within experimental error.

In comparison to other mercury complexes previously reported by our group, it is clear that the reaction between amines and $Hg(CN)_2$ is more favorable than with $Hg(SCN)_2$ and $Hg(SeCN)_2$ because the signals at CN region for all complexes are obtained [100,102]. This shows that the $Hg(CN)_2$ complex is the most stable, while the $Hg(SCN)_2$ and $Hg(SeCN)_2$ complex is least stable with some exceptions. In a similar point of view, in the case of d^{10} metals, a comparison of the shift differences in C≡N region for $Zn(CN)_2$, $Cd(CN)_2$ and $Hg(CN)_2$ are worthy enough to mention. It is observed that the

shift difference is greater for Zn(II) complexes and less for Hg(II) and Cd(II) complexes [103,145]. This suggests that cyanide forms more stable complexes with Zn(II) than with Hg(II) and Cd(II).

Table 5.17 Mid-IR data of Hg(II)$(CN)_2$-diamine complexes

Compound	ν(N-H)	ν(C-N)	ν(C≡N)
$Hg(CN)_2$	---	---	2191
en	3393	1033	---
[(en)$Hg(CN)_2$] **(19)**	3378	1571	2158
pn	3282	1093	---
[(pn)$Hg(CN)_2$] **(20)**	3280	1558	2154
N-Me-*en*	3282	1130	---
[(N-Me-en)$Hg(CN)_2$] **(21)**	3294	1590	2166
N,N'-Me_2-*en*	3288	1148 w, 1103 m	---
[(N, N´-Me-en)$Hg(CN)_2$] **(22)**	3253	1454	2169
N,N'-Et_2-*en*	3235	1125	---
[(N, N´-Et-en)$Hg(CN)_2$] **(23)**	3245	1448	2166
N,N'-ipr_2-*en*	3249	1173	---
[(N, N´-iPr-en)$Hg(CN)_2$] **(24)**	3247	1495	2168

5.3.2 Solution state NMR studies

The ^{13}C and ^{15}N NMR chemical shifts of various complexes are summarized in Table 5.18 and Table 5.19 respectively. In all prepared complexes, upfield ^{13}C NMR chemical shifts were observed with respect to the free ligands. Similar to the polymeric [*bn*-$Hg(CN)_2$] complex, the ^{13}C NMR spectrum of [*en*-$Hg(CN)_2$] shows no significant shift in the cyanide signal upon complexation with *en* ligand, while a downfield shift of around 3 ppm was observed for the *en* ligand carbons. This shift may be due to the flow of electron density from C to N, in the complexes [98,103,146–149].

On the other hand, the ^{15}N NMR signal of complex **2** is shifted downfield compared that of the free ligand, 1,3-diaminopropane (*pn*). However, no significant shift difference was observed between the complexes. For example, ^{15}N NMR chemical shift of ethylenediamine ring nitrogens in complexes (**22** and **24**) is very similar to that of the propylenediamine ring in complex (**20**).

The ^{13}C and ^{15}N NMR chemical shifts of various complexes are summarized in Table 5.18 and Table 5.19 respectively. With few exceptions, upfield ^{13}C NMR chemical shifts were observed with respect to the free ligands. Similar to the polymeric [*bn*-$Hg(CN)_2$] [150], the ^{13}C NMR spectrum of [*en*-$Hg(CN)_2$] shows shift in cyanide signal upon complexation with en, while a downfield shift of around 3 ppm was observed for the ethylenediamine (en) carbons. This shift may be due to the flow of electron density from C to N, in the complexes [98,146,147,149]. The ^{15}N NMR signal of complex (**20)** is shifted upfield compared to that of pn·HCl. However, shift difference was observed between the complexes. For example, ^{15}N NMR chemical shift of ethylenediamine ring nitrogen atoms in complexes (**22** and **24**) is very similar to that of the propylenediamine ring in complex (**20**).

Table 5.18 ^{13}C NMR chemical shifts of $Hg(CN)_2$-diamine complexes

Compound	^{13}C-N	C-1	C-2	C-3
$Hg(CN)_2$	145.15			
en		45.05		
[(en)$Hg(CN)_2$] **(19)**	144.24	42.12		
pn		39.86	37.33	
[(pn)$Hg(CN)_2$] **(20)**	143.28	38.02	35.45	
N-Me-en		36.26	46.37	
[(N-Me-en)$Hg(CN)_2$] **(21)**	144.42	41.48	31.26	
N, N'-Me_2-*en*		51.43	36.49	
[(N, N'-Me_2-*en*)$Hg(CN)_2$] **(22)**	143.28	50.17	35.99	
N, N'-ipr_2-*en*		48.82	47.57	23.09
[(N, N'-ipr_2-*en*)$Hg(CN)_2$] **(24)**	143.46	49.03	47.11	22.21

Table 5.19 ^{15}N NMR chemical shifts of $Hg(CN)_2$-diamine complexes

Compound	^{15}N (δ in ppm)
pn•HCl	-343.12
[(*pn*)$Hg(CN)_2$] **(20)**	-363.52
[(N, N'-Me_2-*en*)$Hg(CN)_2$] **(22)**	-363.19
[(N, N'-ipr_2-*en*)$Hg(CN)_2$] **(24)**	-362.34

5.3.3 Solid state CPMAS NMR characterization

Table 5.20 shows Solid state NMR data for the complexes studied. ^{199}Hg signals in the complexes are almost 1000 ppm de-shielded from those in $Hg(CN)_2$, with the change in geometry and coordination of two nitrogen atoms to ^{199}Hg (Figure 5.17 and Figure 5.18). This is a clear confirmation that the complexes are formed. As reported for some mercury cyanide/chloride double salts, these complexes have a see-saw effective coordination geometry based upon characteristic linear coordination [151]. The C–Hg–C bond angles in their complexes are the range 150–160 º. The Hg anisotropies are 2300–3400 ppm in our earlier studies [100] on $Hg(CN)_2$ complexes with imidazolidine-2-thiones and its derivatives, the anisotropies of ^{199}Hg (1400–2000 ppm) have been rationalized in terms of stronger coordination of sulfur compared to chloride, making the C–Hg–C angle less than 150 º; that is closer to a highly distorted tetrahedral geometry. The computed C–Hg–C bond angle for (**19**) described here is 157.89 º and the diamine is weakly coordinated. So, the ^{199}Hg anisotropies in the complexes under study here are 1000 ppm, perhaps indicating weaker binding of diamines to $Hg(CN)_2$; that is also indicated by the calculated structural parameters. ^{13}C and ^{15}N CPMAS spectra show two distinct resonances for CN for complexes (**23**, **22 and 24**) as shown in Figure 5.19, Figure 5.20 and Figure 5.21 respectively, indicating two chemically different environments for CN. This suggests that two distinct molecules may exist in a unit cell, or one CN is H-bonded and the other is free. The nitrogen resonances in CN show skew values of 1.00 indicating that axial symmetry is maintained, whereas the carbon resonances show skew values less than 1.00. The ^{15}N signals from $–NH_2$ or NH is slightly overlapped with CN side bands and we can only pick out one type of resonance for this nucleus.

Table 5.20 Solid state ^{13}C, ^{15}N and ^{199}Hg isotropic chemical shifts (δ_{iso}) and principle shielding tensors (σ_{xx}) of Hg(II) cyanide complexes with diamines

Complex	Nucleus	δ_{iso}	σ_{11}	σ_{22}	σ_{33}	Ω (Span[a])	κ (Skew[b])
$[Hg(CN)_2]$	$^{13}C_{(CN)}$	---					
	^{119}Hg	-1396					
(**19**)	$^{13}C_{(CN)}$	163.7	282.22	192.84	13.94	267	0.6
	^{15}N	-125.2					
	^{15}N(en)	-315.5					
	^{199}Hg	-503	30.79	-555.35	-985.61	1016	0.805
(**22**)	i) $^{13}C_{(CN)}$	145.3	291.9	207.7	-63.7	355.6	0.53
	ii) $^{3}C_{(CN)}$	143.5	274.8	235.8	-80.1	354.9	0.78
	i)$^{15}N_{(CN)}$	-92.5	110.3	110.3	-498.3	608.3	1
	ii)$^{15}N_{(CN)}$	-95.9	101.1	101.1	-489.9	590.9	1
	$^{15}N_{(en)}$	-348.5					
	^{119}Hg	-311.5					
(**23**)	i)$^{13}C_{(CN)}$	142.9	214.5	214.5	-0.39	214.9	1
	ii)$^{13}C_{(CN)}$	145.8	217.4	217.4	2.5	214.9	1
	i) ^{119}Hg	-365.7	157.5	-306.9	-947.7	1105.2	0.16
	ii) ^{119}Hg	-371.6	159.5	-332.5	-942	1101.5	0.11
(**24**)	$^{13}C_{(CN)}$	146.5	249.1	249.1	-58.7	307.9	1
	$^{15}N_{(CN)}$	-91.9	72.7	72.7	-421	493.7	1
	$^{15}N_{(en)}$	-316.3					
	^{119}Hg	-504.3	-29.4	-408.6	-1074.4	1045.4	0.28

[a] Isotropic shielding, $\sigma_{iso} = (\sigma_{11} + \sigma_{22} + \sigma_{33})/3$

$\Delta\sigma = \sigma_{33} - 0.5(\sigma_{11} + \sigma_{22})$

[b] $\eta = 3(\sigma_{22} - \sigma_{11}) / 2\Delta\sigma$

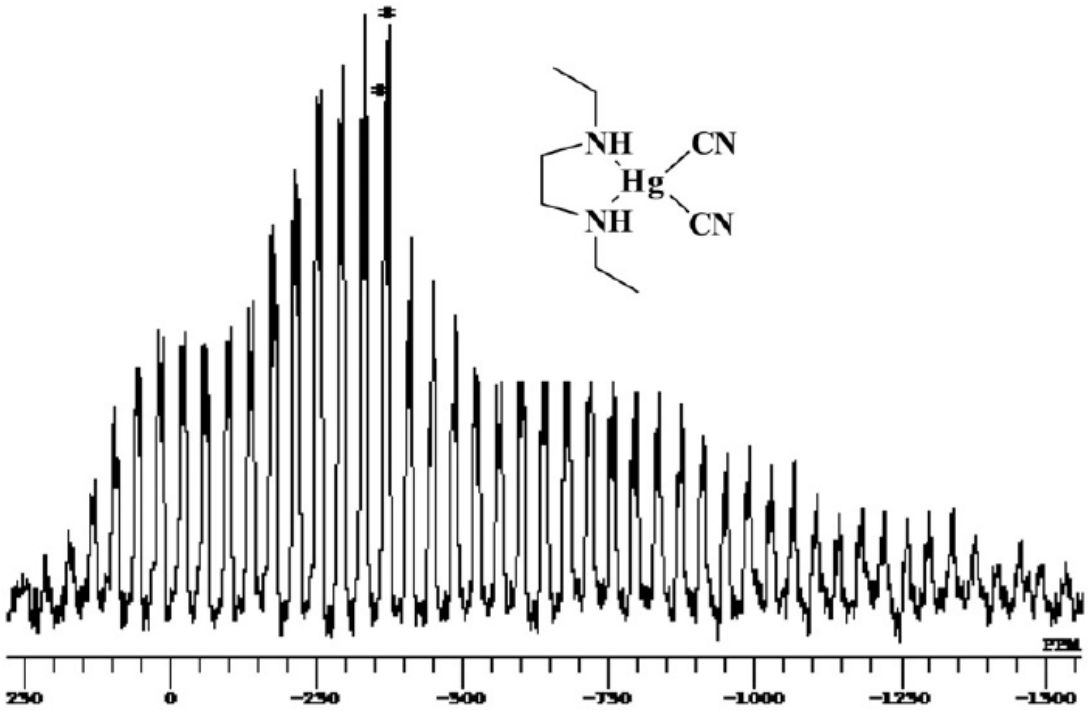

Figure 5.17 ^{199}Hg CPMAS spectrum of (23).

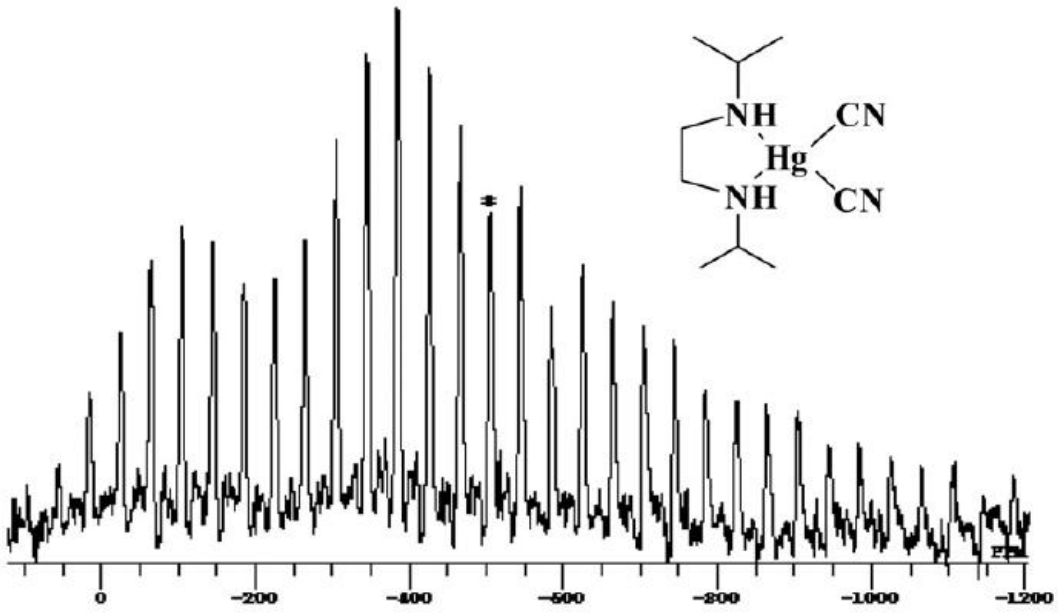

Figure 5.18 ^{199}Hg CPMAS spectrum of (24).

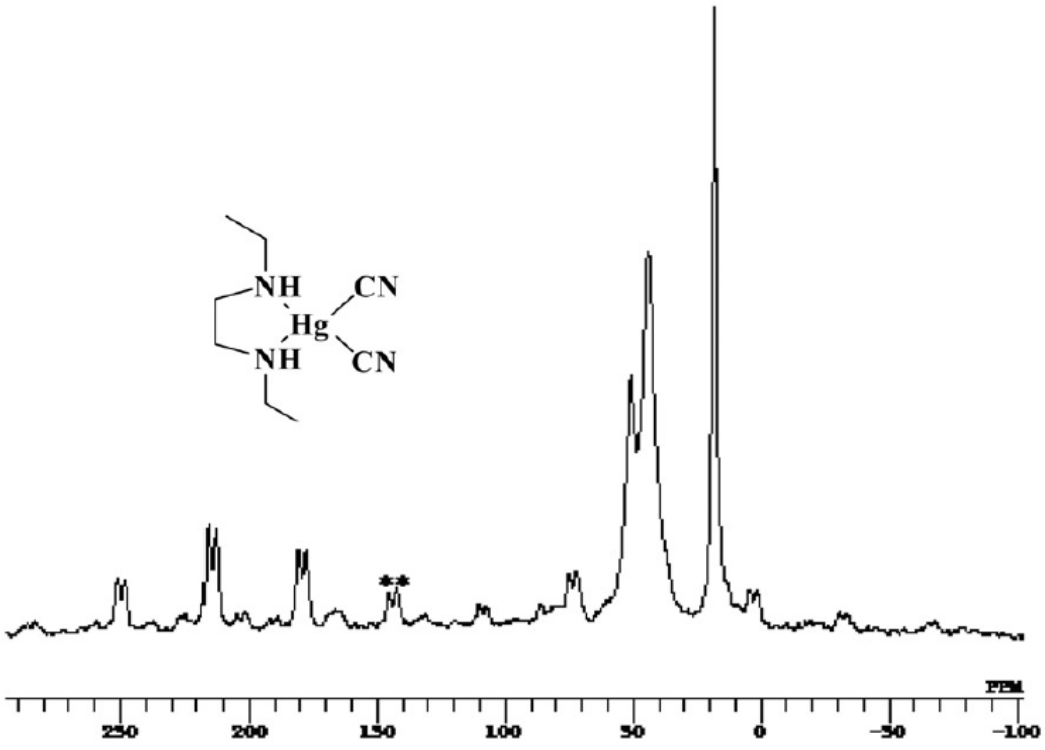

Figure 5.19 ^{13}C CPMAS spectrum of (23).

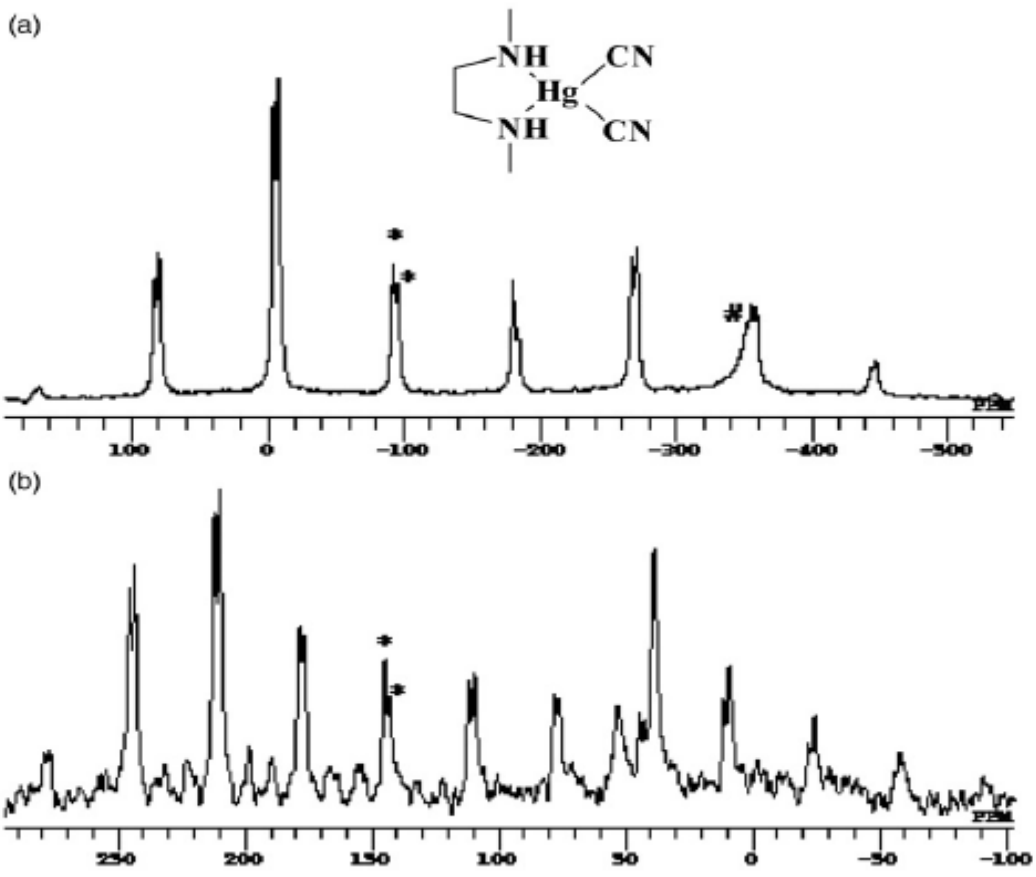

Figure 5.20 (a) ^{15}N and (b) ^{13}C CPMAS spectra of (22)

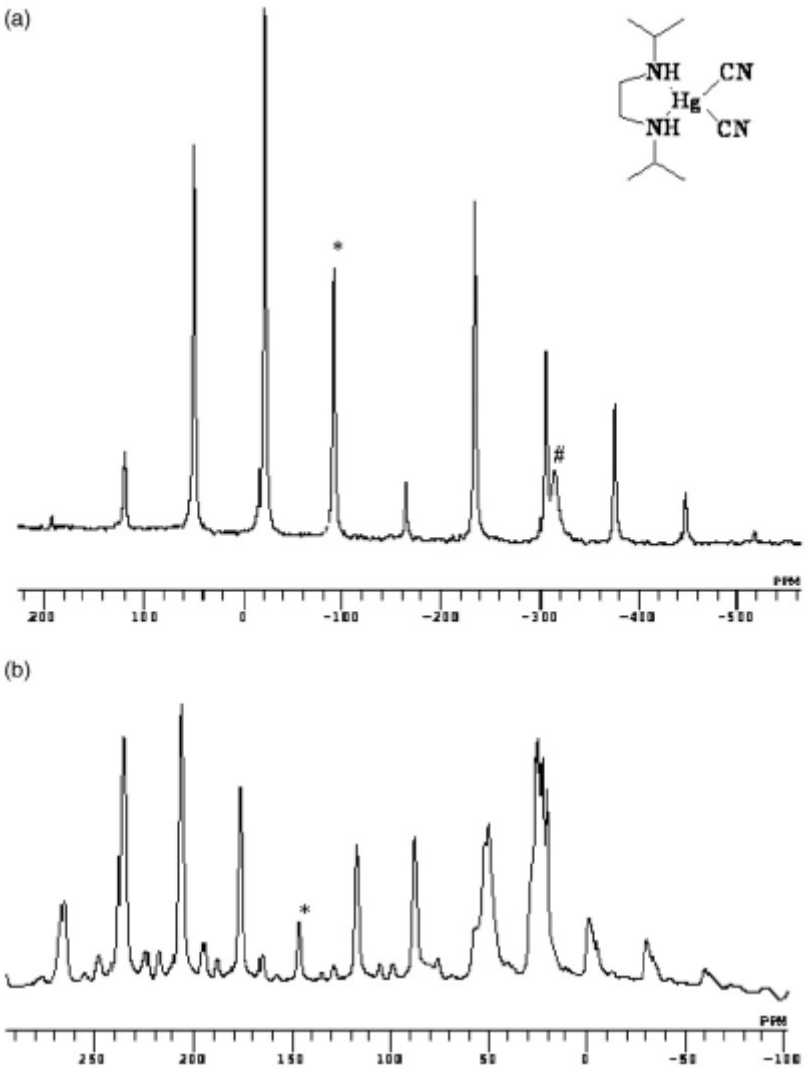

Figure 5.21 (a) ^{15}N and (b) ^{13}C CPMAS spectra of (24).

5.3.4 Computational analysis

The computationally optimized structures of **19** and **20** are shown in Figure 5.22. The selected bond lengths and bond angles of the optimized structures are presented in Table 5.21 and Table 5.22 respectively. In both complexes, Hg atom exhibits a severly distorted tetrahedral geometry completed by the two N atoms of diamines and two C atoms of the cyanide groups. The Hg-N and Hg-C bond distances and most of the bond angle values are in agreement with those observed in other reported complexes [150,152–154].

In both **19** and **20**, the Hg-C distance is slightly longer than that in the structure of $Hg(CN)_2$ (2.015(3) Å) [48]. The C-Hg-C angles in **19** and **20** are 157.89^o and 156.36^o respectively, which are much larger than the normal tetrahedral value of 109.5^o. These large angles are counter balanced by the very small N-Hg-N bond angles of 72.20^o and 81.06^o for **19** and **20** respectively. This tetrahedral distortion as well as somewhat longer Hg-N distances than those in $[Hg(CN)_2$-*bn*$]_n$ indicate a weak binding of diamine ligands to Hg(II). The C-Hg-N bond angles in **19** and **20** are 97.45 and 100.91 respectively. In comparison to *bn* (1,4-diaminobutane), which formed a linear polymeric complex $[Hg(CN)_2$-*bn*$]_n$, the diamines used in this study, *en* and *pn* are found to form chelates, **19** and **20**. As indicated by the N-Hg-N bong angles, the chelate formed by *pn* is less strained than that of *en*.

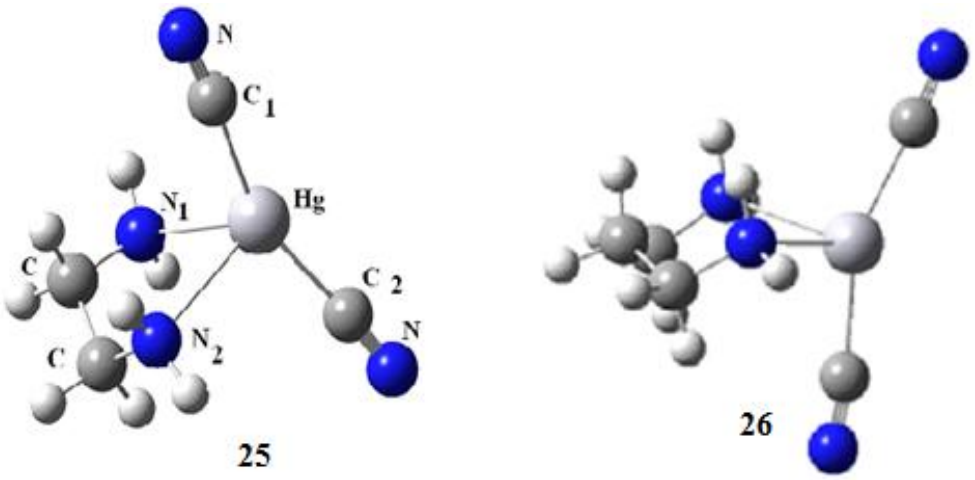

Figure 5.22 Computationally optimized structure of complexes (25 and 26)

Table 5.21 Selected bond lengths derived computationally for 19 and 20 complexes

Complex	Bond	Length (Å)
19	C≡N	1.189
	Hg-C	2.208
	Hg-N	2.59
	C-N	1.496
	C-C	1.541
20	C≡N	1.189
	Hg-C4	2.211
	Hg-C5	2.218
	Hg-N1	2.568
	Hg-N2	2.568
	C1-N2	1.498
	C3-N1	1.498
	C1-C2	1.544

Table 5.22 Selected bond angles derived computationally for 19 and 20 complexes

Complex	Bonds	Angle (^{o})
19	Hg-C≡N	175.53
	C-Hg-C	157.89
	C1-Hg-N1	97.45
	C2-Hg-N1	100.5
	C-N-Hg	106.87
	N-Hg-N	72.2
20	Hg-C4-N3	176.43
	C4-Hg-C5	156.36
	C4-Hg-N1	100.92
	C2-Hg-N2	100.92
	C1-N2-Hg	112.37
	C3-N1-Hg	112.38
	N1-Hg-N2	81.07

5.3.5 Bioactivity studies

The antibacterial activities of $Hg(CN)_2$ and two of its complexes estimated by minimum inhibitory concentrations (MIC; μg mL^{-1}) are given in Table 5.23. The results show that the complex **19** in DMSO is particularly effective in inhibiting the growth of tested bacteria. The compound **20** although shows some activity against two of the microbes, in general, it was found to be highly resistant against all four bacteria. A comparison between the activity of **19** and **20** against the most sensitive organism, *E. coli* shows that the minimum concentration increased from 775 to 930 μg/mL in water and 720 to 950 μg/mL in DMSO as we move from **19** to **20**. The greater activity of **19** may be related to its less stability originated from a more strained ring of the chelate so that the ligand could be easily replaced by biological ligands.

Table 5.23 Antibacterial activities of Hg(II)$(CN)_2$-diamine complexes

Test organism	$Hg(CN)_2$ in water	$Hg(CN)_2$ in DMSO	**19** in water	**19** in DMSO	**20** in water	**20** in DMSO
HPC	>1000	950	850	825	>1000	>1000
P. Aeruginosa	950	900	800	750	>1000	>1000
F. Streptococcus	>1000	>1000	800	750	975	940
E. Coli	850	800	775	720	930	950

5.4 Cadium(II) and Mercury(II) Selenocyanate Complexes

This work reports the synthesis and characterization of some Cd(II) and Hg(II) selenocyanate complexes with general formula [(L)M(II)(selenocyanate)$_2$] where selenocyanate = $SeCN^-$; M(II) = Cd(II) or Hg(II) and L=Gly or His.

5.4.1 Mid-IR studies

The C≡N stretching frequency for $Hg(SeCN)_2$ is higher than that of $Cd(SeCN)_2$. It means that C-N bond in $Hg(SeCN)_2$ is relatively stronger than that in $Cd(SeCN)_2$. It is because of less electron density at the selenium atom that derives more π-back donation from Hg to Se. In Table 5.24, the mid-IR data shows highest red shift for selenocyanate stretching frequency for histidine complex of mercury. It means that there is the highest π-back donation from the metal to the selenocyanate in histidine complex owing to the greater donation to the anti-bonding π-orbitals of the cyanate from selenium atom. It is clearly an indication of stronger histidine mercury bonding than that of the rest of the complexes series.

In general, there is a good agreement of the experimental and theoretical mid-IR stretching bands observed for the prepared complexes with some blue shift of the calculated results due to the intermolecular interaction in the real mid-IR experiment.

Table 5.24 Mid-IR frequencies, ν(cm^{-1}) $M(SeCN)_2$ complexes with Gly and His

Compound	ν(C=O) Exp.	ν(C=O) Theo.	ν(SeCN) Exp.	ν(SeCN) Theo.	ν(NH_2) Exp.	ν(NH_2) Theo.
KSeCN	-	-	2070[a]	-	-	-
L-Gly	1606 s	-	-	-	3424	-
L-Hist	1634 s	-	-	-	3127	-
$Cd(SeCN)_2$	-	-	2107	-	-	-
[(L-Gly)$Cd(SeCN)_2$] **(25)**	1611 s	1759	2107	2127	3450	3455
[(L-Hist)$Cd(SeCN)_2$] **(26)**	1631 s	1718	2109	2112	3460	3402
$Hg(SeCN)_2$	-	-	2127	-	-	-
[(L-Gly)$Hg(SeCN)_2$] **(27)**	1611 s	1742	2130	2137	3447	3476
[(L-Hist)$Hg(SeCN)_2$] **(28)**	1636 s	1716	2111	2118	3422	3423

[a]Published Paper [155]

5.4.2 Solution state NMR studies

The ^{13}C solution NMR data of all complexes are shown in Table 5.25. Downfield chemical shifts were observed for the prepared complexes: (Gly)$Cd(SeCN)_2$ at 194.9 ppm and (Gly)$Hg(SeCN)_2$ at 189.24 ppm with respect to the free ligand, glycine at 173.1 ppm. These high downfield shifts resulted from the electron donation from glycine carboxylate to metal thereby causing about 20 ppm shifts of carbonyl carbon, while this shift was not observed in the histidine complexes because in this case, imidazole nitrogen and α-amine are involved in coordination to the metal center, which agrees with the reported binding mode of histidine to mercury metal ion [156].

The decrease in electron density observed by downfield shift for the de-shielded Se bound to Hg (-109 ppm) compared with Se bound to Cd (-272 ppm) as shown by ^{77}Se NMR (Table 5.26). In the case of histidine complexes of $Hg(SeCN)_2$, the selenium atom becomes more shielded and shifted up-field (-169.71 ppm) because the donation from histidine to the metal center, which causes even stronger π-back donation to selenium.

The ^{77}Se NMR data clearly showed greater deshielding effect at the selenium via complexing to histidine, which bind through two nitrogen atoms [157].

Table 5.25 ^{13}C NMR data for $Hg(SeCN)_2$ and $Cd(SeCN)_2$ with Gly and His

Compound	SeCN	C=O	C-1	C-2	C-3	C-4	C-5
His	-	174.7	136.2	135	117.9	55.1	29
Gly	-	173.1	42.5				
$[Cd(SeCN)_2]$	116.9						
$[(His)Cd(SeCN)_2]$ (**25)**	115.4	173	136.6	134.5	117	53.5	28.1
$[(Gly)Cd(SeCN)_2]$ (**26)**	119	194.9					
$[Hg(SeCN)_2]$	103.3						
$[(His)Hg(SeCN)_2]$ (**27)**	109.8	170.3	135	132.3	116.4	53.3	27.4
$[(Gly)Hg(SeCN)_2]$ (**28)**	116.5	189.2					

Table 5.26 ^{77}Se NMR data for $Cd(SeCN)_2$, $Hg(SeCN)_2$, and complex 27

Compound	^{77}**Se** (ppm)
$Cd(SeCN)_2$	-272.94
$Hg(SeCN)_2$	-109.18
$[(His)Hg(SeCN)_2]$ **(27)**	-169.71

5.4.3 Solid state CPMAS NMR

The solid state CPMAS NMR spectral data for complexes $(Gly)Cd(SeCN)_2$ and $(His)Cd(SeCN)_2$ for ^{13}C and $(Gly)Hg(SeCN)_2$ and $(His)Hg(SeCN)_2$ for ^{15}N are shown in Table 5.27and Table 5.28 respectively. The solid state ^{13}C and ^{15}N NMR spectra are shown in Figure 5.23 and Figure 5.24 respectively. The corresponding peaks are denoted by asterisk. The calculated chemical shift tensors are also compiled in Table 5.27 and Table 5.28, along with the span, Ω, which describes the breadth of the chemical shift tensor and skew, κ, describing the shape of the powder pattern. From Table 5.27, solid state ^{13}C NMR of glycine and histidine cadmium complexes show an increase in the chemical shift of the $Se^{13}CN$ (~2 ppm) for mercury (II) complex because the involvement of selenium in binding to the metal center, causing deshielding at the SeCN carbon. But in the case of the ^{15}N NMR data in Table 5.28, histidine and glycine complexes show a significant downfield shift of the nitrogen atom signal of the amine group. Additionally, histidine shows downfield shift for the imidazole moiety, which facilitates the involvement of imidazole nitrogen in binding to metal.

Table 5.27 Solid state ^{13}C Isotropic Chemical Shifts (δ_{iso}) and principle shielding tensors (σ_{xx}) [a] of Cd(II)-Selenocyanate complexes with Gly and His

Compound	Nucleus	δ_{iso}	σ_{11}	σ_{22}	σ_{33}	$\Delta\sigma$	[b]η
$Cd(SeCN)_2$	^{113}Cd	211.9	322	283	30	291	0.73
	^{77}Se	-119.6	53	41	-452	505	0.96
	^{13}C	117	222	205	-76	298	0.89
$[(Gly)Cd(SeCN)_2]$ **(25)**	^{13}C	170.8	242	171	98	-109	0.98
	^{13}C	119.9	212	124	23	-146	0.9
$[(His)Cd(SeCN)_2]$ (**26**)	^{13}C	169.3	236	169	102	-101	0.99
	^{13}C	108.4	181	103	41	-101	0.86
	^{13}C	132	202	136	58	-111	0.9
	^{13}C	129.2	196	130	61	-102	0.96
	^{13}C	119.5	213	120	23	-142	0.97

[a] isotropic shielding, $\sigma_{iso} = (\sigma_{11} + \sigma_{22} + \sigma_{33})/3$

$\Delta\sigma = \sigma_{33} - 0.5(\sigma_{11} + \sigma_{22})$

[b] $\eta = 3(\sigma_{22} - \sigma_{11}) / 2\Delta\sigma$

Table 5.28 Solid state ^{15}N isotropic chemical shifts (δ_{iso}) and principle shielding tensors (σ_{xx}) [a] of Hg(II)-selenocyanate complexes with Gly and His

Compound	Nucleus	δ_{iso}	δ_{11}	δ_{22}	δ_{33}	$\Delta\sigma$	η^b
His	^{15}N	-202.55	-97.76	-181	-328.85	-189.45 -	0.66 -
	^{15}N	-331.02	-	-	-		
[(His)Hg(SeCN)$_2$] (**27**)	^{15}N	-156.73	-27.66	-169.72	-272.8	-174.11	0.8
	^{15}N	-146.5	-		-	-	-
Gly	^{15}N	-345.56	-	-	-	-	-
[(Gly)Hg(SeCN)$_2$] (**28**)	^{15}N	-311.01	-	-	-	-	-

[a.] isotropic shielding, $\sigma_{iso} = (\sigma_{11} + \sigma_{22} + \sigma_{33})/3$

$\Delta\sigma = \sigma_{33} - 0.5(\sigma_{11} + \sigma_{22})$

$\eta^b = 3(\sigma_{22} - \sigma_{11}) / 2\Delta\sigma$

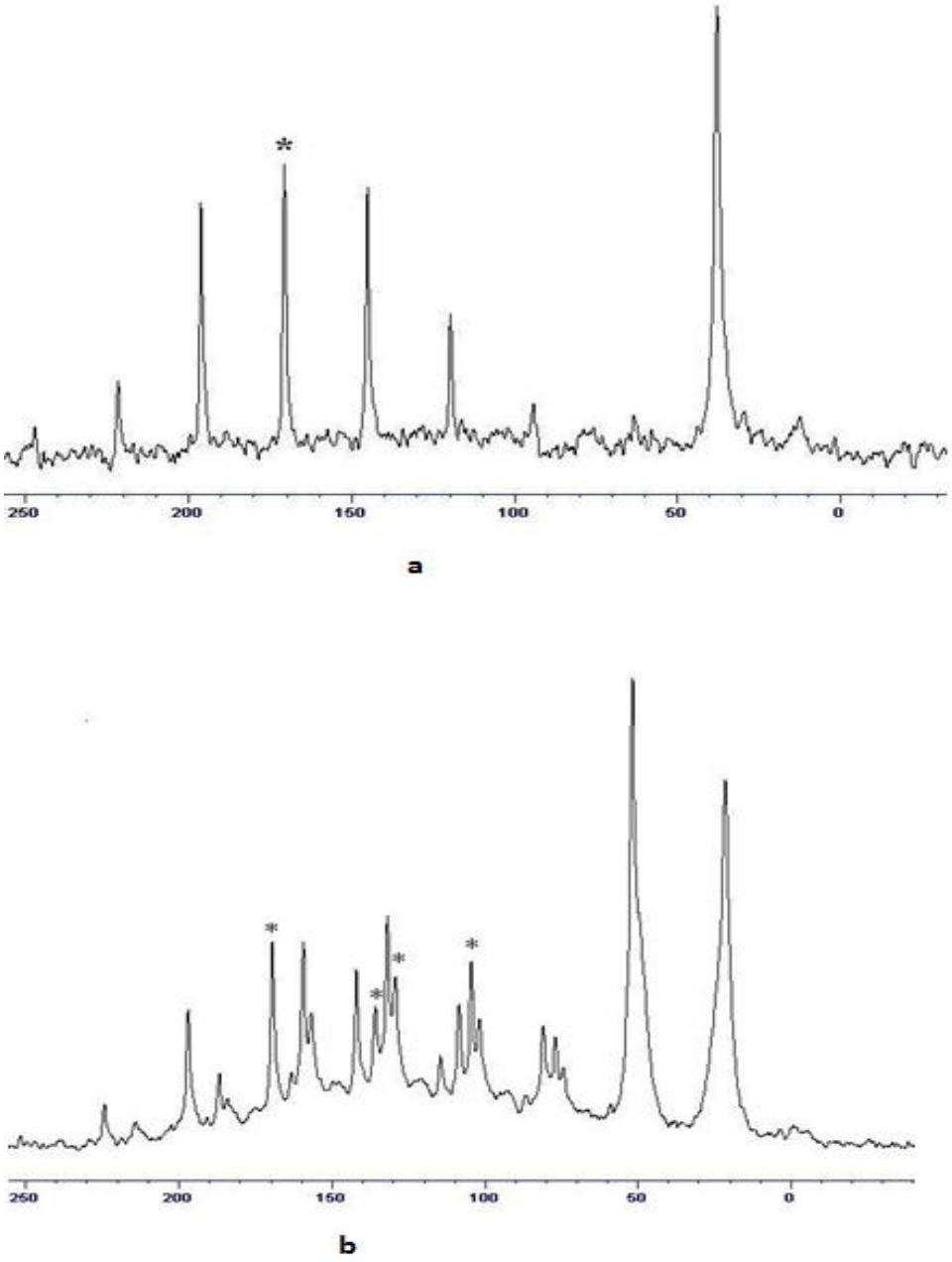

Figure 5.23 ^{13}C CPMAS spectra of (a) $(Gly)Cd(SeCN)_2$ and (b) $(His)Cd(SeCN)_2$

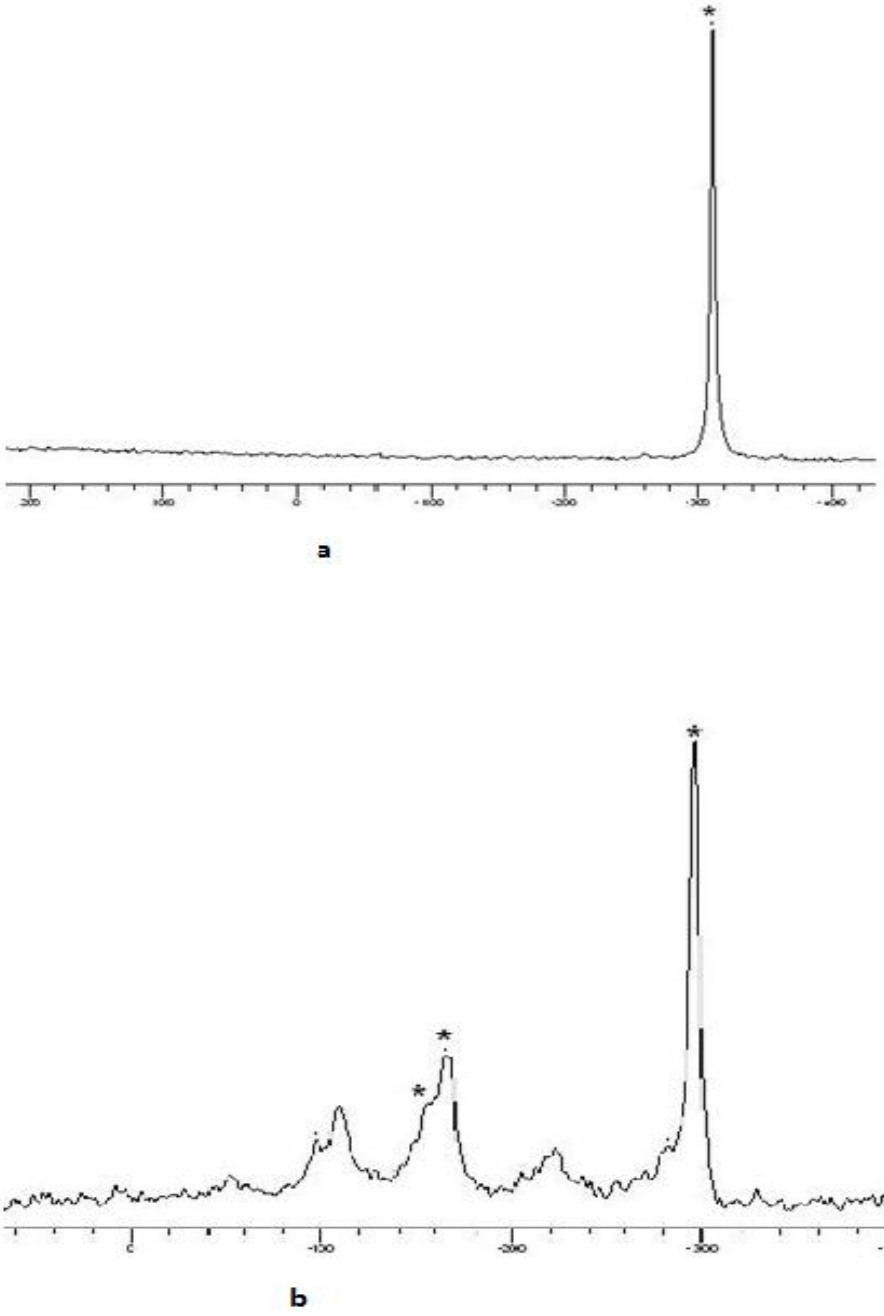

Figure 5.24 ^{15}N NMR spectra of (a) (Gly)Hg(SeCN)$_2$ and (b) (His)Hg(SeCN)$_2$

5.4.4 Computational analysis

Computational study shows that Glycine (C=O) and (C-O) bonds in the optimized structure (Figure 5.25) are shorter in Cd complex than in Hg complex (Table 5.29 and Table 5.30), which agrees with experimental ^{13}C NMR results, while no difference in (C=O) and (C-O) bonds were observed in Histidine complexes indicating less contribution of carboxylate in binding. Se-Cd is shorter than Se-Hg because of the proximity in the atomic sizes of Se and Cd. It is worth-mentioning here that the calculated bond lengths are comparable to the reported experimental bond length for Se-Cd obtained by single crystals (2.723 and 2.828 Å) [158,159]. It is also observed that Hg-N and Hg-O is longer than Cd-N and Cd-O because Cd is harder than Hg, leading to better interaction. This may cause higher stability of Cd complexes in general. Nitrogen is less electronegative atom than oxygen so it can donate electron more easily to the metal and forms stronger bonds with metals, which results in stronger chelation through two nitrogens than chelation through nitrogen and oxygen. L-Histidine complexes of Hg and Cd have shorter bonds than Glycine complexes indicating stronger bonding of Histidine to theses metals. This agrees with the higher electron donation indicated from ^{77}Se NMR data.

Table 5.29 Bond lengths (Å) derived computationlly for [LM(SeCN)$_2$] structures

$Hg(SeCN)_2$ + His		$Cd(SeCN)_2$ + His		$Hg(SeCN)_2$ + Gly		$Cd(SeCN)_2$ + Gly	
Hg-Se1	2.765	Cd-Se1	2.718	Hg-Se1	2.699	Cd-Se1	2.656
Hg-Se2	2.795	Cd-Se2	2.745	Hg-Se2	2.731	Cd-Se2	2.691
Hg-N1	2.434	Cd-N1	2.302	Hg-N1	2.576	Cd-N1	2.415
Hg-N2	2.537	Cd-N2	2.399	Hg-O1	2.656	Cd-O1	2.423
C=O	1.236	C=O	1.236	C=O	1.232	C=O	1.228
C-O	1.386	C-O	1.386	C-O	1.402	C-O	1.412

Table 5.30 Torsion angles (°) derived computationlly for [LM(SeCN)$_2$] structures

$Hg(SeCN)_2$ + His		$Cd(SeCN)_2$ + His		$Hg(SeCN)_2$ + Gly		$Cd(SeCN)_2$ + Gly	
Se1-C-N4	178.79	Se1-C-N4	178.45	Se1-C-N3	178.03	Se1-C-N2	178.2
Se2-C-N5	176.36	Se2-C-N5	175.84	Se2-C-N2	177.04	Se2-C-N3	176.32
N1-Hg-N2	83.87	N1-Cd-N2	87.79	N1-Hg-O1	64.67	N1-Cd-O1	96.81
Se1-Hg-Se2	125.79	Se1-Cd-Se2	121.32	Se1-Hg-Se2	149.92	Se1-Cd-Se2	139.71
Se1-Hg-N1	108.92	Se1-Cd-N1	111.15	Se1-Hg-N1	107.5	Se1-Cd-N1	112.35
Se2-Hg-N2	99.18	Se2-Cd-N2	101.26	Se2-Hg-O1	111.58	Se2-Cd-O1	112.17
Se1-Hg-N2	118.69	Se1-Cd-N2	116.85	Se1-Hg-O1	89.99	Se1-Cd-O1	96.81
Se2-Hg-N1	112.6	Se2-Cd-N1	113.3	Se2-Hg-N1	100.81	Se2-Cd-N1	103.86

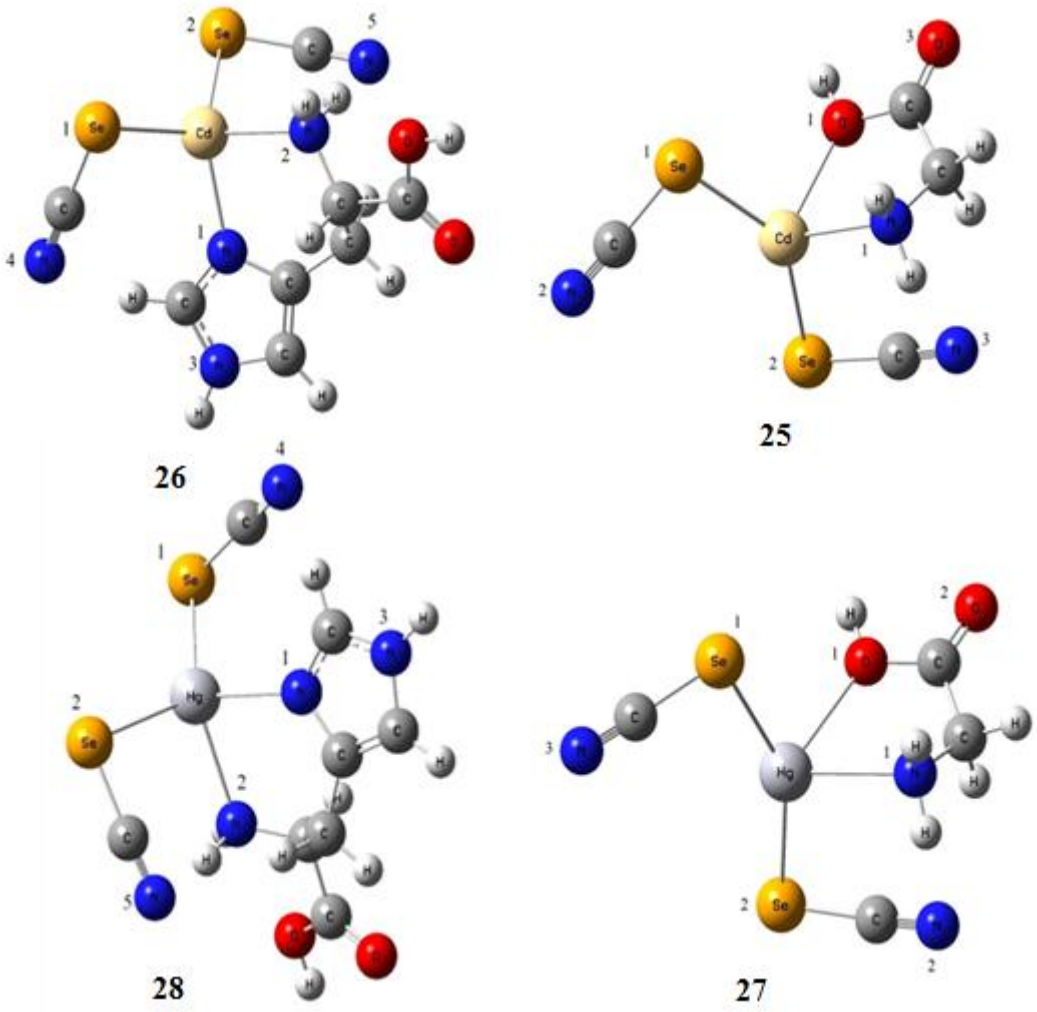

Figure 5.25 Compuationally optimized structures of [LM(SeCN)$_2$] complexes

5.4.5 Antibacterial activity

The *in vitro* anti-bacterial activity studies were performed with Cd(II) complexes against both gram positive as well as gram negative bacteria. Two complexes, (His)$Cd(SeCN)_2$ and (Gly)$Cd(SeCN)_2$ exhibited antibacterial activity compared to the $Cd(SeCN)_2$ except for *K. pneumoniae*, which showed resistance to all the tested compounds. The inhibition of $Hg(SeCN)_2$was reported previously [160], while mercury complexes with glycine and histidine did not show significant antibacterial activity. The activities of the complexes are summarized in Table 5.31**.**

Table 5.31 Antibacterial activities of [$LM(SeCN)_2$] complexes

Microorganisms	Zone of Inhibition (mm)			
	$Hg(SeCN)_2$*	$Cd(SeCN)_2$	[(His)$Cd(SeCN)_2$]	[(Gly)$Cd(SeCN)_2$]
E. coli	-	25	35	22
P. aeruginosa	10	20	18	32
S. typhi	10	28	32	29
S. aureus	22	20	22	20
K. pneumonia	22	--	--	--

*Published work [160]

5.5 Interaction studies of Gold(III) complex using NMR spectroscopy

This work reports the interaction of $[Au(pn)]^{3+}$ with some biologically important ligands such as Imt, Gly, Met, Im and His as shown in Figure 5.26 using ^{1}H and ^{13}C NMR measurements.

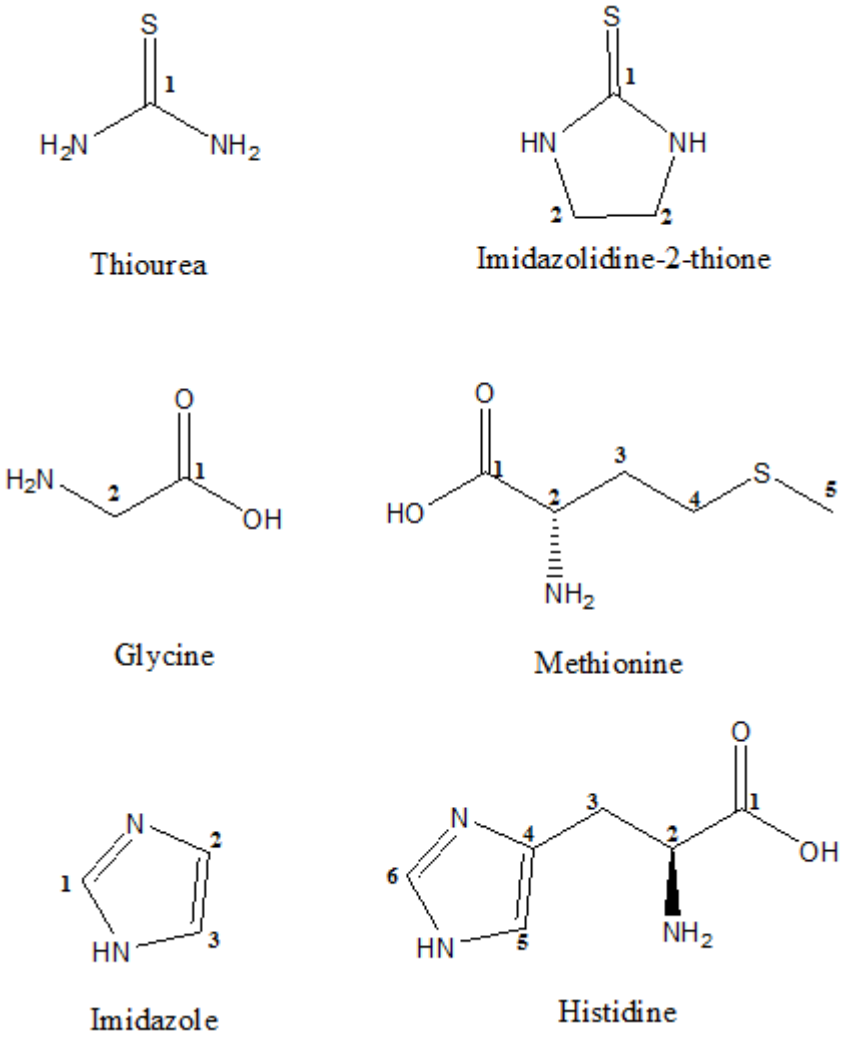

Figure 5.26 Structures of ligands with carbon numbering for NMR studies

5.5.1 Interaction of $[Au(pn)_2]Cl_3$ with Thiourea and Imidazolidine-2-thione

The interaction of Thiourea (Tu) and Imidazolidine-2-thione (Imt) was studied by ^1H NMR. The ^1H chemical shifts of free *pn*, $[Au(pn)_2]^{3+}$ and interacted ligands such as Tu and Imt are shown in the Table 5.32.

The proton spectrum of free thiourea (Tu) in D_2O at 298 K shows a signal at 7.05 ppm corresponds to N-H protons. The study of interaction of $[Au(pn)_2]^{3+}$ and Tu shows a change in chemical shifts of N-H protons correspond to coordinated *pn* in gold complex. The interaction of Imidazolidine-2-thione (Imt) with $[Au(pn)_2]^{3+}$ at 298 K in D_2O was followed by ^1H NMR. The proton spectrum of free Imidazolidine-2-thione in D_2O shows signals at 3.50 and 7.94 ppm corresponding to C-H and N-H protons respectively. The study of interaction of $[Au(pn)_2]^{3+}$ and Imt shows a change in chemical shifts of C-H and N-H protons of *pn* in the gold complex.

The interaction of Tu and Imt was also studied by ^{13}C NMR. The ^{13}C chemical shifts of free *pn*, $[Au(pn)_2]^{3+}$ and interacted $[Au(pn)_2]^{3+}$ with Tu and Imt are given in the Table 5.33.

The carbon spectrum of free thiourea (Tu) in D_2O is taken at 298 K. Signal at 182.72 ppm corresponds to carbon (C=S) of Tu. An upfield chemical shift from 182.72 ppm to 157.73 ppm of C=S carbon of the interacted Tu accounts for complexation with Au(III) centre. As a result, such complexation leads to one of the bound *pn* as mono-dentate ligand in the complex. The interaction of $[Au(pn)_2]^{3+}$ complex with Tu also leads to an into upfield chemical shift of carbons of the coordinated *pn*.

The carbon spectrum of free Imidazolidine-2-thione (Imt) in D_2O is taken at 298 K. Signals at 44.07 and 183.07 ppm correspond to C-1 (CH_2) and C-2 (C=S) carbons respectively. The larger change in chemical shift for C=S carbon of Imt is observed which could be attributed to ligation of C=S sulfur of Imt to Au(III). The evidence of S binding of Imt is also corroborated by the downfield shift of CH_2 carbon of Imt. The smaller upfield chemical shift of CH_2 carbon and the larger downfield chemical shift of C=S carbon indicate the binding of C=S sulphur of Imt towords Au(III) as a metal center. As a result, one of NH_2 nitrogen bound *pn* may be replaced by C=S sulphur of Imt in $[Au(pn)_2]^{3+}$ complex. Therefore, one of coordinated bi-dentate *pn* may become mono-dentate ligand in the gold(III) complex.

From this study, it appeared that the binding of thione like Imidazolidine-2-thione (Imt) and thiourea (Tu) is probably occurring through S atom of Tu and Imt towards Au(III) centre in the complex at 298 K in D_2O. The ^{13}C NMR spectra of the interacted Au(III) complex show the deshielding of carbons of the bound *pn* as result of interaction with Tu and Imt.

Table 5.32 ^{1}H NMR data of $[Au(pn)_2]^{3+}$ and interacted $[Au(pn)_2]^{3+}$ with Imt and Tu

Compound	H1-pn	H2-pn			
Free pn	2.76	1.59			
$[Au(pn)_2]^{3+}$	2.96	1.93			
			C-H Imt	N-H Imt	
Free Imt			3.5	7.94	
Imt + $[Au(pn)_2]^{3+}$	3.17	1.81	3.6	7.98	
					N-H Tu
Free Tu					7.05
Tu + $[Au(pn)_2]^{3+}$	2.94	1.9			7.08

Table 5.33 ^{13}C NMR data of $[Au(pn)_2]^{3+}$ and interacted $[Au(pn)_2]^{3+}$ with Imt and Tu

Compound	C2-pn	C1-pn			
Free pn	37.51	39.97			
$[Au(pn)_2]^{3+}$	37.27	41.41			
			C2-Imt	C1-Imt	
Free Imt			44.07	183.35	
Imt + $[Au(pn)_2]^{3+}$	37.74	43.42	45.28	192.39	
					C=S(Tu)
Free Tu					182.72
Tu + $[Au(pn)_2]^{3+}$	37.6	41.93			157.73

5.5.2 Interaction of $[Au(pn)_2]Cl_3$ with Glycine and Methionine

The interaction of Glycine (Gly) and Histidine (His) was also studied by ^1H NMR. The ^1H chemical shifts of free *pn*, $[Au(pn)_2]^{3+}$ and interacted ligands such as His and Gly are shown in the Table 5.34.

The interaction of Glycine (Gly) with $[Au(pn)_2]^{3+}$ at 298 K in D_2O was followed by ^1H NMR. The proton spectrum of free Glycine in D_2O shows signals at 3.40 ppm corresponding to C-H proton. The study of interaction of $[Au(pn)_2]^{+3}$ and Gly shows no appreciable change in chemical shifts of C-H protons corresponding to the bound *pn* in the gold complex.

The proton spectrum of free L-methionine (Met) in D_2O at 298 K shows signals at 2.06, 2.53, 2.00 and 3.73 ppm that correspond to protons numbered 5, 4, 3 and 2 respectively

There is a slight change in chemical shifts of protons associated with bound *pn* in the gold complex as a result of interaction with Met.

The interaction of Gly and Met was also studied by ^{13}C NMR. The ^{13}C chemical shifts of free *pn*, $[Au(pn)_2]^{3+}$ and interacted $[Au(pn)_2]^{3+}$ with Gly and Met are given in the Table 5.35.

The carbon spectrum of free Glycine (Gly) in D_2O was taken at 298 K. Signals at 44.26 and 173.26 ppm correspond to C-1 (CH_2) and C-2 (C=O) carbons respectively. The change in chemical shift for C=O carbon of Gly could be attributed to ligation of C=O oxygen of Gly to Au(III). This is also corroborated by the smaller downfield shift of CH_2 carbon of Gly. As a result, one of NH_2 nitrogen in bound *pn* may be replaced by C=O

oxygen of Gly in $[Au(pn)_2]^{3+}$ complex. Therefore, one of coordinated bi-dentate *pn* would become mono-dentate ligand in the gold(III) complex**.**

The interaction of Methionine with $[Au(pn)_2]^{3+}$ complex was also studied by ^{13}C NMR spectroscopy. ^{13}C NMR spectra of free and interacted Met with $[Au(pn)_2]^{3+}$ in D_2O solvent are measured at 298 K. Chemical shifts at 14.76, 29.65, 30.47, 54.71 and 174. 98 ppm corresponds to carbons numbered 5, 4, 3, 2 and 1 of free L-Methionine. The interaction of L-Methionine (Met) with gold(III) complex results in the change of chemical shifts of C-1 and C-2 of coordinated *pn.* The downfield chemical shifts of the *pn* carbons of the complex support the hypothesis of interaction of Met with gold(III) complex as given in Table 5.8. Apart from such changes, there is also a downfield chemical shift of the carbon directly bonded to S of Met. Such changes chemical shifts may be a sign of the interaction of Met through S towards Au(III) centre.

From this study, it appeared that the binding of thioether like L-Methionine (Met) is probably occurring through S atom of Met towards Au(III) centre in the complex at 298 K in D_2O. The ^{13}C NMR spectra of the interacted Au(III) complex show the deshielding of carbons of the bound *pn* as result of interaction with Met.

Table 5.34 ^{1}H NMR data of $[Au(pn)_2]^{3+}$ and interacted $[Au(pn)_2]^{3+}$ with Gly and Met

Compound	H1-pn	H2-pn		
Free pn	2.76	1.59		
$[Au(pn)_2]^{3+}$	2.96	1.93		
			C-H Gly	
Free Gly	-	-	3.4	
Gly + $[Au(pn)_2]^{3+}$	2.96	1.92	3.41	
				H2 Met
Free Met	-	-		3.73
Met + $[Au(pn)_2]^{3+}$	3.05	1.94		4.09

Table 5.35 ^{13}C NMR data of $[Au(pn)_2]^{3+}$ and interacted $[Au(pn)_2]^{3+}$ with Gly and Met

Compound	C2-pn	C1-pn				
Free pn	37.51	39.97				
$Au(pn)_2]^{3+}$	37.27	41.41				
			C-2 Gly	C-1 Gly		
Free Gly			42.26	173.26		
Gly + $[Au(pn)_2]^{3+}$	37.57	41.76	42.34	173.44		
					C4-Met	C1-Met
Free Met					29.65	174.98
Met + $[Au(pn)_2]^{3+}$	37.41	41.7			25.87	176.05

5.5.3 Interaction of $[Au(pn)_2]Cl_3$ with Imidazole and Histidine

The interaction of Imidazole (Im) with $[Au(pn)_2]^{3+}$ complex was also studied by ^1H NMR spectroscopy. The ^1H chemical shifts of free *pn*, $[Au(pn)_2]^{3+}$, interacted Imidazole (Im) and Histidine (His) ligands are given in the Table 5.36 and Table 5.37 respectively.

The interaction of Imidazole (Im) with $[Au(pn)_2]^{3+}$ at 298 K in D_2O was followed by proton NMR. The proton spectrum of free Imidazole (Im) in D_2O shows signals at 6.97 and 7.61 ppm related to **H**C=C**H** (free Im) and N-C**H**=N (free Im) protons respectively. The interaction of $[Au(pn)_2]^{3+}$ with Im causes downfield chemical shifts of **H**C=C**H** (bound Im) and N-C**H**=N (bound Im) protons in gold(III) complex. There is a slight upfield chemical shift of protons associated with the bound *pn* in the gold complex as a result of interaction with Im.

The ^1H spectrum of free Histidine (His) in D_2O at 298 K shows signals at 2.95, 3.06, 3.82, 6.89 and 7.58 ppm that correspond to protons numbered 3(a), 3(b), 2, 5 and 6 respectively. There is a slight upfield chemical shift of protons associated with the bound *pn* in the gold complex as a result of interaction with His.

The interaction of Im and His with gold(III) complex was also studied by ^{13}C NMR spectroscopy at 298 K in D_2O. The ^{13}C chemical shifts of free *pn*, $[Au(pn)_2]^{3+}$, interacted $[Au(pn)_2]^{3+}$ with Im and His are given in the Table 5.38 and Table 5.39 respectively.

Signals at 122.55 ppm and 136.83 ppm corresponds to H**C**=**C**H and N-**C**H=N carbons of free Imidazole. The interaction of Imidazole with $[Au(pn)_2]^{3+}$ results in the downfield chemical shifts of C-1 and C-2 of coordinated *pn* as given in the Table 5.38. The slight upfield chemical shift of H**C**=**C**H and N-**C**H=N carbons of Imidazole may also be a sign

of the interaction of Imidazole through nitrogen donor atom (HC=**N**-CH) towards Au(III) center.

The interaction of Histidine (His) with $[Au(pn)_2]^{3+}$ complex is also studied by ^{13}C NMR spectroscopy. ^{13}C NMR spectra of free and interacted His with $[Au(pn)_2]^{3+}$ in D_2O solvent are measured at 25˚C. Signals at 29.00, 55.66, 117.63, 133.18, 137.18 and 174.72 ppm corresponds to carbons numbered 3, 2, 5, 4, 6 and 1 of free Histidine. The interaction of Histidine with the gold(III) complex results in the change in chemical shifts of C-1 and C-2 of coordinated *pn.* The downfield chemical shifts of the *pn* of complex complex support the hypothesis of interaction of His with gold(III) complex as given in the Table 5.39. Apart from such changes, there are also downfield chemical shifts of Histidine carbons 2, 5 and 4; slightly upfield chemical shifts of carbon numbered 1 and 3 i.e 176.35 ppm and 28.64 ppm respectively; and unchanged chemical shift of carbon numbered 6. Such significant changes in chemical shifts may reveal the interaction of Hist with Au(III) center.

These experiments indicate that the binding of thione like imidazolidine-2-thione (Imt) and thioether (Tu); and thioether like Methionine (Met) through S towards Au(III) center. The ^{13}C NMR spectra of the interacted Au(III) complex show the deshielding of carbons of bound *pn* as result of interaction with Imt, Tu and Met.

Table 5.36 ^{1}H NMR data of $[Au(pn)_2]^{3+}$ and interacted $[Au(pn)_2]^{3+}$ with Im

Compound	H1-pn	H2-pn		
Free pn	2.76	1.59		
$[Au(pn)_2]^{3+}$	2.96	1.93		
			HC=CH Im	N-CH=N Im
Free Im			6.97	7.61
Im + $[Au(pn)_2]^{3+}$	2.94	1.9	7.01	7.74

Table 5.37 ^{1}H NMR data of $[Au(pn)_2]^{3+}$ and interacted $[Au(pn)_2]^{3+}$ with His

Compound	H1-pn	H2-pn					
Free pn	2.76	1.59					
$[Au(pn)_2]^{3+}$	2.96	1.93					
			H3 (a) His	H3 (b) His	H2 His	H5 His	H6 His
Free His			2.95	3.06	3.82	6.89	7.58
			2.70,	3.06(f),	3.76,		7.70(i)
His + $[Au(pn)_2]^{3+}$	2.92	1.88	2.92	3.02(i)	3.63,	6.89	7.59(f)
					3.53		

Table 5.38 ^{13}C NMR data of $[Au(pn)_2]^{3+}$ and interacted $[Au(pn)_2]^{3+}$ with Im.

Compound	C2-pn	C1-pn		
Free pn	37.51	39.97		
$[Au(pn)_2]^{3+}$	37.27	41.41		
			HC=CH Im	N-CH=N Im
Free Im			122.55	136.83
Im + $[Au(pn)_2]^{3+}$	37.52	41.8	122.22	136.55

Table 5.39 ^{13}C NMR data of $[Au(pn)_2]^{3+}$ and interacted $[Au(pn)_2]^{3+}$ with His

Compound	C2-pn	C1-pn						
Free pn	37.51	39.97						
$Au(pn)_2]^{3+}$	37.27	41.41						
			C-3 His	C-2 His	C-5 His	C-4 His	C-6 His	C-1 His
Free His			29	55.66	117.63	133.02	137.18	174.72
His + $[Au(pn)_2]^{3+}$	37.78	38.4	28.64	55.91	117.86	133.38	137.18	176.35

CHAPTER 6

SUMMARYAND CONCLUSIONS

A novel series of gold(III) diamine complexes (**1**-**7**) with general formula, $[Au(diamine)_2]Cl_3$ have successfully been synthesized and characterized by using various analytical and spectroscopic techniques. The NMR and elemental analysis results strongly support the formation of a 1:2 complex of the type $[Au(\textit{diamine})_2]^+$ with chelating ethylenediamine, propylenediamine or akyl substituted ethylenediamine ligands. ^{15}N NMR showed that the nitrogens of five-membered ring of monoethylenediamine complex (**8**) has higher electron donation to gold(III) than that of the bis-ethylenediamine complex. Computational study shows that this complex has a slightly distorted square planar geometry. According to our biological assays, complex (**1**) with ethylenediamine is a more promising candidate as an anticancer agent than complex (**4**). Therefore, $[Au(en)_2]Cl_3$ might be a prospective chemo-preventative and chemotherapeutic agent against human gastric carcinogenesis.

According to IC_{50} data, complex (**1**) with ethylenediamine ligand is a more prospective anticancer agent against prostate cancer PC3 cells. The dose dependent studies showed that complex (**1**) was found to execute a powerful and promising cytotoxic effect on PC3 cells which is comparable to that of cisplatin. These data also indicate that gold(III) complexes with specific ligands incorporated into the structural design such as complexes (**2**-**5**) may have the potential to overcome mechanisms inducing resistance to cisplatin, particularly in the gastric cancer SGC7901 cells.

The MTT results showed the effect of complexes **(8-10**) on prostate PC3 cancer cells growth, where the first two complexes (**8**) and (**9**) demonstrated inhibition in cancer cells growth, while the last complex (**10**) did not show any significant changes in cancer cells growth. Thus, complexes (**8**) and (**9**) might prove to be reasonably good candidates as anticancer drugs for prostate cancer. The MTT results also showed the effect of complexes (**8-10**) on gastric SGC7901 cells growth, where the first complex (**8)** demonstrated inhibition in cancer cells growth, while the last two complexes (**9**) and (**10**) did not show any major changes in cancer cells growth. Thus, complex (**8**) might prove to be practically good candidate as anticancer drug for gastric cancer. The IC_{50} data for cisplatin sensitive A2780 and *cisplatin* resistant A2780 cis ovarian cancer cell lines show that [Au(*en*)Cl_2]Cl (**8**) is relatively better cytotoxic agent than [Au(*en*)$_2$]Cl_3 (**1**).

It is also interesting to note that mono(alkyldiamine)gold(III) complexes, [Au(diamine)Cl_2]$^{1+}$ complexes (**8**) and (**9**) show relatively better anticancer agents in the gastric cancer SGC7901 cells while [Au(diamine)$_2$]$^{3+}$ complexes (**1-5**) display comparatively better anticancer activity against the prostate PC3 cells as well as cisplatin sensitive A2780 and *cisplatin* resistant A2780 cis ovarian cancer cell lines. Since complex [Au(en)$_2$]Cl_3 (**1**) emerged as the best anticancer agent in this study, it is presently subjected to evaluation of *in vivo* anticancer properties.

A new series of gold(III) complexes of general formula [(thione)$_2$Au(diamine)]Cl_3 complexes (**11-18**) are reported here. The solid state IR as well as ^{13}C and ^{15}N NMR data indicate that Au(III) center is bonded via sulfur of thiocarbonyl S=C< site of the thiones and also chelated by the diamines from the *trans* side of coordinated thiones. Spectroscopic data were evaluated by comparisons with calculated data from the built

and optimized structure by GAUSSIAN 09 at the RB3LYP level with LanL2DZ bases set. These new Au(III) complexes based on mixed thione and diamine ligands are almost similar with the square planar structure of tetra-coordinate $[Au(en)_2]Cl_3$ complex.

Since $[Au(en)_2]Cl_3$ type complex are relatively more toxic towards some cancer cell lines, the $[(thione)_2Au(diamine)]Cl_3$ complexes may be a better alternate for $[Au(en)_2]Cl_3$ type complex. The *in vitro* cytotoxic study of thione Au(III) complexes against C6 glioma cell line also leads to the conclusion that the structural features e.g. ring size of thione ligand (Imt and Diaz) as well as Au(III) chelate size with diamine (en, pn and bn) may affect *in vitro* cytotoxicity of the complex.

In addition to the synthesis of gold(III) complexes, a series of $Hg(CN)_2$ complexes (**19-24**) of the type $[Hg(CN)_2(L)]$ (L= en, pn, N-Me-en, N,N'-Me_2-en, N,N'-Et_2-en and N,N'-ipr_2-en) was also synthesized and characterized. The analysis of the complexes showed only one equivalent of alkyl diamine ligand involved in coordination to form a mercury complex. Complexes (**19** and **20**) have shown a good antibacterial activity towards different microorganisms.

Moreover, some Cd(II) and Hg(II) complexes (**25-28**) of the type, $[(L)M(SeCN)_2]$ (L= Histidine or Glycine and M^{2+} = Cd^{2+} or Hg^{2+}), were also prepared and characterized by EA, mid-IR solution and Solid state NMR. The results reveal that the metal complexes with Histidine are more strongly coordinated than that of the corresponding Glycine containing metal complexes. The Cd(II) complexes have shown good zone inhibition towards different microorganisms, while no significant antibacterial activity was observed for the mercury complexes.

6.1 Future Studies

- In the same line of Au(III) diamine complexes, Au(III) bipyridine and Au(III) phenanthroline complexes can also be synthesized and evaluated *in vitro* for potential anticancer activity.
- As *in vitro* anticancer activity of $[Au(en)_2]Cl_3$ and its derivatives was significantly promising towards some cancer cell line, further *in vivo* anticancer evaluation would be worth-while.
- With same frame of mind, N-alkyl substituted imidazolidine-2-thione (N-R-Imt) can also be used to synthesize a new series of complexes with general formula, $[(N\text{-}R\text{-}Imt)_2Au(diamine)]Cl_3$ and evaluated *in-vitro* for potential anticancer activity.
- As $[(Imt)_2Au(pn)]Cl_3$ complex has emerged as an excellent *in vitro* cytotoxic agent against C6 glioma cancer cell line, further *in vivo* cytotoxic evaluation for such complex is needed.

Appendix A -List of Publications

1. S. S. Al-Jaroudi, **M. Monim-ul-Mehboob**, M. Altaf, M. Fettouhi, M. I. M. Wazeer, A. A. Isab, *Synthesis, X-ray structure and Influence of Stereochemistry on Antitumor Activity of Bis(1,2-Diaminocyclohexane)Gold(III) Complexes* submitted to **New J. Chem.** (**2013**)

2. M. Altaf, **M. Monim-ul-Mehboob**, A. A. Isab, M. I. M. Wazeer, *New gold(I) complexes with t-butyl phosphine and dialkyl dithiocarbamate ligands: Synthesis, spectroscopic characterization, crystal structure determination and in vitro cytotoxic evaluation against A549, HeLa and MCF7 human cancer lines*, accepted in **Eur. J. Med. Chem.**, (**2013**).

3. **M. Monim-ul-Mehboob**, Bassem A. Al-Maythalony, Muhammad Altaf, Mohammed I.M. Wazeer, Anvarhusein A. Isab, Saleh Altuwaijri, Ayesha Ahmed, Vikram Dhuna, Gaurav Bhatia. Kshitija Dhuna, Sukhdev Singh Kamboje *New $[(thione)_2Au(diamine)]Cl_3$ complexes: Synthesis, Spectroscopic characterization, Computational study and in vitro Cytotoxicity*, **Spectrochim. Acta Part A,** 115, 641–647 (**2013**).

4. **M. Monim-ul-Mehboob**, M. Altaf, M. Fettouhi , A. A. Isab, M. I. M. Wazeer, M. N. Shaikh, S. Altuwaijri, *Synthesis, Spectroscopic Characterization and Anticancer Properties of new gold(III)-alkanediamine complexes against Gastric, Prostate and Ovarian cancer cells; Crystal structure of $[Au_2(pn)_2(Cl)_2]Cl_2{\cdot}H_2O$*, **Polyhedron**, 61, 225-234 (**2013**).

5. B. A. Al-Maythalony, **M. Monim-ul-Mehboob**, M. I. M. Wazeer Anvarhusein A.A. Isab and M. N. Shaikh, S. Altuwaijri, Synthesis, *CP-MAS NMR Characterization,*

and Anti-bacterial activities of Glycine and Histidine Complexes of $Cd(SeCN)_2$ and $Hg(SeCN)_2$, **Bioinorg. Chem. Appl.**, 2013, 476874 (**2013**).

6. M.N. Shaikh, B.A Al-Maythalony, **M. Monim-ul-Mehboob**, M. Fettouhi, M.I.M Wazeer, A.A Isab, S. Ahmad, *Mercury(II) cyanide complexes with alkyldiamines: Solid state/solution NMR, computational, and antimicrobial studies*, **J. Coord. Chem.**, 65, 2074-2080 (**2012**).

7. A.A Isab, M.N. Shaikh, **M. Monim-ul-Mehboob**, B.A Al-Maythalony, M.I.M Wazeer, S. Altuwaijiri, *Synthesis, characterization and anti proliferative effect of $[Au(en)_2]Cl_3$ and $[Au(N\text{-}propyl\text{-}en)_2]Cl_3$ on human cancer cell lines*, **Spectrochim. Acta - Part A**, 79, 1196-1201 (**2011**).

Appendix B - Conference Presentations

1. Poster presentation entitled "*New $[Au(DACH)_2]Cl_3$ complexes: Synthesis, characterization, in vitro cytotoxicity and influence of stereochemistry on anticancer activity*" accepted in the **247th ACS National Meeting 2014** (March 16-20, **2014)** in Dallas, United States of America.

2. Oral presentation entitled "*Synthesis, characterization of new gold(III)-alkanediamines complexes and their anticancer activity against gastric, prostate and ovarian cancer cell lines*" in the **ChemIndix 2013** on 5th November, **2013** at Gulf Hotel, Kingdom of Bahrain.

3. Poster presentation entitled "*New $[(thione)_2Au(diamine)]Cl_3$ complexes: Synthesis, Spectroscopic characterization and in vitro Cytotoxicity*" in the **4th Scientific Saudi Conference** (SSC4) on 30th April, **2013** at Umm Al-Qura University, Makkah, Kingdom of Saudi Arabia.

4. Poster presentation entitled "*Anticancer activity of new gold(III) complexes of $[Au(en)_2]Cl_3$ and its derivatives against human prostate and gastric cancer cell lines*" in the **3rd Scientific Saudi Conference** (SSC3) on 1st May **2012** at Al-Khobar, Kingdom of Saudi Arabia.

5. Poster presentation entitled "*Synthesis, characterization and antiproliferative effect of $[Au(en)_2]Cl_3$ and $[Au(N\text{-}propyl\text{-}en)_2]Cl_3$ on human cancer cell lines*" in the **2nd Scientific Saudi Conference** (SSC2) on 29th March, **2011** at Jeddah, Kingdom of Saudi Arabia.

References

[1] L. Kelland, The resurgence of platinum-based cancer chemotherapy., Nat. Rev. Cancer. 7 (2007) 573–84.

[2] S. Ahmad, Platinum-DNA interactions and subsequent cellular processes controlling sensitivity to anticancer platinum complexes., Chem. Biodivers. 7 (2010) 543–66.

[3] H.M. Pinto, J.H. Schornagel, Coordination Compounds in Cancer Chemotherapy, (1996).

[4] B. Lippert, Cisplatin Chemistry and Biochemistry of a Leading Anticancer Drug, John Wiley & Sons, 1999.

[5] N. Farrell, Platinum-Based Drugs in Cancer Therapy, Humana Press Inc., Totowa, 2000.

[6] M. Gielen, R. Edward, T. Tiekink, Metallotherapeutic Drugs and Metal-Based Diagnostic Agents: The Use of Metals in Medicine, Wiley, 2005.

[7] D. Wang, S.J. Lippard, Cellular processing of platinum anticancer drugs., Nat. Rev. Drug Discov. 4 (2005) 307–20.

[8] M.A. Fuertes, C. Alonso, J.M. Pérez, Biochemical modulation of Cisplatin mechanisms of action: enhancement of antitumor activity and circumvention of drug resistance., Chem. Rev. 103 (2003) 645–62.

[9] Y.-P. Ho, C.F.A.-Y. Steve, K.K.W. To, Platinum-based anticancer agents: innovative design strategies and biological perspectives., Med. Res. Rev. 23 (2003) 633–55.

[10] C.X. Zhang, S.J. Lippard, New metal complexes as potential therapeutics., Curr. Opin. Chem. Biol. 7 (2003) 481–9.

[11] T.W. Hambley, Platinum binding to DNA: structural controls and consequences, J. Chem. Soc. Dalt. Trans. (2001) 2711–2718.

[12] Y. Jung, S.J. Lippard, Direct cellular responses to platinum-induced DNA damage., Chem. Rev. 107 (2007) 1387–407.

[13] M.A. Fuertes, J. Castilla, C. Alonso, J.M. Pérez, Cisplatin biochemical mechanism of action: from cytotoxicity to induction of cell death through interconnections between apoptotic and necrotic pathways., Curr. Med. Chem. 10 (2003) 257–66.

[14] E. Wong, C.M. Giandomenico, Current status of platinum-based antitumor drugs., Chem. Rev. 99 (1999) 2451–66.

[15] E.R. Jamieson, S.J. Lippard, Structure, Recognition, and Processing of Cisplatin-DNA Adducts., Chem. Rev. 99 (1999) 2467–98.

[16] L.M. Pasetto, M.R. D'Andrea, A.A. Brandes, E. Rossi, S. Monfardini, The development of platinum compounds and their possible combination., Crit. Rev. Oncol. Hematol. 60 (2006) 59–75.

[17] M.J. Silva, P. Costa, A. Dias, M. Valente, H. Louro, M.G. Boavida, Comparative analysis of the mutagenic activity of oxaliplatin and cisplatin in the Hprt gene of CHO cells., Environ. Mol. Mutagen. 46 (2005) 104–15.

[18] L.M. Pasetto, M.R. D'Andrea, E. Rossi, S. Monfardini, Oxaliplatin-related neurotoxicity: how and why?, Crit. Rev. Oncol. Hematol. 59 (2006) 159–68.

[19] S. Ahmad, A.A. Isab, S. Ali, A.R. Al-Arfaj, Perspectives in bioinorganic chemistry of some metal based therapeutic agents, Polyhedron. 25 (2006) 1633–1645.

[20] S. Ahmad, The chemistry of cyano complexes of gold(I) with emphasis on the ligand scrambling reactions, Coord. Chem. Rev. 248 (2004) 231–243.

[21] C.F. Shaw III, Gold-based therapeutic agents., Chem. Rev. 99 (1999) 2589–600.

[22] S.J. Berners-Price, P.J. Sadler, Coordination chemistry of metallodrugs: insights into biological speciation from NMR spectroscopy, Coord. Chem. Rev. 151 (1996) 1–40.

[23] F. Caruso, M. Rossi, J. Tanski, C. Pettinari, F. Marchetti, Antitumor activity of the mixed phosphine gold species chlorotriphenylphosphine-1,3-bis(diphenylphosphino)propanegold(I)., J. Med. Chem. 46 (2003) 1737–42.

[24] T.M. Simon, D.H. Kunishima, G.J. Vibert, A. Lorber, Inhibitory effects of a new oral gold compound on hela cells, Cancer. 44 (1979) 1965–1975.

[25] T.M. Simon, D.H. Kunishima, G.J. Vibert, A. Lorber, Screening Trial with the Coordinated Gold Compound Auranofin Using Mouse Lymphocytic Leukemia P388, Cancer Res. 41 (1981) 94–97.

[26] C.K. Mirabelli, R.K. Johnson, D.T. Hill, L.F. Faucette, G.R. Girard, G.Y. Kuo, et al., Correlation of the in vitro cytotoxic and in vivo antitumor activities of gold(I) coordination complexes., J. Med. Chem. 29 (1986) 218–23.

[27] H.B.. Agrawal, K.C.; Bears, K.B.; Marcus, D.; Jonassen, Gold triphenylphosphine Res., complexes as a new class of potential antitumor agents., in: Am Assoc Cancer Res, 1978: p. 110.

[28] C.F.S. III, H. Schmidbaur, Gold-Progress in Chemistry, Biochemistry and Technology, Wiley, New York, (1999) 259-308., in: Wiley, New York, 1999: pp. 259–308.

[29] A. Casini, C. Hartinger, C. Gabbiani, E. Mini, P.J. Dyson, B.K. Keppler, et al., Gold(III) compounds as anticancer agents: relevance of gold-protein interactions for their mechanism of action., J. Inorg. Biochem. 102 (2008) 564–75.

[30] M. Navarro, C. Hernández, I. Colmenares, P. Hernández, M. Fernández, A. Sierraalta, et al., Synthesis and characterization of [Au(dppz)2]Cl3. DNA interaction studies and biological activity against Leishmania (L) mexicana., J. Inorg. Biochem. 101 (2007) 111–6.

[31] C. Gabbiani, A. Casini, L. Messori, Gold(III) compounds as anticancer drugs, Gold Bull. 40 (2007) 73–81.

[32] L. Messori, G. Marcon, Gold complexes as antitumor agents., Met. Ions Biol. Syst. 42 (2004) 385–424.

[33] L. Messori, G. Marcon, P. Orioli, Gold(III) compounds as new family of anticancer drugs, Bioinorg. Chem. Appl. 1 (2003) 177–187.

[34] E.R.T. Tiekink, Gold compounds in medicine: Potential anti-tumour agents, Gold Bull. 36 (2003) 117–124.

[35] G. Marcon, S. Carotti, M. Coronnello, L. Messori, E. Mini, P. Orioli, et al., Gold(III) Complexes with Bipyridyl Ligands: Solution Chemistry, Cytotoxicity, and DNA Binding Properties, J. Med. Chem. 45 (2002) 1672–1677.

[36] L. Ronconi, C. Marzano, P. Zanello, M. Corsini, G. Miolo, C. Maccà, et al., Gold(III) dithiocarbamate derivatives for the treatment of cancer: solution chemistry, DNA binding, and hemolytic properties., J. Med. Chem. 49 (2006) 1648–57.

[37] L. Messori, F. Abbate, G. Marcon, P. Orioli, M. Fontani, E. Mini, et al., Gold(III) Complexes as Potential Antitumor Agents: Solution Chemistry and Cytotoxic Properties of Some Selected Gold(III) Compounds, J. Med. Chem. 43 (2000) 3541–3548.

[38] N. Shaik, A. Martínez, I. Augustin, H. Giovinazzo, A. Varela-Ramírez, M. Sanaú, et al., Synthesis of apoptosis-inducing iminophosphorane organogold(III) complexes and study of their interactions with biomolecular targets., Inorg. Chem. 48 (2009) 1577–87.

[39] A. Casini, M.C. Diawara, R. Scopelliti, S.M. Zakeeruddin, M. Grätzel, P.J. Dyson, Synthesis, characterisation and biological properties of gold(III) compounds with modified bipyridine and bipyridylamine ligands., Dalton Trans. 39 (2010) 2239–45.

[40] C.-M. Che, R.W.-Y. Sun, Therapeutic applications of gold complexes: lipophilic gold(III) cations and gold(I) complexes for anti-cancer treatment., Chem. Commun. (Camb). 47 (2011) 9554–60.

[41] F. Mendes, M. Groessl, A.A. Nazarov, Y.O. Tsybin, G. Sava, I. Santos, et al., Metal-based inhibition of poly(ADP-ribose) polymerase--the guardian angel of DNA., J. Med. Chem. 54 (2011) 2196–206.

[42] J.J. Yan, A.L.-F. Chow, C.-H. Leung, R.W.-Y. Sun, D.-L. Ma, C.-M. Che, Cyclometalated gold(III) complexes with N-heterocyclic carbene ligands as topoisomerase I poisons., Chem. Commun. (Camb). 46 (2010) 3893–5.

[43] C. Gabbiani, G. Mastrobuoni, F. Sorrentino, B. Dani, M.P. Rigobello, A. Bindoli, et al., Thioredoxin reductase, an emerging target for anticancer metallodrugs. Enzyme inhibition by cytotoxic gold(iii) compounds studied with combined mass spectrometry and biochemical assays, Medchemcomm. 2 (2011) 50.

[44] B. Rosenberg, L. Vancamp, T. Krigas, Inhibition of Cell Division in Escherichia coli by Electrolysis Products from a Platinum Electrode, Nature. 205 (1965) 698–699.

[45] B. Rosenberg, L. Vancamp, J.E. Trosko, V.H. Mansour, Platinum Compounds: a New Class of Potent Antitumour Agents, Nature. 222 (1969) 385–386.

[46] D. Carpenter, Reputation and Power: Organizational Image and Pharmaceutical Regulation at the FDA (Princeton Studies in American Politics: Historical, International, and Comparative P...), Princeton University Press, 2010.

[47] B. Rosenberg, L. VanCamp, The successful regression of large solid sarcoma 180 tumors by platinum compounds., Cancer Res. 30 (1970) 1799–1802.

[48] A. Dorcier, W.H. Ang, S. Bolaño, L. Gonsalvi, L. Juillerat-Jeannerat, G. Laurenczy, et al., In Vitro Evaluation of Rhodium and Osmium RAPTA Analogues: The Case for Organometallic Anticancer Drugs Not Based on Ruthenium, Organometallics. 25 (2006) 4090–4096.

[49] S. Page, Ruthenium compounds as anticancer agents, Educ. Chem. 49 (2012) 26–29.

[50] E. Wong, C.M. Giandornenico, Current status of platinum-based antitumor drugs, Chem. Rev. 99 (1999) 2451–2466.

[51] K.R. Koch, New chemistry with old ligands: N-alkyl- and N,N-dialkyl-N′-acyl(aroyl)thioureas in co-ordination, analytical and process chemistry of the platinum group metals, Coord. Chem. Rev. 216-217 (2001) 473–488.

[52] Z.H. Siddik, Cisplatin: mode of cytotoxic action and molecular basis of resistance., Oncogene. 22 (2003) 7265–79.

[53] L. Ronconi, P.J. Sadler, Using coordination chemistry to design new medicines, Coord. Chem. Rev. 251 (2007) 1633–1648.

[54] E. Meggers, Exploring biologically relevant chemical space with metal complexes., Curr. Opin. Chem. Biol. 11 (2007) 287–92.

[55] N. Shah, D.S. Dizon, New-generation platinum agents for solid tumors., Future Oncol. 5 (2009) 33–42.

[56] P.M. Takahara, C.A. Frederick, S.J. Lippard, Crystal Structure of the Anticancer Drug Cisplatin Bound to Duplex DNA, J. Am. Chem. Soc. 118 (1996) 12309–12321.

[57] S. Ahmad, A.A. Isab, S. Ali, A.R. Al-Arfaj, Perspectives in bioinorganic chemistry of some metal based therapeutic agents, Polyhedron. 25 (2006) 1633–1645.

[58] T.S.L. Vincent, T. Devita, S.A. Rosenberg, Cancer: Principles and Practice of Oncology, in: Lippincott Williams and Wilkins, 2008: pp. 419–426.

[59] A.K. Godwin, A. Meister, P.J. O'Dwyer, Chin Shiou Huang, T.C. Hamilton, M.E. Anderson, High resistance to cisplatin in human ovarian cancer cell lines is associated with marked increase of glutathione synthesis, Proc. Natl. Acad. Sci. U. S. A. 89 (1992) 3070–3074.

[60] P.C.A. Bruijnincx, P.J. Sadler, New trends for metal complexes with anticancer activity, Curr. Opin. Chem. Biol. (2008).

[61] V. Milacic, D. Chen, L. Ronconi, K.R. Landis-Piwowar, D. Fregona, Q.P. Dou, A novel anticancer gold(III) dithiocarbamate compound inhibits the activity of a purified 20S proteasome and 26S proteasome in human breast cancer cell cultures and xenografts., Cancer Res. 66 (2006) 10478–86.

[62] K. Palanichamy, A.C. Ontko, Synthesis, characterization, and aqueous chemistry of cytotoxic Au(III) polypyridyl complexes, Inorganica Chim. Acta. 359 (2006) 44–52.

[63] P. Shi, Q. Jiang, Y. Zhao, Y. Zhang, J. Lin, L. Lin, et al., DNA binding properties of novel cytotoxic gold(III) complexes of terpyridine ligands: the impact of steric and electrostatic effects., J. Biol. Inorg. Chem. 11 (2006) 745–52.

[64] E.R.T. Tiekink, Anti-cancer potential of gold complexes., Inflammopharmacology. 16 (2008) 138–42.

[65] I. Kostova, Gold coordination complexes as anticancer agents., Anticancer. Agents Med. Chem. 6 (2006) 19–32.

[66] X. Wang, Z. Guo, Towards the rational design of platinum(II) and gold(III) complexes as antitumour agents., Dalton Trans. (2008) 1521–32.

[67] M.J. McKeage, L. Maharaj, S.J. Berners-Price, Mechanisms of cytotoxicity and antitumor activity of gold(I) phosphine complexes: the possible role of mitochondria, Coord. Chem. Rev. 232 (2002) 127–135.

[68] M.J. McKeage, Gold opens mitochondrial pathways to apoptosis, Br. J. Pharmacol. 136 (2002) 1081–1082.

[69] A. Garza-Ortiz, F. der W. en Natuurwetenschappen, Design, synthesis, characterization and biological studies of ruthenium and gold compounds with anticancer properties, (n.d.).

[70] A. Garza-Ortiz, H. den Dulk, J. Brouwer, H. Kooijman, A.L. Spek, J. Reedijk, The synthesis, chemical and biological properties of dichlorido(azpy)gold(III) chloride (azpy=2-(phenylazo)pyridine) and the gold-induced conversion of the azpy ligand to the chloride of the novel tricyclic pyrido[2,1-c][1,2,4]benzotriazin-11-ium cation., J. Inorg. Biochem. 101 (2007) 1922–30.

[71] S. Zhu, W. Gorski, D.R. Powell, J.A. Walmsley, Synthesis, structures, and electrochemistry of gold(III) ethylenediamine complexes and interactions with guanosine 5'-monophosphate., Inorg. Chem. 45 (2006) 2688–94.

[72] F. Abbate, P. Orioli, B. Bruni, G. Marcon, L. Messori, Crystal structure and solution chemistry of the cytotoxic complex 1,2-dichloro(o-phenanthroline)gold(III) chloride, Inorganica Chim. Acta. 311 (2000) 1–5.

[73] P.J. Sadler, M. Nasr, V.L. Narayanan, The design of metal complexes as anticancer drugs," in Platinum Coordination Complexes in Cancer Chemotherapy, in: E. M. P. Hacker, E. B. Douple, and I. H. Krakoff (Ed.), Martinus Nijhoff, Boston, Mass, USA, 1984: pp. 290–304.

[74] R. V. Parish, B.P. Howe, J.P. Wright, J. Mack, R.G. Pritchard, R.G. Buckley, et al., Chemical and Biological Studies of Dichloro(2-((dimethylamino)methyl)phenyl)gold(III), Inorg. Chem. 35 (1996) 1659–1666.

[75] R.G. Buckley, A.M. Elsome, S.P. Fricker, G.R. Henderson, B.R. Theobald, R. V Parish, et al., Antitumor properties of some 2-[(dimethylamino)methyl]phenylgold(III) complexes., J. Med. Chem. 39 (1996) 5208–14.

[76] R.V. Parish, B.P. Howe, J.P. Wright, J. Mack, R.G. Pritchard, R.G. Buckley, et al., Chemical and Biological Studies of Dichloro(2-((dimethylamino)methyl)phenyl)gold(III), Inorg. Chem. 35 (1996) 1659–1666.

[77] C.-M. Che, R.W.-Y. Sun, W.-Y. Yu, C.-B. Ko, N. Zhu, H. Sun, Gold(III) porphyrins as a new class of anticancer drugs: Cytotoxicity, DNA binding and induction of apoptosis in human cervix epitheloid cancer cells, Chem. Commun. 9 (2003) 1718–1719.

[78] G. Marcon, L. Messori, P. Orioli, Gold(III) complexes as a new family of cytotoxic and antitumor agents, Expert Rev. Anticancer Ther. 2 (2002) 337–346.

[79] S. Nobili, I. Landini, B. Giglioni, E. Mini, Pharmacological Strategies for Overcoming Multidrug Resistance, Curr. Drug Targets. 7 (2006) 861–879.

[80] A. Casini, M.A. Cinellu, G. Minghetti, C. Gabbiani, M. Coronnello, E. Mini, et al., Structural and solution chemistry, antiproliferative effects, and DNA and protein binding properties of a series of dinuclear gold(III) compounds with bipyridyl ligands., J. Med. Chem. 49 (2006) 5524–31.

[81] A. Bindoli, M.P. Rigobello, G. Scutari, C. Gabbiani, A. Casini, L. Messori, Thioredoxin reductase: A target for gold compounds acting as potential anticancer drugs, Coord. Chem. Rev. 253 (2009) 1692–1707.

[82] S. Nobili, E. Mini, I. Landini, C. Gabbiani, A. Casini, L. Messori, Gold compounds as anticancer agents: chemistry, cellular pharmacology, and preclinical studies., Med. Res. Rev. 30 (2010) 550–80.

[83] A. Mani, E.P. Gelmann, The ubiquitin-proteasome pathway and its role in cancer., J. Clin. Oncol. 23 (2005) 4776–89.

[84] D. Horn, Histone deacetylases., Adv. Exp. Med. Biol. 625 (2008) 81–6.

[85] A. Hadnagy, R. Beaulieu, D. Balicki, Histone tail modifications and noncanonical functions of histones: perspectives in cancer epigenetics., Mol. Cancer Ther. 7 (2008) 740–8.

[86] A.S. Ali, S. Ali, B.F. El-Rayes, P.A. Philip, F.H. Sarkar, Exploitation of protein kinase C: a useful target for cancer therapy., Cancer Treat. Rev. 35 (2009) 1–8.

[87] H.J. Mackay, C.J. Twelves, Targeting the protein kinase C family: are we there yet?, Nat. Rev. Cancer. 7 (2007) 554–62.

[88] L. Maiore, M.A. Cinellu, S. Nobili, I. Landini, E. Mini, C. Gabbiani, et al., Gold(III) complexes with 2-substituted pyridines as experimental anticancer agents: solution behavior, reactions with model proteins, antiproliferative properties., J. Inorg. Biochem. 108 (2012) 123–7.

[89] K. Palanichamy, N. Sreejayan, A.C. Ontko, Overcoming cisplatin resistance using gold(III) mimics: anticancer activity of novel gold(III) polypyridyl complexes., J. Inorg. Biochem. 106 (2012) 32–42.

[90] C. Gabbiani, M.A. Cinellu, L. Maiore, L. Massai, F. Scaletti, L. Messori, Chemistry and biology of three representative gold(III) compounds as prospective anticancer agents, Inorganica Chim. Acta. 393 (2012) 115–124.

[91] M.N. Kouodom, G. Boscutti, M. Celegato, M. Crisma, S. Sitran, D. Aldinucci, et al., Rational design of gold(III)-dithiocarbamato peptidomimetics for the targeted anticancer chemotherapy., J. Inorg. Biochem. 117 (2012) 248–60.

[92] J.A. Lessa, K.S.O. Ferraz, J.C. Guerra, L.F. de Miranda, C.F.D. Romeiro, E.M. Souza-Fagundes, et al., Spectroscopic and electrochemical characterization of gold(I) and gold(III) complexes with glyoxaldehyde bis(thiosemicarbazones): cytotoxicity against human tumor cell lines and inhibition of thioredoxin reductase activity., Biometals. 25 (2012) 587–98.

[93] A.A. Isab, M.N. Shaikh, M. Monim-ul-Mehboob, B.A. Al-Maythalony, M.I.M. Wazeer, S. Altuwaijri, Synthesis, characterization and anti proliferative effect of [Au(en)2]Cl3 and [Au(N-propyl-en)2]Cl3 on human cancer cell lines., Spectrochim. Acta. A. Mol. Biomol. Spectrosc. 79 (2011) 1196–201.

[94] B.A. Al-Maythalony, M.I.M. Wazeer, A.A. Isab, Synthesis and characterization of gold(III) complexes with alkyldiamine ligands, Inorganica Chim. Acta. 362 (2009) 3109–3113.

[95] A. Ahmed, D.M. Al Tamimi, A.A. Isab, A.M.M. Alkhawajah, M.A. Shawarby, Histological changes in kidney and liver of rats due to gold (III) compound [Au(en)Cl(2)]Cl., PLoS One. 7 (2012) e51889.

[96] S.S. Al-Jaroudi, M. Fettouhi, M.I.M. Wazeer, A.A. Isab, S. Altuwaijri, Synthesis, characterization and cytotoxicity of new gold(III) complexes with 1,2-diaminocyclohexane: Influence of stereochemistry on antitumor activity, Polyhedron. 50 (2013) 434–442.

[97] J. Kasparkova, O. Novakova, N. Farrell, V. Brabec, DNA binding by antitumor trans-[PtCl2(NH3)(thiazole)]. Protein recognition and nucleotide excision repair of monofunctional adducts., Biochemistry. 42 (2003) 792–800.

[98] S. Ahmad, A.A. Isab, H.P. Perzanowski, Ligand scrambling reactions of cyano(thione)gold(I) complexes and determination of their equilibrium constants, Can. J. Chem. 80 (2002) 1279–1284.

[99] D.J. Williams, D. VanDerveer, L.A. Lipscomb, R.L. Jones, Main group metal halide complexes with sterically hindered thioureas XII. Crystallographic studies of lead(II) and cadmium(II) thiocyanate complexes with 1,3-dimethyl-2(3H)-imidazolethione, Inorganica Chim. Acta. 192 (1992) 51–57.

[100] M.I.M. Wazeer, A.A. Isab, Complexations of Hg(CN)(2) with imidazolidine-2-thione and its derivatives: solid state, solution NMR and antimicrobial activity studies., Spectrochim. Acta. A. Mol. Biomol. Spectrosc. 68 (2007) 1207–12.

[101] M.I.M. Wazeer, A.A. Isab, M. Fettouhi, New cadmium chloride complexes with imidazolidine-2-thione and its derivatives: X-ray structures, solid state and solution NMR and antimicrobial activity studies, Polyhedron. 26 (2007) 1725–1730.

[102] M.I.M. Wazeer, A.A. Isab, Solid state and solution NMR studies of some new complexes of mercury selenocyanate with imidazolidine-2-thione and its derivatives, J. Coord. Chem. 60 (2007) 2649–2657.

[103] M. Fettouhi, M.I.M. Wazeer, A.A. Isab, A novel polymeric Cd[SSe2N2] central core five-coordinate complex: Synthesis, X-ray structure and 113Cd, 77Se CP MAS NMR characterization of catena(bis(μ2-selenocyanato-N,Se)-(N,N′-dimethylimidazolidine- 2-thione-S)-cadmium(II)), Inorg. Chem. Commun. 11 (2008) 252–255.

[104] P.J. Cox*, P. Aslanidis*, P. Karagiannidis, S. Hadjikakou, Silver(I) complexes with heterocyclic thiones and tertiary phosphines as ligands. Part 4. Dinuclear complexes of silver(I) bromide: the crystal structure of bis[bromo-(pyrimidine-2-thione)(triphenylphosphine)silver(I)], Inorganica Chim. Acta. 310 (2000) 268–272.

[105] M. Milovanović, A. Djeković, V. Volarević, B. Petrović, N. Arsenijević, Ž.D. Bugarčić, Ligand substitution reactions and cytotoxic properties of [Au(L)Cl2]+ and [AuCl2(DMSO)2]+ complexes (L=ethylenediamine and S-methyl-l-cysteine), J. Inorg. Biochem. 104 (2010) 944–949.

[106] A. Casini, C. Hartinger, C. Gabbiani, E. Mini, P.J. Dyson, B.K. Keppler, et al., Gold(III) compounds as anticancer agents: relevance of gold-protein interactions for their mechanism of action., J. Inorg. Biochem. 102 (2008) 564–75.

[107] W. Kemp, NMR in Chemistry-A Multinuclear Introduction, 2nd ed., Macmillan Education Ltd., London, 1986.

[108] S. Hayashi, K. Hayamizu, Spinning-rate dependence of, Chem. Phys. 157 (1991) 381–389.

[109] K. Eichele and R.E. Wasylischen, W: simulation package,, (2001).

[110] M.M. Maricq, J.S. Waugh, NMR in rotating solids, J. Chem. Phys. 70 (1979) 3300–3316.

[111] J.M. Hook, P.A.W. Dean, L.C.M. van Gorkom, Solid-state mercury-199 NMR of hexakis (dimethyl sulphoxidé) mercury (II) trifluoromethanesulphonate: A new standard for mercury-199 CP/MAS experiments, Magn. Reson. Chem. 33 (1995) 77–79.

[112] SMART APEX Software (5.05) for SMART APEX Detector,, (2001).

[113] SAINT Software (5.0) for SMART APEX Detector, (2001).

[114] G.M. Sheldrick, SADABS Program for Empirical Absorption correction of Area detector Data, (1996).

[115] G.M. Sheldrick, SHELXTL V5.1 Software, (1997).

[116] G.M. Sheldrick, SHELXTL 97, (1997).

[117] L.J. Farrugia, ORTEP-3 for windows - A version of ORTEP-III with a graphical user interface (GUI), J. Appl. Crystallogr. 30 (1997).

[118] C.F. Macrae, I.J. Bruno, J.A. Chisholm, P.R. Edgington, P. McCabe, E. Pidcock, et al., Mercury CSD 2.0 – new features for the visualization and investigation of crystal structures, J. Appl. Crystallogr. 41 (2008) 466–470.

[119] M.J. Frisch, G.W. Trucks, H.B. Schlegel, G.E. Scuseria, M.A. Robb, J.R. Cheeseman, et al., Gaussian 09, Revision A.1, (2009).

[120] M.J. Frisch, G.W. Trucks, H.B. Schlegel, G.E. Scuseria, M.A. Robb, J.R. Cheeseman, et al., GAUSSIAN03, Revision B.04, (2003).

[121] N.U. Zhanpeisov, M. Matsuoka, H. Yamashita, M. Anpo, Cluster quantum chemical ab initio study on the interaction of NO molecules with highly dispersed titanium oxides incorporated into silicalite and zeolites, J. Phys. Chem. B. 102 (1998) 6915–6920.

[122] A. Nicklass, M. Dolg, H. Stoll, H. Preuss, Ab initio energy-adjusted pseudopotentials for the noble gases Ne through Xe: Calculation of atomic dipole and quadrupole polarizabilities, J. Chem. Phys. 102 (1995) 8942–8952.

[123] M.J. Stewart, I.D. Watson, Standard units for expressing drug concentrations in biological fluids, Br. J. Clin. Pharmacol. 16 (1983) 3–7.

[124] K. Nomiya, S. Yamamoto, R. Noguchi, H. Yokoyama, N.C. Kasuga, K. Ohyama, et al., Ligand-exchangeability of 2-coordinate phosphinegold(I) complexes with AuSP and AuNP cores showing selective antimicrobial activities against Gram-positive bacteria. Crystal structures of [Au(2-Hmpa)(PPh3)] and [Au(6-Hmna)(PPh3)] (2-H2mpa=2-mercaptopropio, J. Inorg. Biochem. 95 (2003) 208–220.

[125] N.C. Kasuga, K. Sekino, M. Ishikawa, A. Honda, M. Yokoyama, S. Nakano, et al., Synthesis, structural characterization and antimicrobial activities of 12 zinc(II) complexes with four thiosemicarbazone and two semicarbazone ligands, J. Inorg. Biochem. 96 (2003) 298–310.

[126] V. Navarro, M.L. Villarreal, G. Rojas, X. Lozoya, Antimicrobial evaluation of some plants used in Mexican traditional medicine for the treatment of infectious diseases, J. Ethnopharmacol. 53 (1996) 143–147.

[127] W. Beck, W.P. Fehlhammer, P. Pöllmann, E. Schuierer, K. Feldl, Darstellung, IR- und Elektronenspektren von Azido-Metall-Komplexen, Chem. Ber. 100 (1967) 2335–2361.

[128] K. Esumi, M. Nawa, N. Aihara, K. Usui, Growth of rodlike Au/Pt particles in cationic micelles by UV irradiation, New J. Chem. 22 (1998) 719–720.

[129] I. V. Mironov, V.A. Afanas'eva, Gold(III) amine complexes in aqueous alkali solutions, Russ. J. Inorg. Chem. 55 (2010) 1156–1161.

[130] V.A. Afanas'eva, L.A. Glinskaya, R.F. Klevtsova, I. V. Mironov, Dinuclear complex of gold(III) with 1,3-diaminopropane (HL), [Au2(HL)(L)2](ClO4)3(OH): Synthesis and crystal and molecular structures, Russ. J. Coord. Chem. 36 (2010) 697–703.

[131] E. V. Makotchenko, I.A. Baidina, Structural investigation of [Au(en)2]Cl(ReO4)2 and [Au(en)2](ReO4)3 complexes, J. Struct. Chem. 52 (2011) 556–559.

[132] G. Nardin, L. Randaccio, G. Annibale, G. Natile, B. Pitteri, Comparison of structure and reactivity of bis(2-aminoethyl)amine- and bis(2-aminoethyl)amido-chlorogold(III) complexes, J. Chem. Soc. Dalt. Trans. (1980) 220.

[133] A. Casini, G. Kelter, C. Gabbiani, M.A. Cinellu, G. Minghetti, D. Fregona, et al., Chemistry, antiproliferative properties, tumor selectivity, and molecular mechanisms of novel gold(III) compounds for cancer treatment: a systematic study., J. Biol. Inorg. Chem. 14 (2009) 1139–49.

[134] S. Mansilla, L. Llovera, J. Portugal, Chemotherapeutic targeting of cell death pathways, Anticancer. Agents Med. Chem. 12 (2012) 226–238.

[135] A. Deeraksa, J. Pan, Y. Sha, X.-D. Liu, N.T. Eissa, S.-H. Lin, et al., Plk1 is upregulated in androgen-insensitive prostate cancer cells and its inhibition leads to necroptosis., Oncogene. 32 (2013) 2973–83.

[136] J. Portugal, M. Bataller, S. Mansilla, Cell death pathways in response to antitumor therapy, Tumori. 95 (2009) 409–421.

[137] R. Kolanoś, W. Wysocka, T. Brukwicki, A comparative study of NMR chemical shifts of sparteine thiolactams and lactams, Tetrahedron. 59 (2003) 5531–5537.

[138] B.A. Al-Maythalony, A.A. Isab, M.I.M. Wazeer, A. Ibdah, Investigation of the interaction of gold(III)–alkyldiamine complexes with l-histidine and imidazole ligands by 1H and 13C NMR, and UV spectrophotometry, Inorganica Chim. Acta. 363 (2010) 3200–3207.

[139] M.I.M. Wazeer, A.A. Isab, A. El-Rayyes, Solid state NMR study of 1,3-imidazolidine-2-thione, 1,3-imidazolidine-2- selenone and some of their N-substituted derivatives, Spectroscopy. 18 (2004) 113–119.

[140] J.M. Lazić, L. Vucićević, S. Grgurić-Sipka, K. Janjetović, G.N. Kaluderović, M. Misirkić, et al., Synthesis and in vitro anticancer activity of octahedral platinum(IV) complexes with cyclohexyl-functionalized ethylenediamine-N,N'-diacetate-type ligands., ChemMedChem. 5 (2010) 881–9.

[141] H. Yildirim, F. Kockar, C. Nakiboglu, Antiproliferative activity of some novel platinum complexes on C6 glioma and MCF-7 breast cancer cells, African J. Biotechnol. 11 (2012) 12422–12428.

[142] T. Pivetta, M.D. Cannas, F. Demartin, C. Castellano, S. Vascellari, G. Verani, et al., Synthesis, structural characterization, formation constants and in vitro cytotoxicity of phenanthroline and imidazolidine-2-thione copper(II) complexes., J. Inorg. Biochem. 105 (2011) 329–38.

[143] V. Sharma, T.A. Lansdell, S. Peddibhotla, J.J. Tepe, Sensitization of Tumor Cells toward Chemotherapy: Enhancing the Efficacy of Camptothecin with Imidazolines, Chem. Biol. 11 (2004) 1689–1699.

[144] V. Sharma, S. Peddibhotla, J.J. Tepe, Sensitization of cancer cells to DNA damaging agents by imidazolines., J. Am. Chem. Soc. 128 (2006) 9137–43.

[145] A.A. Isab, M.I.M. Wazeer, M. Fettouhi, S. Ahmad, W. Ashraf, Synthesis and characterization of mercury(II) complexes of selones: X-ray structures, CP MAS and solution NMR studies, Polyhedron. 25 (2006) 2629–2636.

[146] A.A. Isab, H.P. Perzanowski, 1H, 13C and 199Hg NMR studies of the —NHCS-containing ligands with mercuric halides, Polyhedron. 15 (1996) 2397–2401.

[147] Z. Popović, G. Pavlović, D. Matković-Čalogović, Ž. Soldin, M. Rajić, D. Vikić-Topić, et al., Mercury(II) complexes of heterocyclic thiones., Inorganica Chim. Acta. 306 (2000) 142–152.

[148] A.A. Isab, M.I.M. Wazeer, W. Ashraf, Cadmium cyanide complexes with heterocyclic thiones: solid state and solution NMR studies., Spectrochim. Acta. A. Mol. Biomol. Spectrosc. 72 (2009) 218–21.

[149] S. Ahmad, A.A. Isab, A.P. Arnold, Synthesis and Spectroscopic Characterization of Silver(I) Complexes of Selenones, J. Coord. Chem. 56 (2003) 539–544.

[150] B.A. Al-Maythalony, M. Fettouhi, M.I.M. Wazeer, A.A. Isab, A novel polymeric Hg[(CN)2N2] central core four-coordinate complex: Synthesis, X-ray structure and 199Hg, 13C and 15N CP MAS NMR characterization of catena((μ2-1,4-diaminobutane-N,N′)dicyanomercury(II)), Inorg. Chem. Commun. 12 (2009) 540–543.

[151] N.D. Draper, R.J. Batchelor, P.M. Aguiar, S. Kroeker, D.B. Leznoff, Factors affecting the solid-state structure and dimensionality of mercury cyanide/chloride double salts, and NMR characterization of coordination geometries., Inorg. Chem. 43 (2004) 6557–67.

[152] A.A. Isab, M. Fettouhi, M.R. Malik, S. Ali, A. Fazal, S. Ahmad, Mercury(II) cyanide complexes of thioureas and the crystal structure of [(N-methylthiourea)2 Hg(CN)2], Russ. J. Coord. Chem. 37 (2011) 180–185.

[153] M. Altaf, H. Stoeckli-Evans, S. Ahmad, A.A. Isab, A.R. Al-Arfaj, M.R. Malik, et al., Crystal Structure of a Trinuclear Mercury(II) Cyanide Complex of Tetramethylthiourea, [{(Tetramethylthiourea)2Hg(CN)2}2·Hg(CN)2], J. Chem. Crystallogr. 40 (2010) 1175–1179.

[154] S. Ahmad, H. Sadaf, M. Akkurt, S. Sharif, I.U. Khan, Bis(1,3-dibutylthiourea)dicyanido-mercury(II)., Acta Crystallogr. Sect. E. Struct. Rep. Online. 65 (2009) m1191–2.

[155] S.-L. Li, J.-Y. Wu, Y.-P. Tian, H. Ming, P. Wang, M.-H. Jiang, et al., Design, Crystal Growth, Characterization, and Second-Order Nonlinear Optical Properties of Two New Three-Dimensional Coordination Polymers Containing Selenocyanate Ligands, Eur. J. Inorg. Chem. 2006 (2006) 2900–2907.

[156] P. Brooks, N. Davidson, Mercury (II) complexes of imidazole and histidine, J. Am. Chem. Soc. 82 (1960) 2118–2123.

[157] A. Renuka, K. Shakuntala, P.C. Srinivasan, Controlled release of mercury into aqueous L-(-) histidine solutions : Biological implications of electrochemical studies, Indian J. Chem. - Sect. A Inorganic, Phys. Theor. Anal. Chem. 37 (1998) 596–605.

[158] S. Sain, T.K. Maji, G. Mostafa, T.-H. Lu, M.Y. Chiang, N.R. Chaudhuri, Self assembly towards the construction of molecular ladder and rectangular grid of cadmium(II)-selenocyanate, Polyhedron. 21 (2002) 2293–2299.

[159] T.K. Maji, S. Sain, G. Mostafa, D. Das, T.-H. Lu, N.R. Chaudhuri, Synthesis and crystal structure of selenocyanato bridged two dimensional supramolecular coordination compounds of cadmium(II), J. Chem. Soc. Dalt. Trans. (2001) 3149–3153.

[160] M. Nasiruzzaman Shaikh, B.A. Al-Maythalony, M.I.M. Wazeer, A.A. Isab, Complexations of 2-thiouracil and 2,4-dithiouracil with Cd(SeCN), Spectroscopy. 25 (2011) 187–195.

Vitae

Name :Muhammad Monim-ul-Mehboob

Nationality :Pakistani

Date of Birth : 27/12/1969

Email :mmmehboob786@gmail.com

Address :5-D, Main Boulevard, Sabzazar, Lahore-54780, Pakistan

Academic Background :PhD in Chemistry with specialization in Inorganic Chemistry, King Fahd University of Petroleum and Minerals (KFUPM), Dhahran-Saudi Aabia (October 2008- October 2013)